THE ISO HANDBOOK

Volume VI:

SWS –
The Short Wavelength Spectrometer

K. Leech[1] for Thijs de Graauw[2], Mario van den Ancker[2], Otto H. Bauer[3], Douwe Beintema[2], Danny Boxhoorn[2], Siegfried Drapatz[3], Helmut Feuchtgruber[3], Leo Haser[3], Anna Heras[1], Karl van der Hucht[5], Rik Huygen[4], Reinhard Katterloher[3], Do Kester[2], Dietmar Kunze[3], Fred Lahuis[2], Dieter Lutz[3], Patrick Morris[5], Peter Roelfsema[2], Alberto Salama[1], Stephan Schaeidt[3], Russell Shipman[2], Henrik Spoon[3], Eckhard Sturm[3], Edwin Valentijn[2], Bart Vandenbussche[4], Ekkehard Wieprecht[3], Erich Wiezorrek[3]

SAI/2000-008/Dc, Version 1.1

January 23, 2001

[1] ISO Data Centre, Astrophysics Division, Space Science Department of ESA, Villafranca, P.O. Box 50727, E-28080 Madrid, Spain

[2] SRON, P.O. Box 800, 9700 AV Groningen, The Netherlands

[3] Max-Planck-Institut für extraterrestrische Physik, Postfach 1603, D-85740 Garching, Germany

[4] Instituut voor Sterrekunde K.U.Leuven, B-3001 Heverlee, Belgium

[5] SRON, Sorbonnelaan 2, 3584 CA Utrecht, The Netherlands

Document Information

Document:	The ISO Handbook
Volume:	VI
Title:	SWS – The Short Wavelength Spectrometer
Reference Number:	SAI/2000-008/Dc
Issue:	Version 1.1
Issue Date:	9 January 2001
Authors:	K. Leech & The SWS Team
Editors:	K. Leech
Web-Editor:	J. Matagne

Document History

The ISO Handbook, Volume VI: SWS – The Short Wavelength Spectrometer, is based on the documents listed in the bibliography.

Document Change Record

Date	**Revision**	**Comments**
Jan 2000	Version 1.0	Derived from SWS Instrument Data Manual
Jan 2001	Version 1.1	update
planned		
Apr 2001	Version 1.2	update
Oct 2001	Version 2.0	Final version

The SWS Consortium

- **Principal Investigator:**
  T. de Graauw, SRON, Groningen, The Netherlands

- **Scientific Associates**
  H. J. G. L. M. Lamers, SRON, Utrecht, The Netherlands
  LBFM Waters, Astronomical Institute Anton Pannekoek, Amsterdam, The Netherlands
  Christoffel Waelkens, Instituut voor Sterrekunde K.U.Leuven, Belgium

- **Management**
  Otto H. Bauer, MPE, Garching, Germany
  Siegfried Drapatz, MPE, Garching, Germany
  Reinhard Genzel, MPE, Garching, Germany
  Gerhard Haerendel, MPE, Garching, Germany
  Leo Haser, MPE, Garching, Germany
  Rik Huygen, Instituut voor Sterrekunde K.U.Leuven, Belgium
  Reinhard Katterloher, MPE, Garching, Germany
  Dieter Lutz, MPE, Garching, Germany
  Peter Roelfsema, SRON, Groningen, The Netherlands
  Berhard Scheiner, MPE, Garching, The Netherlands
  Paul Wesselius, SRON, Groningen, The Netherlands

- **Development of SWS**
  H. van Agthoven, TPD, Delft, The Netherlands
  Mario van den Ancker, SRON, Groningen, The Netherlands
  Lothar Barl, MPE, Garching, Germany
  Douwe Beintema, SRON, Groningen, The Netherlands
  H.E.G. Bekenkamp, SRON, Groningen, The Netherlands
  Geert Bex, Instituut voor Sterrekunde K.U.Leuven, Belgium
  A-J. Boonstra, SRON, Groningen, The Netherlands
  J. Cote, SRON, Groningen, The Netherlands
  Stephan Czempiel, MPE, Garching, Germany
  C. van Dijkhiuzen, SRON, Utrecht, The Netherlands
  J. Evers, SRON, Groningen, The Netherlands
  M. Frericks, SRON, Utrecht, The Netherlands
  Werner Goebel, MPE, Garching, Germany
  P. de Groene, SRON, Utrecht, The Netherlands
  Karl van der Hucht, SRON, Utrecht, The Netherlands
  Thijs van der Hulst, Kapteyn Astronomical Institute, Groningen
  H. Jacobs, SRON, Utrecht, The Netherlands
  Gerd Jakob, MPE, Garching, Germany
  Norbert Kamm, MPE, Garching, Germany
  Th. Kamperman, SRON, Utrecht, The Netherlands
  Do Kester, SRON, Groningen, The Netherlands
  D. Kussendrager, SRON, Groningen, The Netherlands
  Hans Loidl, MPE, Garching, Germany
  Friedhelm Melzner, MPE, Garching, Germany
  Berhard Merz, MPE, Garching, Germany
  Jörg Niekerke, MPE, Garching, Germany

D. van Nguyen, SRON, Groningen
Uwe Pagel, MPE, Garching, Germany
Günther Pfaller, MPE, Garching, Germany
G. Ploeger, SRON, Groningen
S. Price, Air Force Philips Laboratory, USA
Peter Reiss, MPE, Garching, Germany
Christel Schäfer, MPE, Garching, Germany
N. Sijm, SRON, Utrecht, The Netherlands
C. Smoorenburg, TPD, Delft, The Netherlands
Heinrich Späth, MPE, Garching, Germany
Wilhelm Stüberl, MPE, Garching, Germany
Jacob Stöcker, MPE, Garching, Germany
Edwin Valentijn, SRON, Groningen, The Netherlands
J. Wensink,, SRON, Groningen, The Netherlands
J.J Wijnbergen, SRON, Groningen, The Netherlands
K.J. Wildeman, SRON, Groningen, The Netherlands
E. Young, Steward Observatory, Arizona, USA

- **SWS Instrument Dedicated Team in Villafranca**
  Danny Boxhoorn, SRON, Groningen, The Netherlands
  Helmut Feuchtgruber, MPE, Garching, Germany
  Ana Heras, ESA
  Kieron Leech, ESA
  Fred Lahuis, SRON, Groningen, The Netherlands
  Rosario Lorente, INSA, Spain
  Patrick Morris, SRON, Utrecht, The Netherlands
  Alberto Salama, ESA
  Stephan Schaeidt, MPE, Garching, Germany
  Bart Vandenbussche, Instituut voor Sterrekunde K.U.Leuven, Belgium
  Ekkehard Wieprecht, MPE, Garching, Germany

- **ISO Spectrometer Datacentres**
  Harald Baumgartner, MPE, Garching, Germany
  Kurt Becher, MPE, Garching, Germany
  Norbert Heinecke, MPE, Garching, Germany
  Dietmar Kunze, MPE, Garching, Germany
  Georg Orthuber, MPE, Garching, Germany
  Sabine Osterhage, MPE, Garching, Germany
  Dimitra Rigopoulou, MPE, Garching, Germany
  Dirk Rosenthal, MPE, Garching, Germany
  Karla Seidenschwang, MPE, Garching, Germany
  Russell Shipman, SRON, Groningen, The Netherlands
  Henrik Spoon, MPE, Garching, Germany
  Michael Steinmayer, MPE, Garching, Germany
  Eckhard Sturm, MPE, Garching, Germany
  Dan Tran, MPE, Garching, Germany
  Erich Wiezorrek, MPE, Garching, Germany

Contents

List of Figures

List of Tables

Chapter 1

Introduction

1.1 Purpose

This Handbook is one in a series of six documents that explain the operations of the Infrared Space Observatory (ISO) and its four instruments, the data received from the instruments and the processing carried out on the data. Volume 1 of the six gives an overview of the entire ISO mission, Volume 2 explains the operations of the ISO satellite while the remaining four explain the individual instruments (CAM, LWS, PHOT and SWS).

The Explanatory Documentation provides all information relevant to the ISO data user, concerning the satellite, the instruments and the observational and technical data products. It is be a comprehensive description of systems and parameters relevant to ISO data products, how these products were derived, and what are the known limitations and caveats. It will allow the data users to do further data analysis beyond the scope of the automatic Off Line Processing (OLP).

This document describes data processed with version 9 or later of the Off-Line Processing (OLP) system, available from the ISO DATA Archive (IDA) at http://www.iso.vilspa.esa.es/.

1.2 What's new

This section describes major document changes between versions and is an expanded version of the Document Change Record found on page 2.

1.2.1 Issue 1

This was the first version, released in January 2000. It was produced using information from the SWS Instrument & Data Manual (SWS ISDM), updated as necessary.

1.2.2 Issue 1.1

This version was released in December 2000 along with SWS OLP 9.5. The following sections were changed:

1 "Derive-SPD" section 4.2 was re-written based on OLP 9.5.

2 "Overall Calibration", section 5.2, in the previous version was subsumed into the relevant sections. This left space for a new section 5.2, "Determination of the focal plane geometry".

3 “Flux Calibration, section 5.2, was updated.

4 Preliminary section on Straylight written, section 2.3.4.

5 Section “Cross AOT Flux Comparisons”, 5.6.4, moved from chapter 3 to chapter 5.

6 And other minor changes.

1.3 How to contact ESA or other institutes

There are two ways to contact or to get information from ESA concerning ISO.

1 Send a question to the ISO helpdesk, ‘helpdesk@iso.vilspa.esa.es’.

2 Look at the ISO WWW page, at “http://www.iso.vilspa.esa.es/”. There is a SWS page linked to this, accessed via ‘Users Information’.

American observers can also obtain information from IPAC by:

1 Sending a question to the IPAC helpdesk, ‘iso@ipac.caltech.edu’.

2 Looking at the IPAC ISO WWW page, at “http://www.ipac.caltech.edu/iso/iso.html”.

The Short Wavelength Spectrometer team maintains two websites through which they may be contacted. Space Research Organization Netherlands (SRON) Groningen has an ISO page at http://www.sron.rug.nl/iso/ and the ISO Spectrometer Data Centre at the Max-Planck-Institut für extraterrestrische Physik (MPE), Garching, Germany has a web page at http://www.mpe-garching.mpg.de/iso/isosdc.html.

1.4 Processing SWS Data

There are two software packages specifically written to further process SWS data beyond the standard pipeline products: the ISO Spectral Analysis Package for SWS and LWS Auto Analysis Results (ISAP); and the Observers SWS Interactive Analysis (OSIA). Users are encouraged to obtain both these packages from the ISO Web site http://www.iso.vilspa.esa.es/, under Data Analysis. Recipes are also available at this web site to guide you in the reduction of your data.

Users wishing to process SWS data with their favourite data analysis package are recommended to read the ISAP and OSIA recipes and the following sections in order to understand what has to be done to the data.

Users are pointed to these packages and recipes at the relevant place in the following document.

1.5 Current Caveats on SWS Data Products

Excellent results have been obtained from SWS, with very low noise measured, especially in band 1. The basic Off-Line Processing (OLP) products can be used in the analysis of your data, with special processing only needed for exceptional cases.

There are, however, some points to be aware of concerning the data products from OLP Version 9.5, primarily that the AOT testcases do not cover the entire parameter space of SWS observations and there are sets of input data for which the code gives non-optimal results. Many AOT testcases have been selected to test OLP V9, and all have been reduced and checked. However, these do not cover the entire range of possible SWS observations. Thus while there is no reason to believe the pipeline does not work correctly, it has not been proven correct for all input data.

Cases for which the pipeline is not optimised, and is therefore known to fail include:

1 Memory Effects

Memory effects are not accounted for in OLP V9.5 and so may affect the data. See section 6.8, "Memory Effects", for a discussion of this.

2 Low flux cases. Pulse shape problems are the most important problems at low fluxes. Flux jumps and slow changes of up to 10 μV/s exist and cause problems for the dark current subtraction. Memory effects are much more important at higher (>100 μV/s) flux levels.

Cases where the continuum is weak can cause problems for dark current subtraction from two effects.

When the flux level falling on the detectors is very low, jumps and slow changes in the detectors can cause the output to change by 10 μV/s over an observation (equivalent to the flux from the source). This jump or drift makes dark current subtraction very problematical.

At higher flux levels (equivalent to 100 μV/s), memory effects will also cause problems of a similar magnitude. When the amount of flux falling on the detector is small, there may be cases where (flux plus dark current plus noise) is less than the (dark current plus noise). Dark current subtraction then results in negative fluxes in the AAR product. The limiting flux for this can be quite high, e.g. of the order of a few Jy for band 2, and the actual level might be determined by the scan rate and/or number of scans at a required S/N. See section 6.4, "Detector Noise & Dark Current" for a discussion of dark currents and noise.

Such problems can also manifest themselves as distortions in the spectral energy distributions of low flux sources, especially noticeable in AOTs 1 & 6.

3 Fast SWS01 AOTs

There are two possible problems with fast AOT 1's.

- Datapoints of unresolved lines marked as glitched. Since the SWS grating is changing positions during an integration of an AOT1, an unresolved line may be inadvertently flagged as a radiation hit. This can effect both the wings and the center of the line. This effect depends on the strength of the line as well as the resolution of the grating at the wavelength of the line. An examination of the FLAG of the data product will indicate if a particular wavelength has been treated as a radiation hit ('Glitch'). See section 4.5, "Glitch removal effects on spectral lines in fast speed AOT1 observations", for more information on this.

- The calculated flux for a line depending on actual wavelength of the peak of the line. This is because the observed fringe pattern is smeared version of the Relative Spectral Response Function (RSRF), due to the grating moving.

The result of both these effects is that the net line flux and the line profiles can be appreciably affected.

4 Flux/aperture points

SWS has three apertures (four if the virtual Fabry-Pérot aperture is counted) of different sizes and, for the grating, four detector bands each with detectors of different sizes. This causes an effect when switching between apertures/detector bands. The fluxes of extended sources may change as the apertures/detector bands change, due to the different areas of the sky observed. The fluxes of point sources may change if the entered coordinates are incorrect by a few arcseconds, as the apertures are slightly offset wrt each other.

Chapter 2

Instrument overview

2.1 Introduction

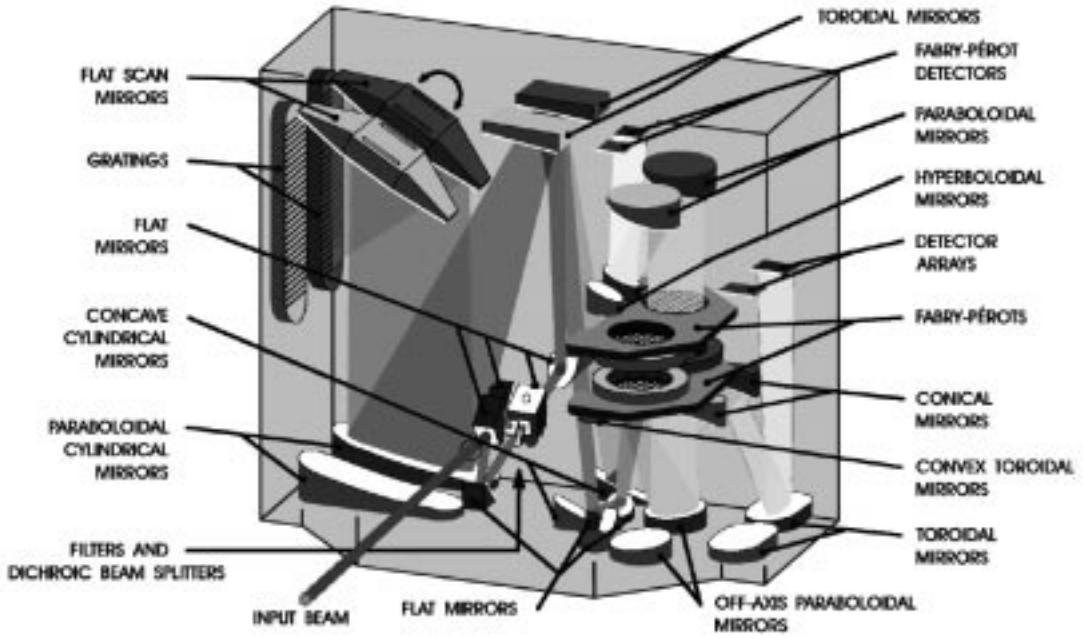

Figure 2.1: *The layout of SWS.*

The Short Wavelength Spectrometer (SWS, see figure 2.1) onboard ESA's Infrared Space Observatory (ISO) provided medium and high spectral resolution in the wavelength region 2.38–45.2 μm. Its two nearly independent grating spectrometers had a spectral resolution of $R \approx 1{,}000$–$2{,}000$, corresponding to

a velocity resolution of $\Delta v \approx 300$–150 km s^{-1}. By inserting Fabry-Pérot (FP) filters, one for the range 15–26 μm (with capability down to 11.4 μm at reduced resolution) and the other for the region 26–35 μm (with capability to 44.5 μm at reduced sensitivity), the resolution could be increased to $R \approx 30,000$, $\Delta v \approx 10$ km s^{-1}.

The SWS wavelength range is of great scientific interest, not only because it is here that cool objects in the temperature range 1500–80 K radiate the bulk of their energy, but also because of its rich variety of atomic, ionic, molecular and solid-state spectral features. These provide unique and excellent tools for studies of the physical and chemical processes in the universe, especially of those regions optically hidden by interstellar dust. The SWS spectral resolution allows probing of kinematic processes in a variety of objects ranging from nuclei of galaxies to planetary atmospheres.

2.2 The Instrument

Figure 2.2 gives an impression of the lay-out of the SWS, an optical block diagram is shown in figure 2.4, and an optical schematic is shown in figure 2.5. Figure 2.3 shows one of the early grating scanners.

Light from the telescope is reflected into the SWS by the ISO pyramidal mirror. The SWS had three entrance apertures, each with its own dichroic beamsplitter feeding the Short Wavelength section and the Long Wavelength section. The appropriate entrance aperture was selected by specific pointing of the ISO satellite. A four-position selection mechanism permitted opening of any one of these apertures or blocking of all three – see section 2.3.1 for further details.

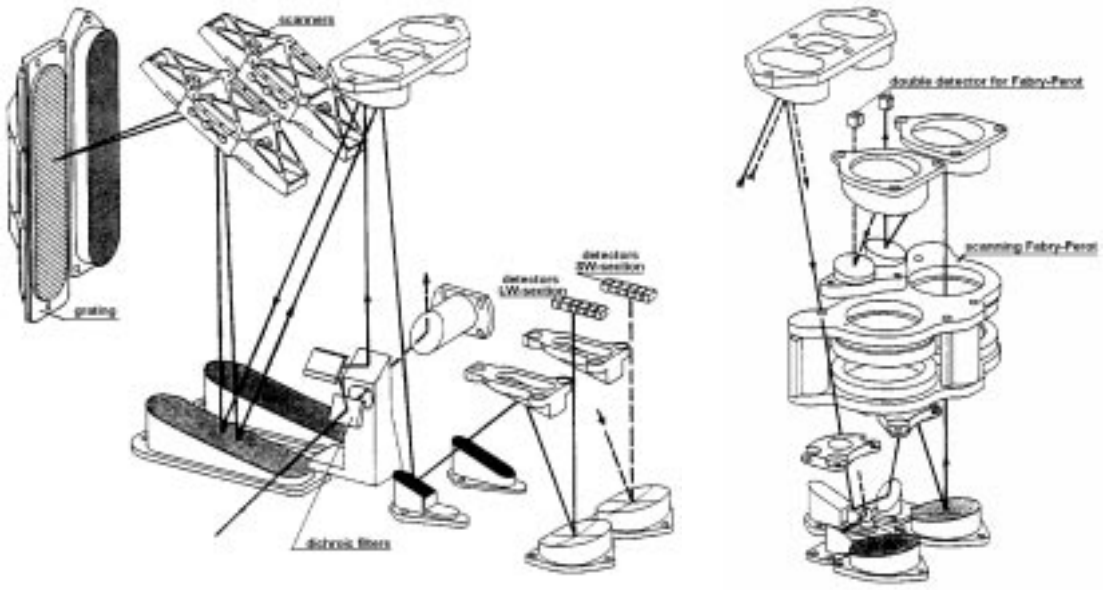

Figure 2.2: *Internal lay-out of the Short Wavelength Spectrometer (SWS). On the left is the light-path for grating observations, while on the right an abbreviated light-path for Fabry-Pérot observations is shown.*

Each grating had its own scanning mechanism, enabling the use of both parts of the spectrograph at the same time, albeit through the same aperture. Wavelength scanning was achieved by rotating a flat mirror close to each grating in discrete scan steps.

After reflection from the gratings, the light almost retraced its path and, by means of small-diameter re-imaging relay optics, the high resolution spectral image of each wavelength band was re-imaged onto

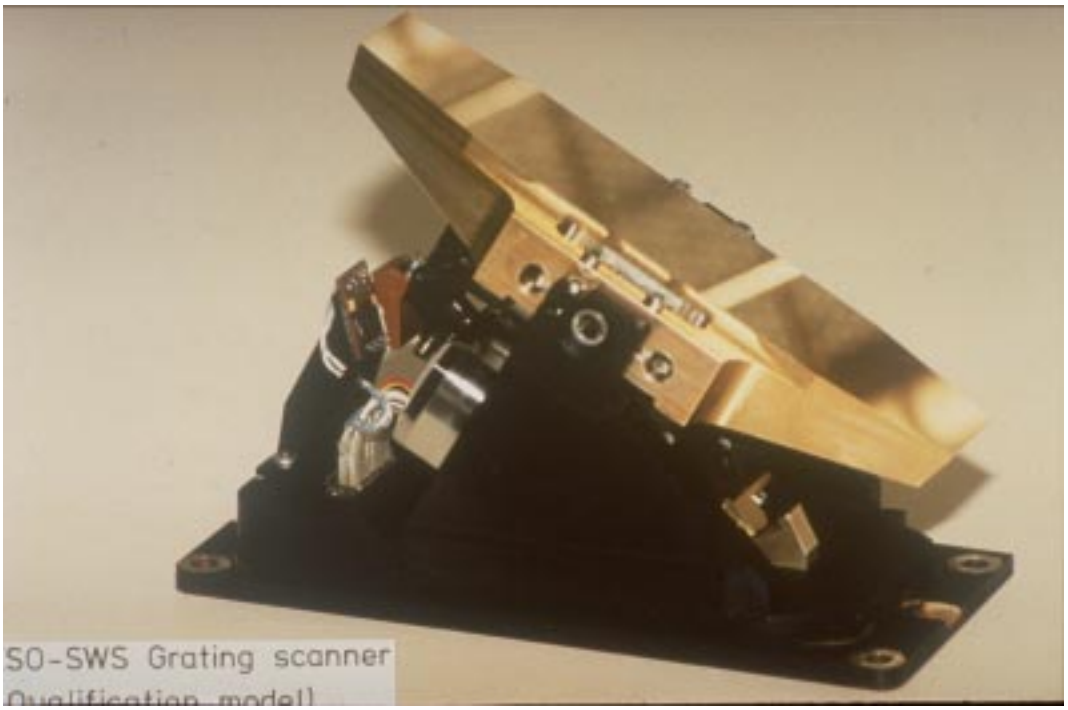

Figure 2.3: *A early QM SWS Grating scanner.*

the detector block. These relay optics have various functions:
– they relayed the high resolution image to a more easily-accessible location on the detector block,
– they changed the relative opening of the beam to a value that was optimised to the detector dimensions,
– they enabled efficient straylight rejection.

To use the F-P's, the radiation returning from the LW grating was collimated again, transmitted through a tunable F-P interference filter and imaged onto separate detectors in the detector block. This second light path is also shown in Figure 2.4. The two F-P's were mounted on a single pair of parallel plates. Their separation and parallelism could be varied by changing the currents in three pull coils.

The wavelength coverage of the SWS is broken down into 12 grating bands and 5 FP bands. For historical reasons they are named Astronomical Observation Templates (AOT) bands, and are listed in tables 2.1 and 2.2. The AOT bands are combinations of detector array, aperture and grating orders such that the relevant detector array sees an unique order. Other detector arrays may see only one order or may see a mixture of orders. The wavelengths of the SWS data products will not be on an equidistant wavelength grid and there may be gaps over certain wavelength ranges. There may also be flux jumps between spectra taken in adjacent AOT bands.

The SW and LW gratings are associated with 4 different detector arrays of 12 elements each. The 2 SWS Fabry-Pérots are associated with 2 double detectors. All $4 \times 12 + 2 \times 2 = 52$ detectors are operated simultaneously. The correspondence between detector number, bands and detector material is shown in table 2.1. At any given time, the astronomical source of interest to the observer was centered into one and only one of the three SWS apertures, feeding light on many, or all, of the 52 detector elements via two rotatable scanning mirrors, one for each grating system. While it was possible to find scanner settings such that all of the detector arrays will contain valid data, the instrument was normally operated such that only one or two of the detector arrays received *one* order of the grating spectrometer, the other four or five receiving a mixture of orders. The observer will, however, receive data from all 52 detectors.

Table 2.1: *Detector definition for the SWS AOT bands*

	band		order	aperture			area[5]	detector	detector	wavelength[8]
	name	number[15]				filter	($''\times''$)	type	number	(μm)
SW[1]	1A	1	4	1	t[3]	Al_2O_3	14-20	InSb	1 - 12	2.38 – 2.60
SW	1B	2	3	1	t	Al_2O_3	14-20	InSb	1 - 12	2.60 – 3.02
SW	1D	3	3	2	t	LiF	14-20	InSb	1 - 12	3.02 – 3.52
SW	1E[13]	4	2	2	t	LiF	14-20	InSb	1 - 12	3.52 – 4.08
SW	2A[13]	5	2	2	t	LiF	14-20	Si:Ga	13 - 24	4.08 – 5.30
SW	2B	6	1	2	t	LiF	14-20	Si:Ga	13 - 24	5.30 – 7.00
SW	2C[9]	7	1	3	t	SrF_2	14-20	Si:Ga	13 - 24	7.00 – 12.0
LW[2]	3A	9	2	1	r[4]	Al_2O_3	14-27	Si:As[14]	25 – 36	12.0 - 16.5
LW	3C	10	2	2	r	LiF	14-27	Si:As[14]	25 – 36	16.5 - 19.5
LW	3D	11	1	2	r	LiF	14-27	Si:As[14]	25 – 36	19.5 - 27.5
LW	3E	12	1	3	r	SrF_2	20-27	Si:As[14]	25 – 36	27.5 - 29.0
LW	4	13	1	3	r	SrF_2	20-33	Ge:Be	37 – 48	29.0 - 45.2
F-P1	5A	15	3	1	r	Al_2O_3	10-39	Si:Sb	49 – 50[10]	11.4 – 12.2
F-P1	5B	16	2	1	r	Al_2O_3	10-39	Si:Sb	49 – 50[10]	12.2 – 16.0
F-P1	5C	17	2	2	r	LiF	10-39	Si:Sb	49 – 50[10]	16.0 – 19.0
F-P1	5D	18	1	2	r	LiF	10-39	Si:Sb	49 – 50[10]	19.0 – 26.0
F-P2	6	19	1	3[12]	r	SrF_2	17-40	Ge:Be	51 – 52[11]	26.0 – 44.5

Notes:

1. SW = short-wavelength grating region

2. LW = long-wavelength grating region

3. t = transmission

4. r = reflection

5. 'Aperture area' refers to the dimensions of the SWS detectors projected through the entrance apertures projected onto the sky – see section 2.3

8. AOTs SWS06 and SWS07 (SW grating) use finite (but small) band overlaps

9. Band 2C ends at 13.16 μm for AOT SWS07.

10. Detector 49 is used for FP observations in band 5.

11. Detector 51 is used for FP observations in band 6.

12. These observations are made through the virtual aperture 4 (see section 3.6) but are flagged in the data as being through aperture 3.

13. The band 1E/2A limit changed from 4.05 to 4.08 μm after the end of PV.

14. These are Back-illuminated Blocked impurity Band (BIBIB) detectors.

15. Band numbers are stored in the AAR and are explained in section A.4.2, "SWAALINE and SWAASCNT".

Table 2.2: *Wavelength range definition of the SWS AOT bands*

	band		detector	wavelength[8]	resolution[6]	L^{7}_{AOT}
	name	number[15]	number	(μm)	($R = \lambda/\Delta\lambda$)	
SW[1]	1A	1	1 - 12	2.38 - 2.60	1870 - 2110	756
SW	1B	2	1 - 12	2.60 - 3.02	1470 - 1750	1043
SW	1D	3	1 - 12	3.02 - 3.52	1750 - 2150	1282
SW	1E[13]	4	1 - 12	3.52 - 4.08	1290 - 1540	867
SW	2A[13]	5	13 - 24	4.08 - 5.30	1540 - 2130	2115
SW	2B	6	13 - 24	5.30 - 7.00	930 - 1250	1377
SW	2C[9]	7	13 - 24	7.00 - 12.0	1250 - 2450	4276
LW[2]	3A	9	25 - 36	12.0 - 16.5	1250 - 1760	2047
LW	3C	10	25 - 36	16.5 - 19.5	1760 – 2380	1879
LW	3D	11	25 - 36	19.5 - 27.5	980 – 1270	2524
LW	3E	12	25 - 36	27.5 - 29.0	1300	500
LW	4	13	37 - 48	29.0 - 45.2	1020 – 1630	4324
F-P1	5A	15	49 - 50[10]	11.4 – 12.2	20600 – 24000	
F-P1	5B	16	49 - 50[10]	12.2 – 16.0	24000 – 32000	
F-P1	5C	17	49 - 50[10]	16.0 – 19.0	32000 – 34500	
F-P1	5D	18	49 - 50[10]	19.0 – 26.0	34500 – 35500	
F-P2	6	19	51 - 52[11]	26.0 – 44.5	29000 – 31000	

Notes:

1. SW = short-wavelength grating region

2. LW = long-wavelength grating region

6. The resolution given is that obtained when observing an extended source

7. L_{AOT} = total number of scan steps in AOT band

8. AOTs SWS06 and SWS07 (SW grating) use finite (but small) band overlaps

9. Band 2C ends at 13.16 μm for AOT SWS07.

10. Detector 49 is used for FP observations in band 5.

11. Detector 51 is used for FP observations in band 6.

13. The band 1E/2A limit changed from 4.05 to 4.08 μm after the end of PV.

15. Band numbers are stored in the AAR and are explained in section A.4.2, “SWAALINE and SWAASCNT”.

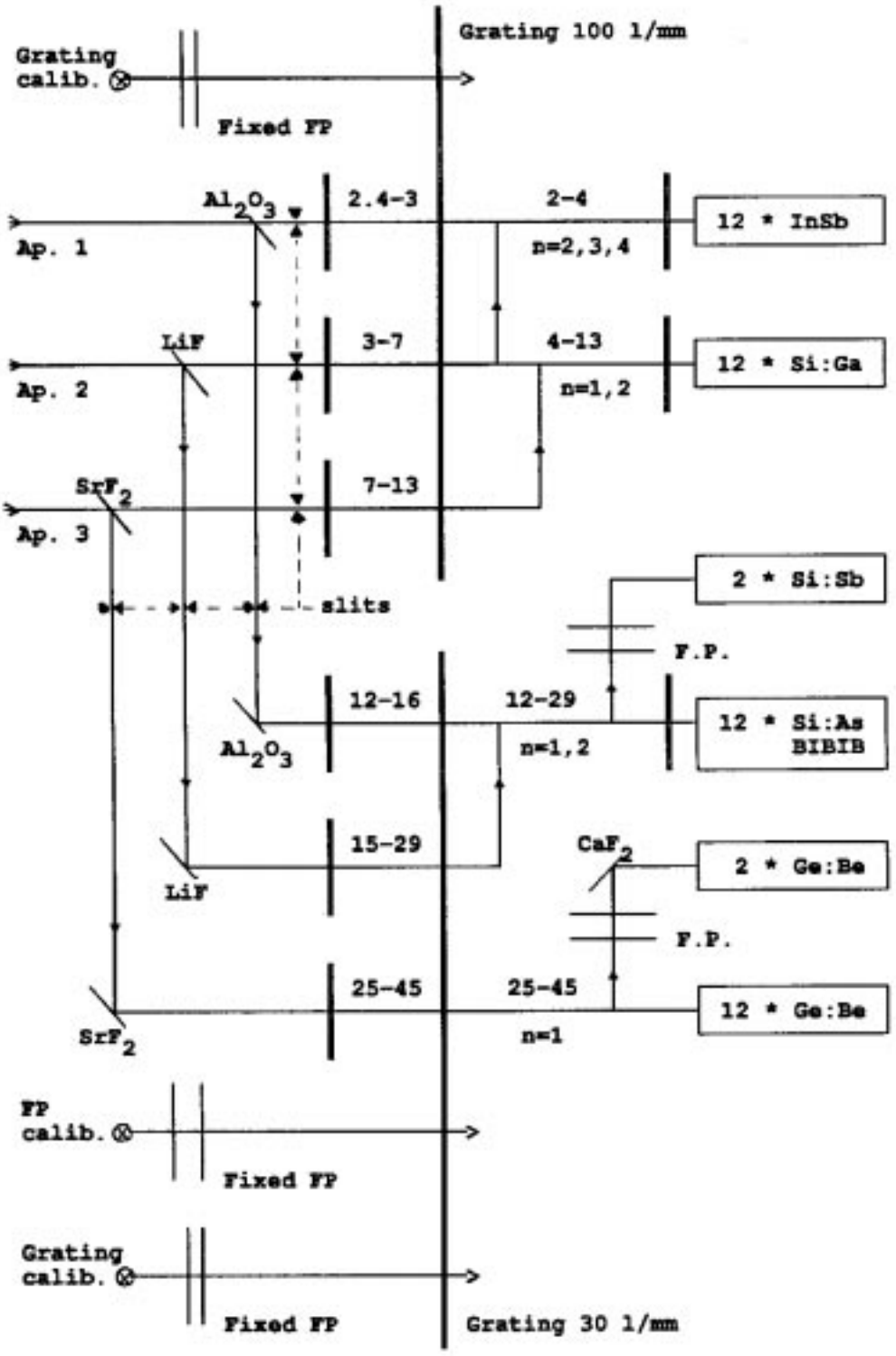

Figure 2.4: *Block diagram of the SWS. The diagram shows the optical functions of the spectrometer, excluding its internal calibration sources, but including the shutter, the collimation and the imaging optics. It excludes band 3E.*

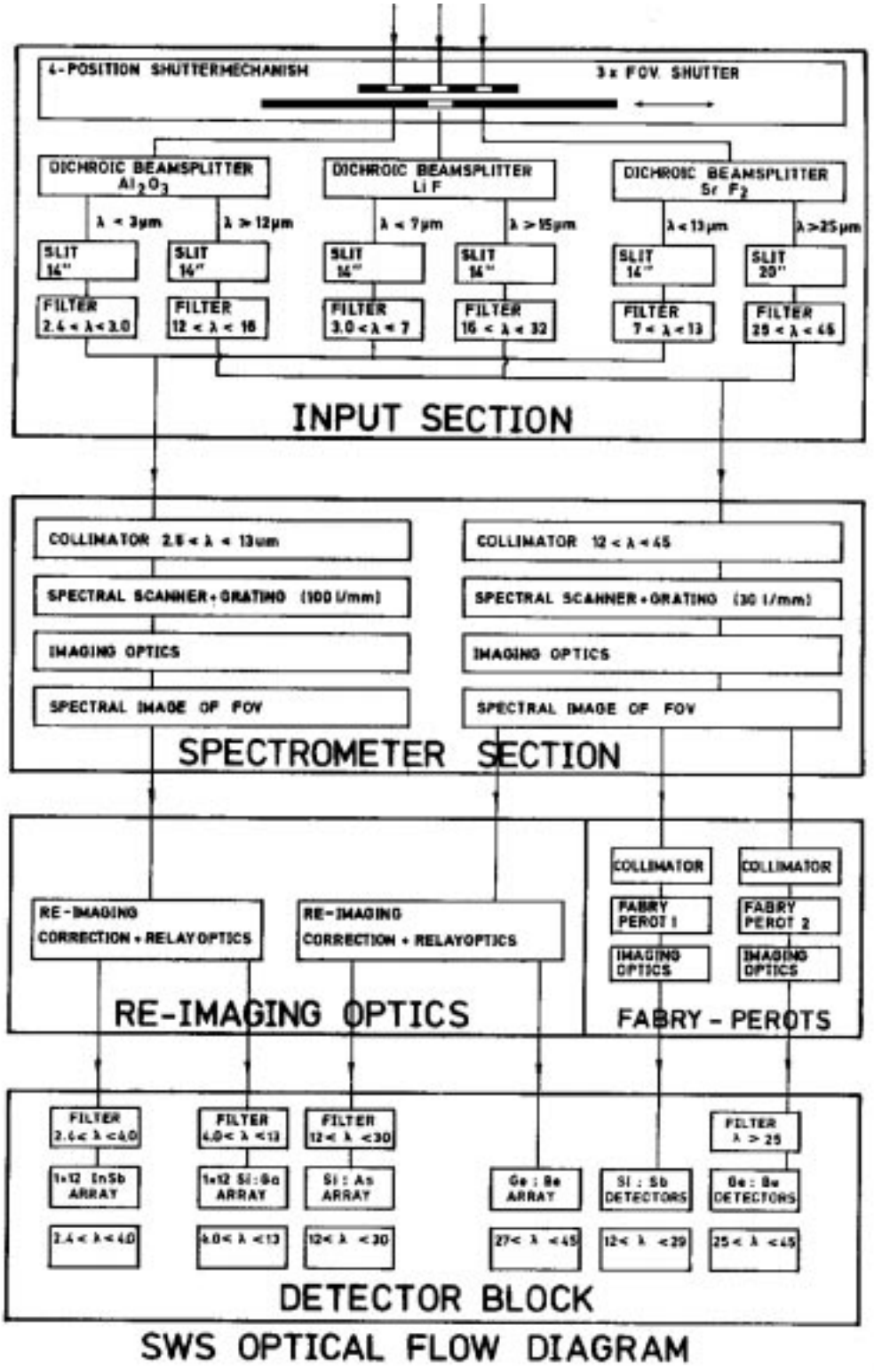

Figure 2.5: *Optical schematic of the SWS. The diagram indicates the location of the six separate entrance slits behind the dichroics after the three apertures. It shows all the spectral order-separation filters and the internal wavelength calibrators. The shutters, collimation and imaging optics and band 3E have been left out.*

2.3 Entrance Apertures

2.3.1 Optics and detector fields of view

SWS has three different physical apertures. A shutter system allows the selection of one aperture, while closing off the other two (the spacecraft pointing has to be adjusted so that the target is imaged onto the selected aperture). There is a virtual aperture 4, used by the LW FP, with a central position offset slightly from aperture 3. Aperture 4 was implemented because of a slight misalignment between the LW grating detectors and the FP detectors. Its introduction increased the amount of light falling onto the FP detectors and hence improved their efficiency. See section 3.6.

Each aperture is used for two wavelength ranges, one for the short-wavelength (SW) section of the spectrometer and one for the long-wavelength (LW) section. Since those two sections are otherwise independent, two wavelength ranges can be observed simultaneously.

Beamsplitters, consisting of Reststrahlen crystal filters (Al_2O_3, LiF and SrF_2), are located behind the apertures. The beams transmitted by the first crystal enter the SW section; the reflected beams enter the LW section, after a second reflection against identical material. As is seen in the schematic (figure 2.5), the actual entrance slits are located behind the beam-splitting crystal. In this way, each of the 6 possible input beams has its own slit. All slits have been given the same width, except for the SrF_2 reflected input, which has a larger width, adapted to the larger diffraction image at these wavelengths (see Table 2.2). The slits are in the focus of the telescope, in the plane where the sky is imaged.

In the direction perpendicular to the dispersion, the slits are oversized. There the fields-of-view are determined by the dimensions of the detectors. The cross-dispersion dimensions are different for almost all detector bands. Since the imaging of the slits onto the detectors (or *vice versa*) is imperfect due to aberrations and diffraction, the short sides of the fields of view (detector edges) are more fuzzy than the long sides (the slit jaws).

Small offsets of the fields of view perpendicular to the dispersion can be caused by alignment errors. The internal alignment specification adhered to amounts to 10% of the detector size alias spectrum width.

The monochromatic images of the grating detectors fill about 55% of the slit widths. This means that the spectral resolution for point sources is significantly higher than for extended sources, in a ratio that is affected, of course, by diffraction.

For the Fabry-Pérot section the situation is more complex. There the monochromatic detector images just fill the slit width. With the spectral channeling by the FPs, a subtle interplay arises between spectral and spatial properties. Effectively, the spatial resolution may increase due to the narrowness of the F resonance. Point sources have less leakage in unwanted FP orders than extended sources. Spatial extent does not influence the spectral resolution of the FPs.

2.3.2 Entrance apertures and spacecraft axis

The edges of the apertures are oriented along the spacecraft y- and z-axis.

y-axis (sometimes called m in calibration documents), parallel to the spacecraft y-axis, is the non-dispersion, or cross-dispersion, direction.

z-axis (sometimes called n), parallel to the spacecraft z-axis, is the dispersion direction.

Along the y-axis, the effective size of the aperture is determined by the projection of the detector array on the sky. This amounts to 20, 27 or 33″ for bands 1A to 4, and from 39 to 40″ for the FP bands 5A to 6.

Along the z-axis, the aperture size is determined by entrance slit width (14 or 20″) for bands 1A to 4. For the FP bands 5A to 6, the aperture is effectively as wide as a detector image on the sky, i.e. either 10 or 17″.

To derive the position angle of an aperture information on the spacecrafts position on the sky must be used. This can be found in the header keywords INSTRA, INSTDEC, INSTROLL found, for example, in the AAR. Specifically, INSTROLL is the angle, measured anticlockwise, between north and the spacecraft z-axis (ref. the ISO Handbook Volume 2 for a description of these keywords). See also section 6.10.

Information on how the spacecraft pointing can affect observations of extended objects can be read in Feuchtgruber 1998, [6]. In observations of NGC 6543 line fluxes varied by 10% over the course of several months. This was attributed to the spatial extent of NGC 6543, the SWS slit size projected on the sky and the change in roll angle between the observations. This is also discussed in section 6.10.

2.3.3 Beam Profile

Beam profiles for all bands were derived during flight by raster observations of point sources (stars). An example of a band 1 beam profile is shown in figure 2.6. More information on the beam profiles can be found in Salama 1998, [18], which should be consulted by observers needing further information on the beam profile of the various bands.

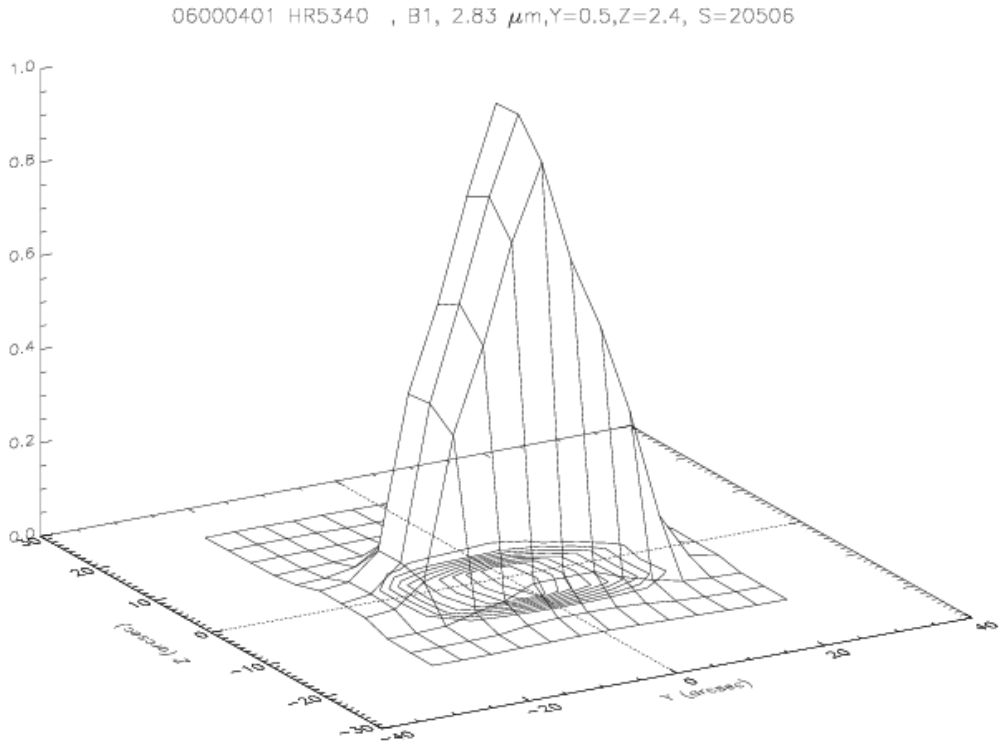

Figure 2.6: *Example beam profile for a band 1 observation at 2.83 μm of a standard star.*

2.3.4 Straylight

Straylight rejection depends on the design and fabrication of the telescope and of the instruments.

One measurement of straylight rejection was performed during observations of Titan. The spectral line due to C_2H_4 at 13.7 μm was measured on Saturn and at a position Y_{off} = -87″, Z_{off} = -163″, corresponding to a total displacement of 3′. By comparing the spectral line at these positions a rejection factor of 10^4 was calculated (ref. Salama 1998, [18]).

2.4 SWS Detectors and operation

The detector material is shown for all bands in table 2.1. The InSb, the Si:As (BIBIB) and the Si:Ga detectors are operated at a temperature of 4-5 K; the Si:Sb detectors for the FP are heated to 10 K (FP); and the Ge:Be detectors are cooled by a thermal conductor to the 2 K cryostat heat sink. The detectors are used with integrating pre-amplifiers with non-destructive read-out, employing heated JFET's.

As photons fall onto the detectors the current generated charges up a capacitor (one per detector). The voltage across this capacitor is read-out non-destructively 24 times a second and digitised into a bit value between 0 and 4095. After a set interval the capacitor is discharged with a destructive readout (basically short-circuited). The time interval between two detector resets is automatically determined from the user's input data (flux and SNR, or execution speed) and is either 1, 2 or 4 seconds. This destructive readout affects the readout electronics, which then take some time to return to normal.

Figures 6.7 and 6.9 give examples of data in which the individual datapoints from the non-destructive readouts and reset pulses can be seen.

To observe faint sources, integrations over several reset intervals are used. Raw data is saved in an Edited Raw Data (ERD) file, with an ERD file for one second consisting of an array of 52 ramps of 24 read-out's each. The Standard Processed Data (SPD) and Auto-Analysis Results (AAR) files contain for each detector a single flux estimate for each reset interval. As mentioned previously, normally only a subset of the array will contain clearly interpretable data.

Examples of ERD, SPD and AAR for each AOT are shown in sections 3.3 to 3.6 with the processing chain that generates SPD & AAR from ERD discussed in chapter 4.

Chapter 3

Instrument Observing Modes

3.1 Introduction

Astronomical observations with ISO were carried out via pre-planned observing modes. These are modes in which the basic operating parameters for the instrument are predefined (e.g. which sub-instrument to use at what wavelength resolution), leaving the user to select wavelengths to scan between, enter flux levels etc. Almost all observations entered by observers used one of four Astronomical Observation Templates, AOTs, while calibration observations used a variety of AOTs and Calibration Observation Templates, COTs. The AOTs are fully described in Beintema & Kunze, 1999, [2], to which users are pointed if this section does not provide them with sufficient information.

The EOHAAOTN keyword, present in the product files (see Appendix A), indicates what type of observation was performed. For normal AOTs it will take the value S01, S02, S06 or S07. For calibration COTs or post-He observations it will take the value S99, while S90 – S98 were reserved for engineering operations such as activation and deactivation.

As AOTs were primarily used for observations COTs will not be discussed in this version of the Handbook.

3.2 AOT overview

There are two main observing modes with the SWS.

1. **Grating-Only Observations (Medium spectral resolution)**. The spectral region of interest is directed to an array of 12 detectors. The spectral range instantaneously covered by the array is about 8 grating resolution elements, with gaps between the individual detectors (except for Band 3). For an observation, the grating is scanned in small steps to fully sample the desired wavelength range and provide a certain redundancy in case of detector failures or detector memory effects. Different scan schemes are used to obtain high fidelity line profiles, scans of wavelength ranges, and quick low-resolution full scans of the SWS wavelength range.

2. **Fabry-Pérot / Grating Combination Observations (High spectral resolution)**. The wavelength is selected by setting the Fabry-Pérot unit to a gap where one of the transmitting orders matches the correct wavelength. The F-P unit is then scanned in steps of about 1/4 F-P resolution element. The grating is used as an order sorter, with the maximum of the grating transmission tuned to the desired wavelength so that unwanted F-P orders are suppressed. Because the two detectors of a F-P detector pair look at slightly different grating resolution elements, this tuning can normally be done only for one detector. The other detector will not simultaneously deliver a useful signal as use of this redundant detector would require commanding of a slightly different grating position.

Figure 3.1 gives an overview of the wavelength ranges that could be simultaneously covered by the SW and LW or FP detector systems.

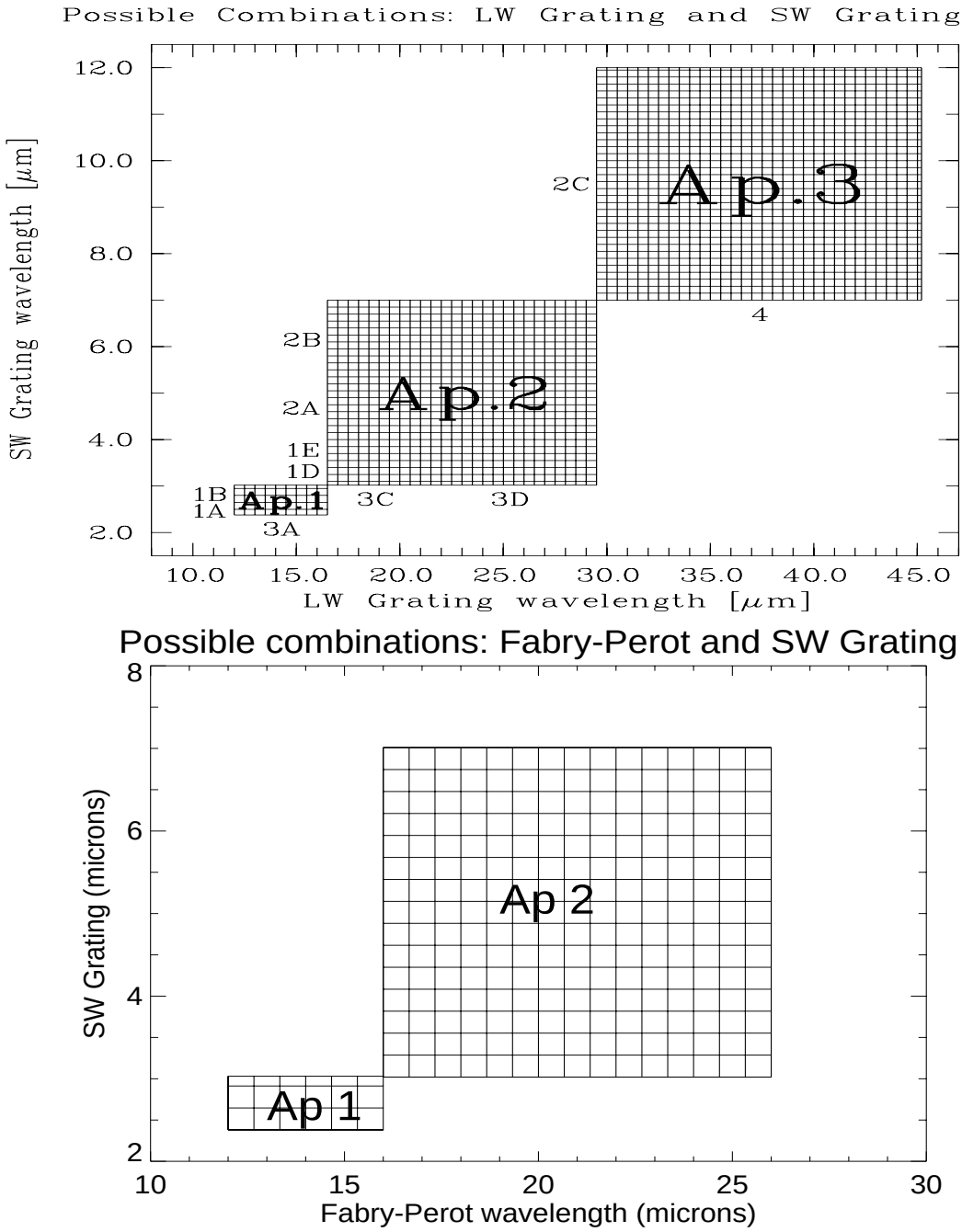

Figure 3.1: *Overview of possibilities for simultaneous use of LW grating and SW grating (top) and FP and SW grating (bottom). Only combinations within the hatched area were allowed, and simultaneous observations through aperture 3 when observing with the FP were not allowed. The corresponding AOT band designations and aperture numbers are indicated.*

During an AOT observation, the source spectrum is measured by rotating the scanning mirror of the grating or varying the gap of the Fabry-Pérot. Each AOT may perform one or more exposures with an internal calibrator for a photometric check and a number of dark current measurements with the aperture closed. Hence, the data produced by any single AOT is generally of several different types.

Four AOT's, listed below, were defined for SWS. Operating modes changed during the mission, and any such changes are noted in this document.

- **AOT 1**: a single up-down scan for each aperture. It has four possible scan speeds and is primarily intended to quickly scan the entire SWS wavelength range at degraded resolution.
- **AOT 2**: slow short up-down scans, designed to measure line profiles.
- **AOT 6**: medium length grating scans with various options. Programmed as long up-down scan, possibly with reference scan. Used to observe long wavelength regions
- **AOT 7**: LW section devoted to FP observations. The SW section does almost the same as in AOT 6. In this AOT priority is given to the FP.

Tables 3.1 and 3.2 summarise their properties. In all of these AOT's the measurements of photometric check, dark current and science data are interleaved in the ERD and SPD, while the AAR only contains science detector data for which an unique wavelength could be assigned to the light falling on that detector. Up-down scans and reference scans are discussed in sections 3.9.1 and 3.9.2.

Table 3.1: *Various SWS AOT options*

AOT #		scan direction	reference scan
1		up-down	no
2		up-down	no
6		up-down	possible
7	LW/FP	up	no
	SW/grating	up-down	possible

Example output from all AOTs are given in sections 3.3 to 3.6.

Table 3.2: *Possible combinations of reset interval t_r, step size L_s in scanner steps, and number of scans n_{scan} for each of the SWS AOT's*

AOT	Band								notes
SWS01	all	t_r	1	2	2	2			
		L_s	4	2	1	1			
		n_{scan}	2	2	2	2			1 up, 1 down
		n_{int}	24	24	24	24			a
		resolution	$R/8$	$R/8$	$R/4$	$R/2$			b
		duration	1172	1944	3846	6570			seconds
SWS02	1	t_r	1	2	4	4		..	
		L_s	1	1	1	1		..	
		n_{scan}	2	2	2	4		..	up, down, etc.
		n_{int}	110	110	110	110		..	b
		duration	1.3	2.7	5.4	10.8		..	minutes
SWS02	2	t_r	1	2	2			..	
	3	L_s	1	1	1			..	
		n_{scan}	2	2	4			..	up, down, etc.
		n_{int}	110	110	110			..	b
		duration	1.3	2.7	5.4			..	minutes
SWS02	4	t_r	1	2	2			..	
		L_s	2	2	2			..	
		n_{scan}	2	2	4			..	up, down, etc.
		n_{int}	90	90	90			..	
		duration	1.3	2.7	5.4			..	minutes
SWS07 F-P	5-6	t_r	1	2				..	
		L_s							1/4 $\Delta\lambda$
		n_{scan}	2	2				..	unidirectional
									3 times or more
SWS06	1	t_r	1	2	2	4	4	4 ..	
+		L_s	4	4	2	2	1	1 ..	
SWS07		n_{scan}	2	2	2	2	2	4 ..	up, down, etc
SW section		n_{int}	27	27	55	55	110	220 ..	
SWS06	2-3	t_r	1	2	2	2	2	..	
+		L_s	4	4	2	1	1	..	
SWS07		n_{scan}	2	2	2	2	4	..	up, down, etc
SW section		n_{int}	27	27	55	110	220	..	
SWS06	4	t_r	1	2	2	2	2	2 ..	
		L_s	6	6	3	2	1	1 ..	
		n_{scan}	2	2	2	2	2	4 ..	up, down, etc
		n_{int}	30	30	60	90	180	360 ..	

Notes:

a. n_{int}, the number of integrations per resolution element. This is the product of n_{scan}, the number of detectors in an array (12), and the ratio between resolution and stepsize.

b. Approximate effective spectral resolution cf AOT 2 – see section 3.3.5.

3.2.1 ICS

In all cases AOTs were actually commanded as sets of ICSs, Instantiated Command Sequences. These are more basic instrument commands to open the shutter, start the grating moving etc. The eight ICSs defined for SWS are listed in table 3.3. The use of these ICSs is described in the following sections, but for a more complete description of them and their use see Beintema & Kunze, 1996, [2].

Table 3.3: *ICSs*

ICS	Use
SS0001	Diffuse cal (not used)
SS0002	Grating cal (dark - on low - wait)
SS0004	SW grating scan for AOT 7
SS0005	SW/LW grating scan for AOTs 1, 2 & 6
SS0006	Dark and Wait for AOTs 1 & 2
SS0007	Reset ICS
SS0008	Reset ICS
SS0009	FP LW

3.3 AOT 1

3.3.1 Introduction

AOT 1 scans the entire SWS wavelength range at a reduced spectral resolution. The scans are effectively continuous, using small and frequent steps, and on a timescale much shorter than the selected reset interval of the detector pre-amplifiers. The integration in time translates into a smoothing of the spectrum, which prevents aliasing problems due to insufficient sampling.

Table 3.4 shows the reset intervals, dwell times, stepsize and number of up-down scans for AOT 1. The reset interval is the time between detector resets, the dwell time is the time during which the grating does not move (and hence each detector is seeing a fixed wavelength) and the stepsize, in LVDT, is the amount by which the grating moves every dwell time. An LVDT is an internal unit of measurement of the grating position and is given the name because it is measured by a Linear Voltage Differential Transducer (see section 5.7.1.1). A movement of 1 LVDT corresponds to approximately 1/8 of a resolution element. The pipeline resolution degradation is discussed in section 3.3.5.

Table 3.4: *AOT 1 parameters*

Speed	Duration sec	Reset interval sec	Dwell time sec	Stepsize LVDT	Number of up-down scans	Pipeline Resolution degradation
1	1172	1	1/8	4	1	7
2	1944	2	1/8	2	1	7
3	3846	2	1/8	1	1	4
4	6570	2	1/4	1	1	2

For an AOT 1 measurement, where the grating moves during a reset interval, the grating position in the SWSPGPOS field of the SPD is set to the start position of the grating during the reset interval. This contrasts with the wavelength in the SWSPWAVE field of the SPD which is the effective wavelength, i.e. calculated from the middle valid sample. For example, for a one second reset interval, the grating position is that of the first sample. As samples are thrown away due to the reset pulse (see section 6.6, operation described in section 4.2.2), the wavelength is that from sample (24 - Cal-G file 3) / 2 (assuming no data contains glitches, is all within limits etc).

3.3.2 AOT SWS01 sample time-line

The timeline an AOT 1 follows is as follows:

1. Acquisition - point aperture 1 to target
2. Dark current measurement (20 sec)
3. Single scan up, bands 1A, 1B, 3A (70 sec)
4. Single scan down, bands 1A, 1B, 3A (70 sec)
5. Dark current (20 sec)
6. Internal photometric calibration (40 sec)
7. Switch to aperture 2 (10 sec)
8. Dark current measurement (20 sec)
9. Single scan up, bands 1D, 1E, 2A, 2B, 3C, 3D (170 sec)
10. Single scan down, bands 1D, 1E, 2A, 2B, 3C, 3D (170 sec)
11. Dark current measurement (20 sec)
12. Switch to aperture 3 (10 sec)
13. Dark current (20 sec)

14. Single scan up, bands 2C, 3E, 4 (150 sec)
15. Single scan down, bands 2C, 3E, 4 (150 sec)
16. Dark current (20 sec)
17. Internal photometric calibration (40 sec)

After resetting the instrument, the AOT is composed of three SS0005 ICSs, one for each aperture. The sequence is aperture 1, 2 then 3. Each ICS 5 starts with a dark, then makes the measurement. An ICS 6 (dark) is used to make another dark current measurement after each ICS 5. A photometric check is made between the aperture 1 ICS 6 and aperture 2 ICS 5. From May 1996 an extra photometric check was added at the end of the AOT.

3.3.3 Example AOT 1 data

Figures 3.2 and 3.3 show ERD data for detectors 1, 13, 25 and 37 (bands 1, 2, 3 & 4) during an example speed 1 (1172 second) AOT 1 observation. The signal is shown in bit values against time (ITK) and only four samples are shown out of the 24 per second for clarity. The periods when apertures 1, 2 & 3 are used, times of dark current measurements and photometric checks are indicated.

Figures 3.4 and 3.5 show the wavelengths seen by the middle detector of each band during the AOT 1 observation along with the scanner position (LVDT). The nature of up-down scans can be seen in the plots, ref section 3.9.1.

Figure 3.6 shows SPD data, in $\mu V/sec$, for detector 1 of each band against time. Figure 3.7 shows the AAR for the same observation, now as flux (Jy) against wavelength. The spread of flux between different detectors in the same band can be seen in the band 4 data. Figure 3.8 shows what can be achieved after further processing of such data in either ISAP or IA.

3.3.4 Use of AOT 1

AOT 1 was designed to do a quick scan over the entire SWS spectral range to get the broad continuum shape of the object under study. In order to do this it was accepted that the spectral resolution it could achieve would be lower than nominal (see section 3.3.5). However, this combined with the OLP processing described in chapter 4, had the undesired effect of reducing the strength of spectral lines in a manner that depended on what wavelength the line was it, what part of a slope it was detected in etc, and was essentially random – see section 4.5 for a description of this.

Therefore AOT 1 observations are primarily useful for obtaining the shape of the continuum of the object under study. Users who wish to look for any spectral lines should proceed with care and re-reduce the data manually.

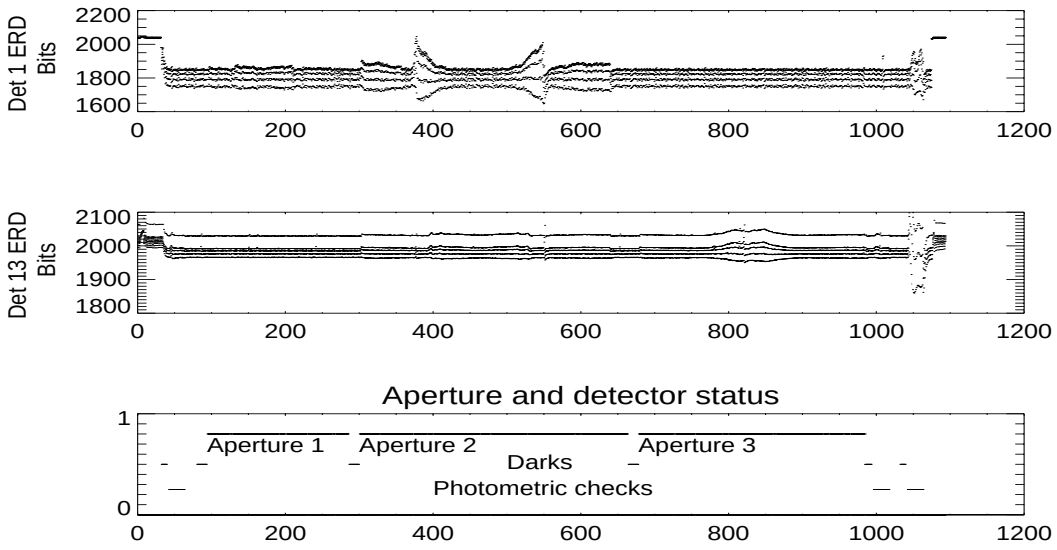

Figure 3.2: *Example ERD data from bands 1 & 2 during an AOT 1 observation. Periods when the detectors are looking through the three apertures, are taking dark current measurements and when the internal illuminators are switched on are indicated.*

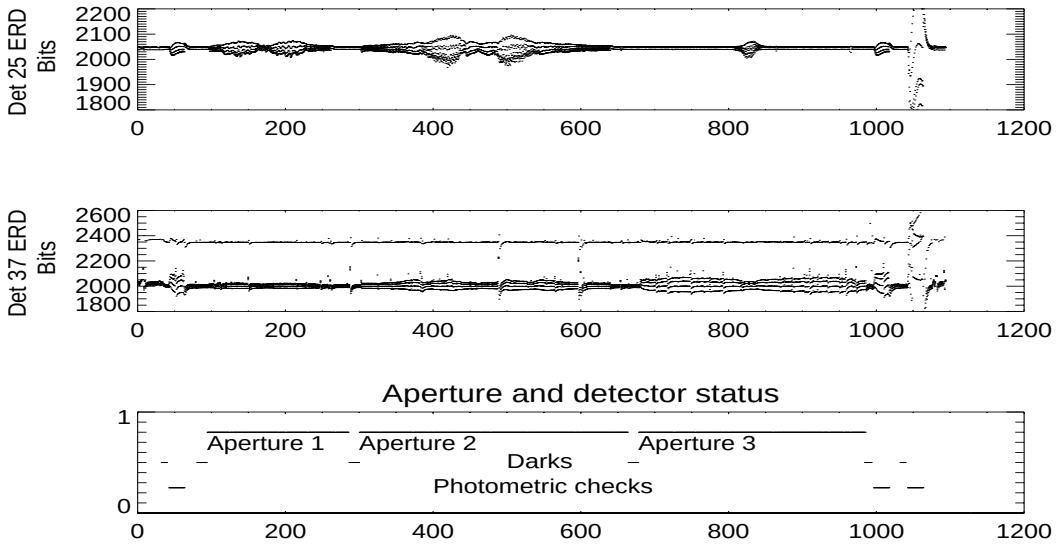

Figure 3.3: *Example ERD data from bands 3 & 4 during an AOT 1 observation. Periods when the detectors are looking through the three apertures, are taking dark current measurements and when the internal illuminators are switched on are indicated.*

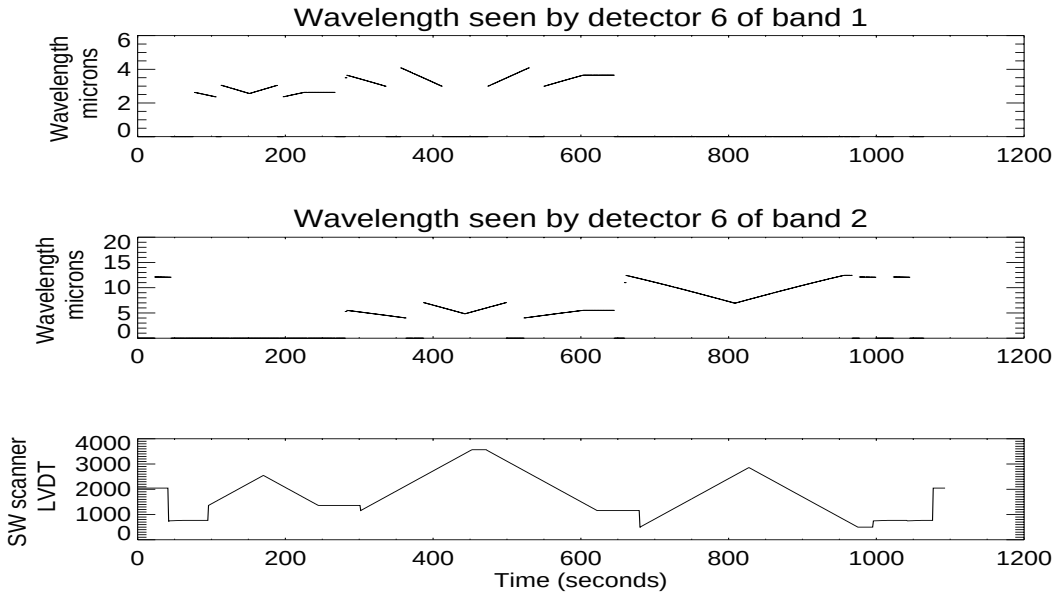

Figure 3.4: *The wavelengths seen by the middle detector in bands 1 & 2 during an AOT 1 are shown along with the grating position.*

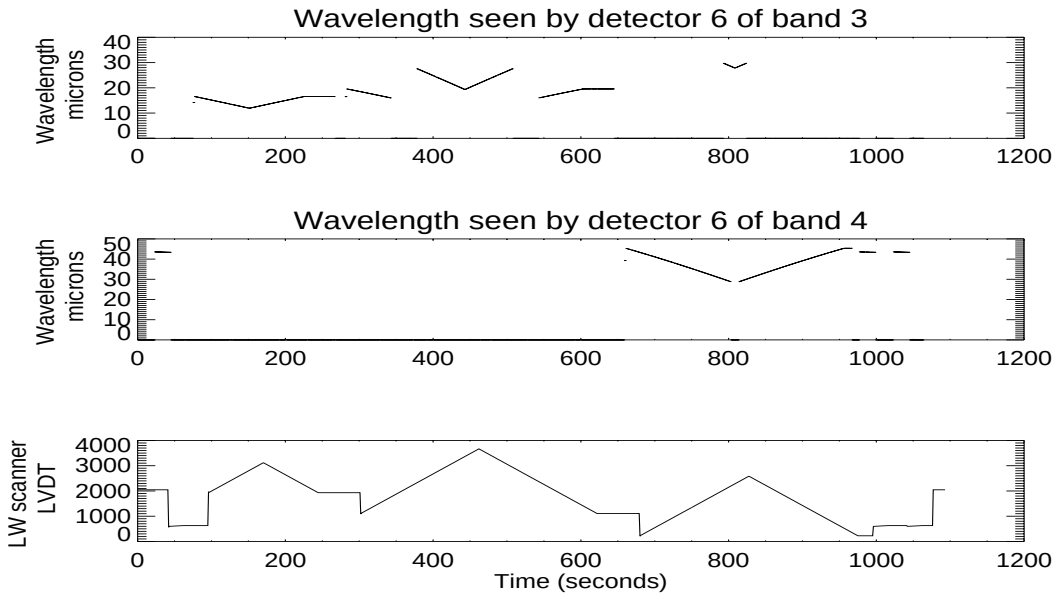

Figure 3.5: *The wavelengths seen by the middle detector in bands 3 & 4 during an AOT 1 are shown along with the grating position.*

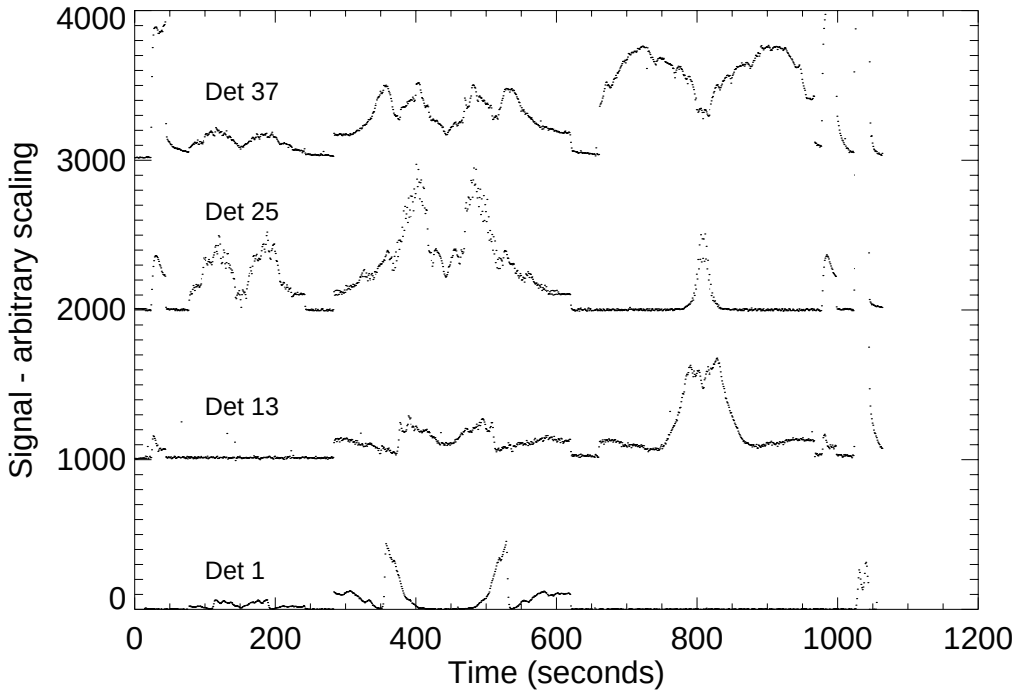

Figure 3.6: *SPD data from the first detector of each band during an AOT 1. The signals have been arbitrarily scaled.*

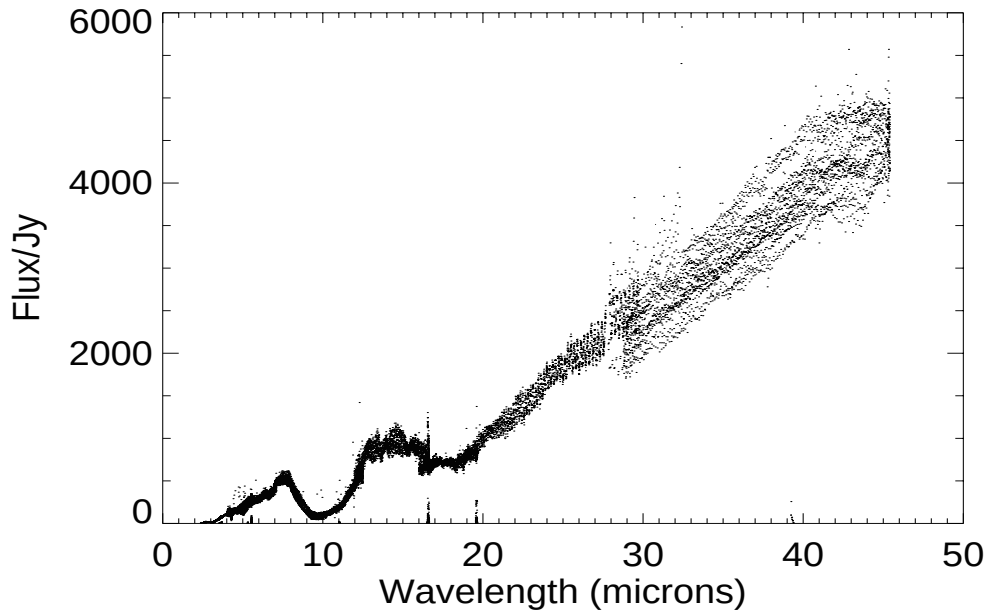

Figure 3.7: *AAR data from all detectors against wavelength during an AOT 1 observation.*

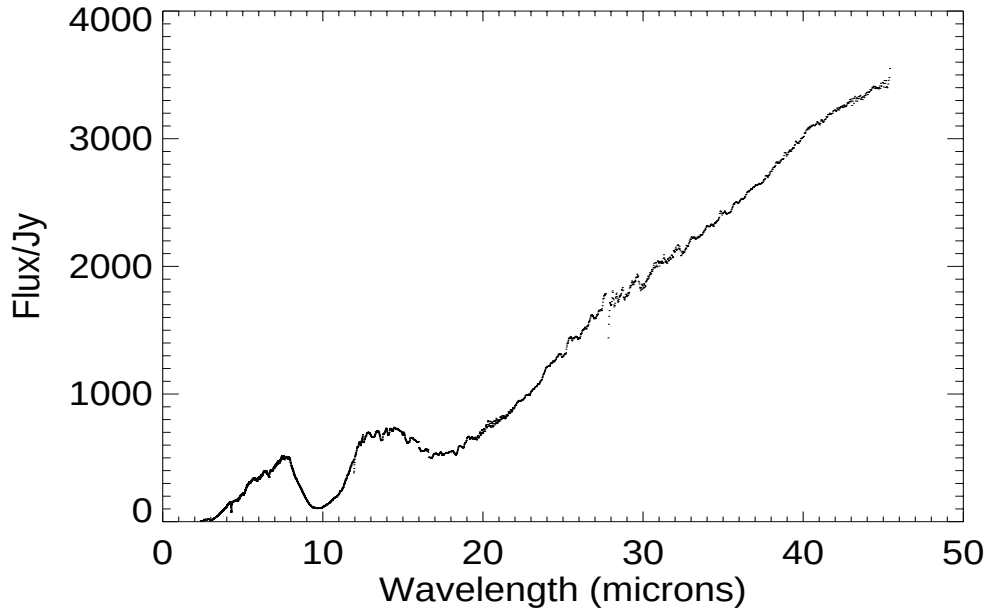

Figure 3.8: *An example of what can be achieved by the further processing of AOT 1 OLP data.*

3.3.5 AOT 1 Spectral Resolution

The pipeline resolution degradation, given in table 3.4 is the amount by which the resolution of the spectrometer is degraded after the data has been processed by the pipeline. The pipeline processes data for blocks of length of the reset interval (1 or 2 seconds), during which the grating will have moved several times. The pipeline effectively smears out the resolution. Both theory and observations can be used to characterise the amount of degradation.

3.3.5.1 Theory

The degradation is given by the equation:

$$Resolution\ degradation = \frac{reset\ time}{dwell\ time} \times \frac{stepsize}{steps\ per\ res.\ element}$$

For a source filling the slit, the number of steps per resolution element is about 4.5, except for bands 3E and 4, where it is about 7.0.

Hence the effective resolution of AOT 1 data processed by the pipeline is between a factor of 2 and 7 worse than that expected from an AOT 2 pipeline product.

3.3.5.2 Observations

Preliminary measurements of the resolution of AOT 01 scans at all four speeds were carried out on observation of the PNe NGC 6543 and a speed 4 observations was carried out on the PNe NGC 7027. The assumption was made that the lines from these objects would not be resolved by the SWS01 scans. NGC 7027 contained by far the most lines of the two objects.

Table 3.5: *NGC 7027 speed 4 AOT 1 resolution*

Wavelength μm	Resolution $\lambda/FWHM$	Wavelength μm	Resolution $\lambda/FWHM$
2.407	1388	7.902	1123
2.626	1216	9.666	1550
3.092	1458	10.51	1697
3.741	1143	12.81	1149
4.052	1236	13.10	1186
4.487	1366	13.52	1176
4.530	1347	14.32	1357
4.654	1422	15.55	1411
5.610	818	18.71	1663
6.986	1144	24.32	1004
7.319	1149	25.89	1049
7.460	1031	34.81	1619
7.653	1227	36.02	1459

The measurements on NGC 7027 give more reliable results than those on NGC 6543. No systematic difference between the speed 4 resolutions of the two objects could be found.

Table 3.6: *NGC 6543 all speeds AOT 1 resolution*

Wavelength μm	Speed 4 Resolution $\lambda/FWHM$	Speed 3 Resolution $\lambda/FWHM$	Speed 2 Resolution $\lambda/FWHM$	Speed 1 Resolution $\lambda/FWHM$
7.46	983	-	-	-
8.99	1332	771	388	393
10.51	1670	-	463	538
15.55	1344	834	-	526
18.71	1718	1060	529	585
33.48	1323	677	-	560
36.00	1426	886	-	603

3.3.5.3 AOT 1 spectral resolution conclusions

The speed 4 resolutions vary between approximately 800 and 1700, increasing with wavelength per order. This is approximately half of the AOT 2 resolution, matching expectations. The FWHM remains nearly constant.

We can compare the resolutions of the different speeds using the NGC 6543 observations. The results, which match expectations, are:

R(3) / R(4) = 0.6

R(2) / R(4) = 0.3

R(1) / R(4) $\approx$ 0.3 - 0.4

3.4 AOT 2

AOT 2 is used to observe up to 64 individual lines in an objects spectrum using the SWS grating mode. The wavelength interval covered when observing a line is approximately 10 resolution elements, i.e., 3,000-1,500 km/s.

Table 3.7 shows the reset intervals, dwell times, stepsize and number of up-down scans for AOT 2. The dwell time may be higher for some merged scans.

Table 3.7: *AOT 2 parameters*

Detector Band	reset interval sec	dwell time sec	stepsize LVDT	Number of up-down scans
1	1, 2, 4	= reset	1	$n \geq 1$
2,3	1, 2	= reset	1	$n \geq 1$
4	1, 2	= reset	2	$n \geq 1$

The start wavelengths for AOT 2 bands are given in table 3.8.

Table 3.8: *AOT 2 wavelength ranges*

Detector Array	Detector material	Aperture	Grating order	Band start μm
1	InSb	1	4	2.38
1	InSb	1	3	2.60
1	InSb	2	3	3.02
1	InSb	2	2	3.52
2	Si:Ga	2	2	4.08[1]
2	Si:Ga	2	1	5.30
2	Si:Ga	3	1	7.00
3	Si:As	1	2	12.0
3	Si:As	2	2	16.5
3	Si:As	2	1	19.5
3	Si:As	3	1	27.5
4	Ge:Be	3	1	29.0

Note:

1. The band 2A start wavelength was changed from 4.05 to 4.08 μm in May 1996, and hence the band 1A end wavelength was moved accordingly.

3.4.1 Example AOT 2 timeline

AOT 2 is executed in the following way:

- The telescope is pointed to the target position.
- A range of 10 resolution elements around each wavelength specified in the AOT is observed. Each range is scanned back and forth to provide redundancy. The minimal scan time is 100 seconds.

- Dark current measurements are only performed before and after the spectral scan.
- A photometric check is performed, using the internal calibrators.

As an example, to observe lines at 10, 12, 35 & 40 μm AOT 2 would carry out the following sequence:

1. Acquisition - point aperture 1 to target
2. Dark current measurement (20 sec)
3. Scan line at 12 μm, up (50 sec)
4. Scan line at 12 μm, down (50 sec)
5. Dark current measurement (20 sec)
6. Switch to aperture 3 (10 sec)
7. Dark current measurement (20 sec)
8. Simultaneously scan lines at 10 and 40 μm, up (100 sec)
9. Simultaneously scan lines at 10 and 40 μm, down (100 sec)
10. Dark current measurement (20 sec)
11. Simultaneously scan lines at 10 and 35 μm, up (100 sec)
12. Simultaneously scan lines at 10 and 35 μm, down (100 sec)
13. Dark current measurement (20 sec)
14. Internal photometric calibration (40 sec)

This timeline is carried out using chains of ICS 5. Each ICS 5 starts with a dark, then observes a line. ICS 6 is used to make a dark measurement when: the gain changes; the reset interval changes; or the aperture changes. Every approximately 3600 s there is a photometric check. If the entire observation takes less than 3600 s a photometric check is done at the end.

The length of the up and down scans in an AOT 2 may occasionally differ by small amounts. This is due to the runflag going down too early, signifying an early end to the observation.

3.4.2 Example AOT 2 data

Figure 3.9 shows the ERD and SPD from detector 25 as SWS scans across one particular line with an AOT 2. Figure 3.10 shows LW scanner positions, aperture information and wavelength seen by detector 25 during the same period, while 3.11 shows the SPD and AAR data from detector 25 during the same period.

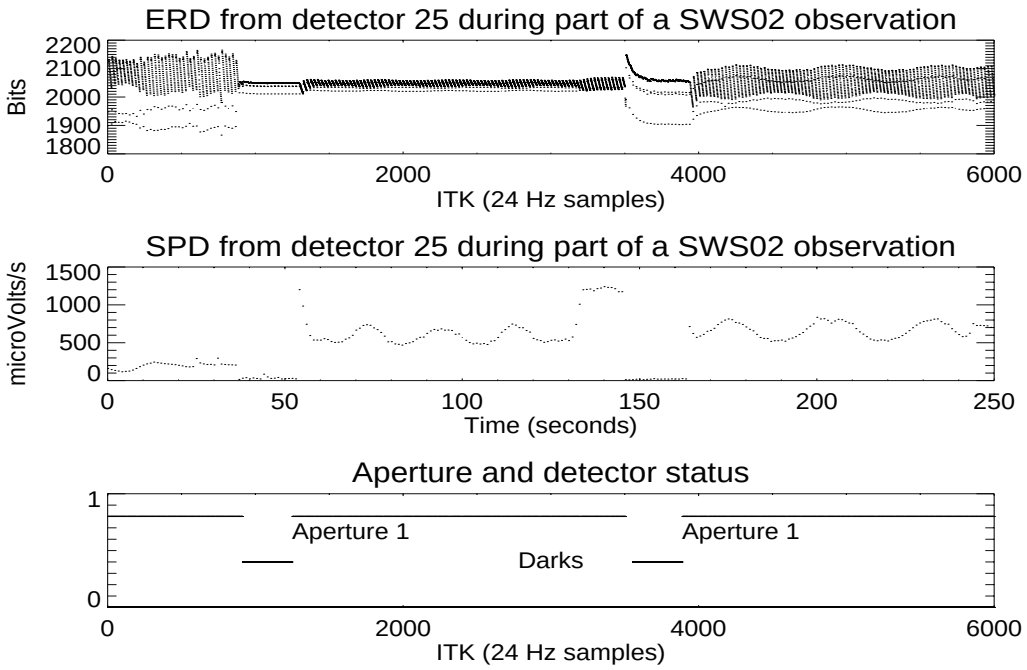

Figure 3.9: *ERD and SPD data for part of an AOT 2 observation. A single line is being scanned with a dark measurement either side of it.*

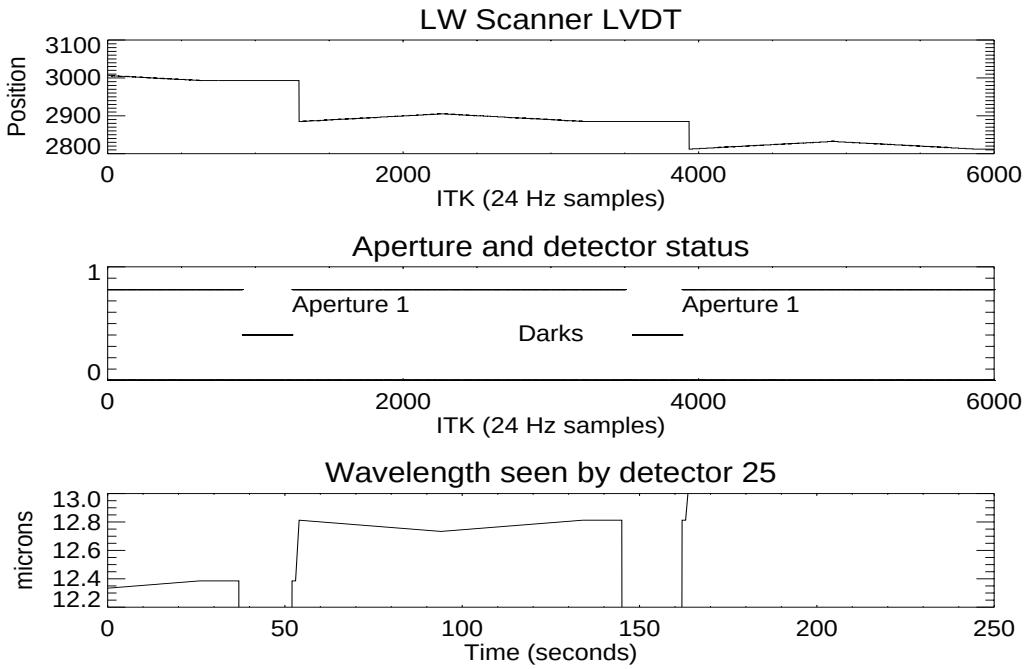

Figure 3.10: *Scanner position, apertures and wavelength seen by detector 25 during the above AOT 2 observation.*

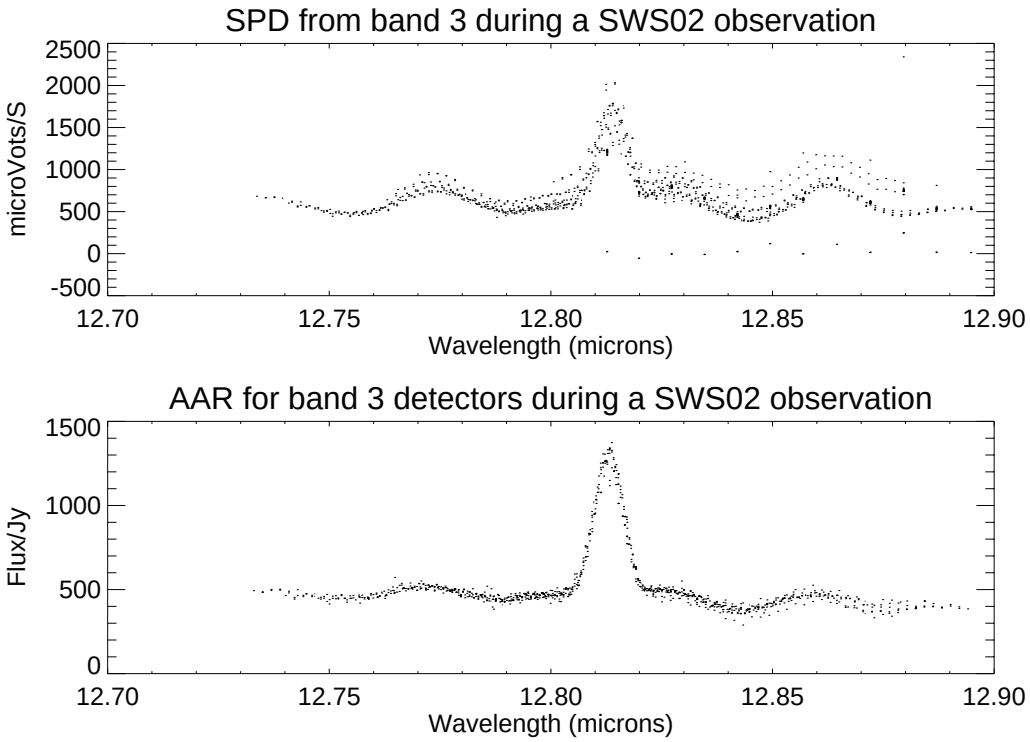

Figure 3.11: *SPD and AAR data from band 3 for AOT 2.*

3.5 AOT 6

AOT 6 was used to make observations over wavelength ranges, as opposed to observing individual lines. Up to 64 wavelength ranges could be chosen anywhere in the SWS grating range, i.e., between 2.38 and 45.2 μm, under the restriction that each range falls within one of the AOT bands (see Table 2.2).

Table 3.9 shows the reset interval, dwell times, stepsize and number of up-down scans for AOT 6. The dwell time stops at 4 secs, and for higher sensitivity the scans repeat. This was not always the case. Earlier versions of the logic (prior to May 1996) had the dwell time increasing. After May 1996 the scanning strategy used to reach the desired S/N ratios was:

- Use 1 sec reset with the max step size.
- If the S/N ratio is insufficient use a reset interval 2 sec.
- While the S/N ratio is insufficient and the stepsize is greater than 2 halve the stepsize.
- If the S/N ratio is still insufficient and it is band 1 then use a reset interval 4 sec.
- If the S/N ratio is still insufficient then increase the number of scans.

Table 3.9: *AOT 6 parameters*

Detector band	reset interval sec	dwell time sec	stepsize LVDT	Number of up-down scans
1	1, 2, 4	$\geq$ reset	1, 2, 4	n
2, 3	1, 2	$\geq$ reset	1, 2, 4	n
4	1, 2	$\geq$ reset	1, 2, 3, 6	n

The wavelength coverage of AOT 6 is given in table 3.10. Note that there is a slight overlap between bands. Band 3E was introduced after PV because band 3D suffered from a light leak at the long wavelength end, rendering observations around 28–29 μm problematical.

3.5.1 Example AOT 6 timeline

AOT SWS06 was executed by pointing the telescope to the target position, and then for each wavelength range (or pair of merged ranges):

- A dark-current measurement is done.
- A measurement on the reference wavelength is performed, if the spectral scan is long enough to need it.
- The wavelength range specified in the AOT is observed. Each range is scanned back and forth to provide redundancy.
- The reference measurement (if any) is repeated.
- A dark current measurements is done.
- Very long observations are interrupted by wavelength switching to the reference wavelength, as an additional photometric check.

Table 3.10: *AOT 6 wavelength ranges*

Detector Array	Detector material	Aperture	Grating order	Band	Band start μm	Band End μm
1	InSb	1	4	1A	2.38	2.61
1	InSb	1	3	1B	2.60	3.03
1	InSb	2	3	1D	3.02	3.53
1	InSb	2	2	1E	3.52	4.08[1]
2	Si:Ga	2	2	2A	4.05	5.31
2	Si:Ga	2	1	2B	5.30	7.01
2	Si:Ga	3	1	2C	7.00	12.1
3	Si:As	1	2	3A	12.0	16.6
3	Si:As	2	2	3C	16.5	19.6
3	Si:As	2	1	3D	19.5	27.6
3	Si:As	3	1	3E	27.5	29.0
4	Ge:Be	3	1	4	28.9	45.2

Note:

1. The band 1E end wavelength was changed to 4.08 μm from 4.05 μm from May 1996 onwards.

- If a single up and down scan does not provide enough sensitivity, the measurement sequence is repeated as often as necessary
- Photometric checks using the internal calibrator are done at regular intervals, at least once per AOT.

As an example, an AOT 6 observation around 10, 12, 33 & 40 μm would have the following timeline:

1. Acquisition - point aperture 1 to target
2. Dark current measurement (16 sec)
3. Scan up around 12 μm (24 sec, fast)
4. Scan down around 12 μm (24 sec, fast)
5. Dark current measurement (16 sec)
6. Switch to aperture 3 (10 sec)
7. Dark current measurement (16 sec)
8. Reference scans near 10 and 33 μm (16 sec)
9. Scans around 10 and 33 μm, up (360 sec)
10. Reference scans near 10 and 33 μm (16 sec)
12. Scans around 10 and 33 μm, up, continued (360 sec)
10. Reference scans near 10 and 33 μm (16 sec)
14. Scans around 10 and 33 μm, down (360 sec)
10. Reference scans near 10 and 33 μm (16 sec)
16. Scans around 10 and 33 μm, down, continued (360 sec)
10. Reference scans near 10 and 33 μm (16 sec)
18. Dark current measurement (16 sec)
19. Dark current measurement (16 sec)
20. Reference scans near 10 and 40 μm (16 sec)
21. Scans around 10 and 40 μm, up (96 sec)
22. Scans around 10 and 40 μm, down (96 sec)
20. Reference scans near 10 and 40 μm (16 sec)
24. Dark current measurement (16 sec)

25. Internal photometric calibration (40 sec)

Only ICS 5's are used (after the instrument has been set up). The ICS starts with a dark current measurement (at the reference wavelength), then makes a reference scan. Then the grating(s) is commanded up to observe a wavelength region. Another reference scan occurs before the down scan of the up-down pair. A final reference scan and dark current measurement are then made. This operation is repeated until all wavelength regions have been scanned.

For short scans the reference scans are dropped, as they take too much time. Every approximately 3600s there was a photometric check. If the entire observation takes less than 3600 s a photometric check was done at the end.

3.5.2 Example AOT 6 data

Figures 3.12 and 3.13 show ERD data from all bands taken during an AOT 6. Data for detectors 1, 13, 25 and 37 (bands 1, 2, 3 & 4) is shown in bit values against time (ITK). Only five samples are shown out of the 24 per second for clarity. The periods when apertures 1, 2 & 3 are used, times of dark current measurements and photometric checks are indicated.

Figures 3.14 and 3.15 show the wavelength as seen by the middle detector of each band, along with the SW and LW scanner position (LVDT) for the same period. Figures 3.16 and 3.17 show the SPD, in $\mu V/sec$ against time, and AAR, flux (in Jy) against wavelength, for the same observation. Figure 3.18 shows what can be achieved after further processing of such data in either ISAP or IA.

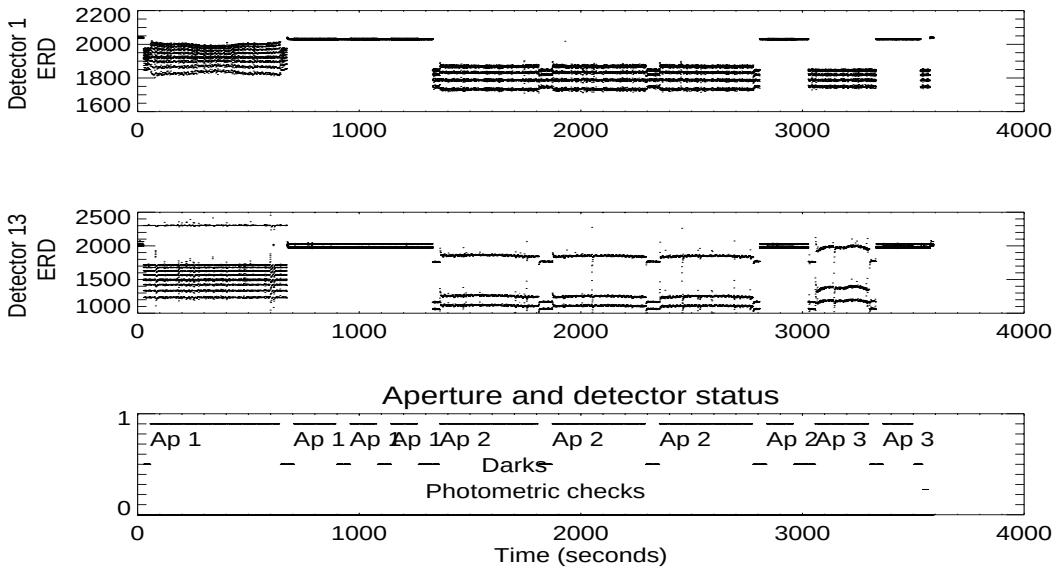

Figure 3.12: *Example ERD data from bands 1 & 2 (detectors 1 and 13) during an AOT 6 observation. Periods when the detectors are looking through the three apertures, are taking dark current measurements and when the internal illuminators are switched on are indicated.*

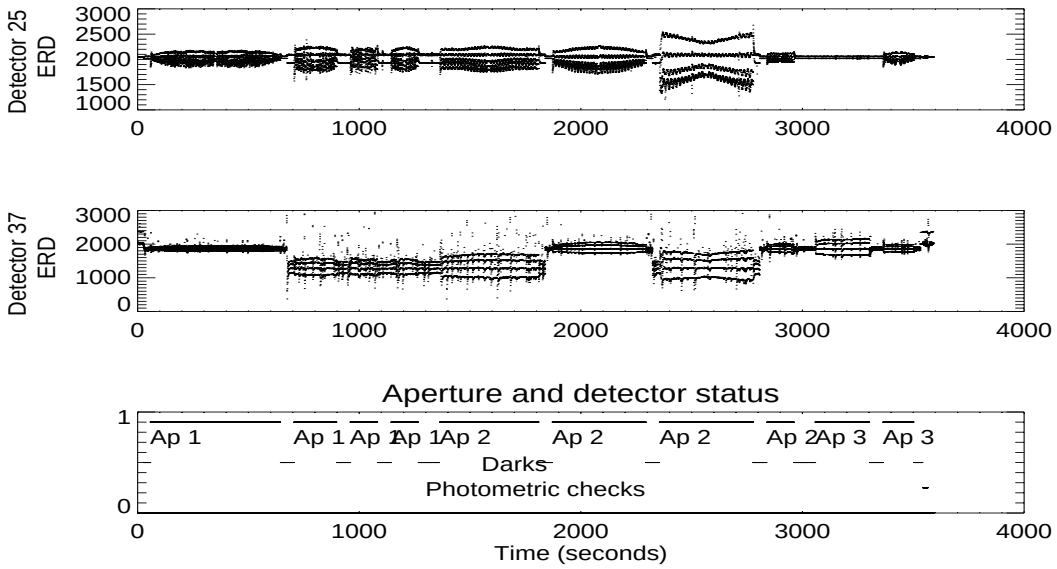

Figure 3.13: *Example ERD data from bands 3 & 4 (detectors 25 and 37) during an AOT 6 observation. Periods when the detectors are looking through the three apertures, are taking dark current measurements and when the internal illuminators are switched on are indicated.*

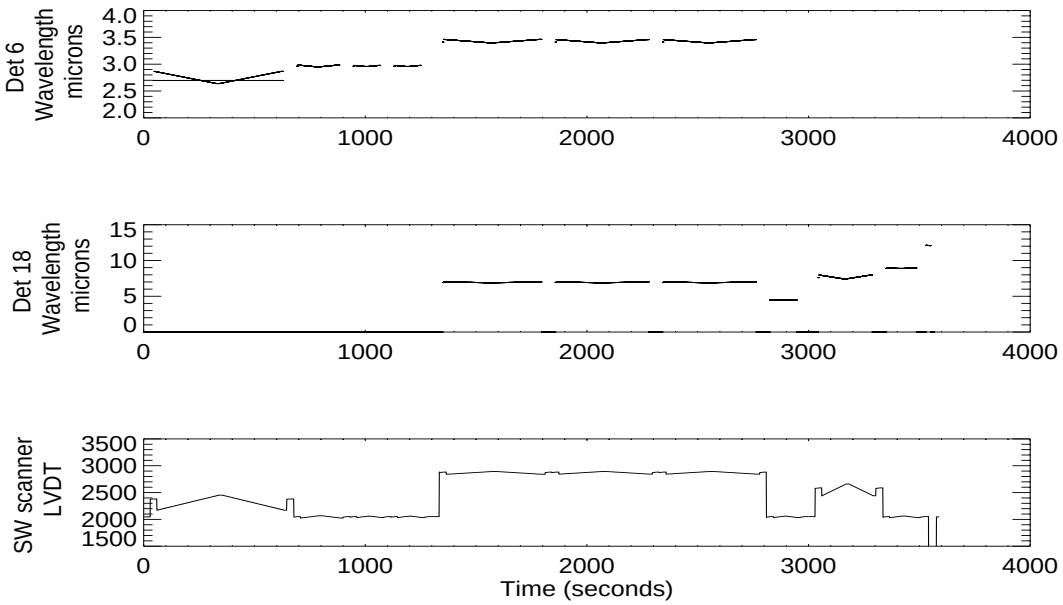

Figure 3.14: *Scanner position and wavelength seen by detector 6 of bands 1 & 2 during an AOT 6 observation.*

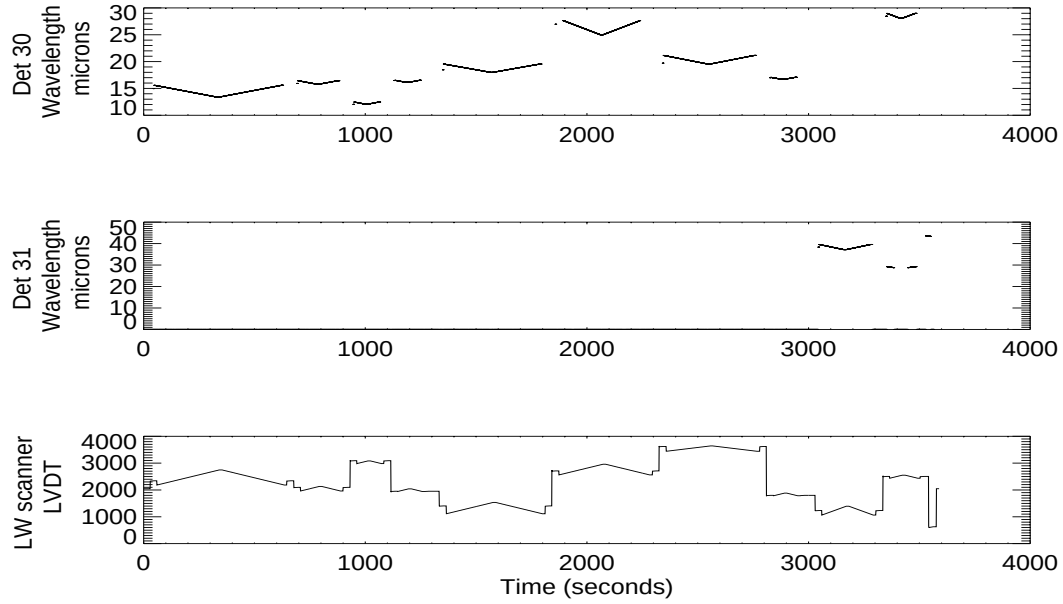

Figure 3.15: *Scanner position and wavelength seen by detector 6 for bands 3 & 4 during an AOT 6 observation.*

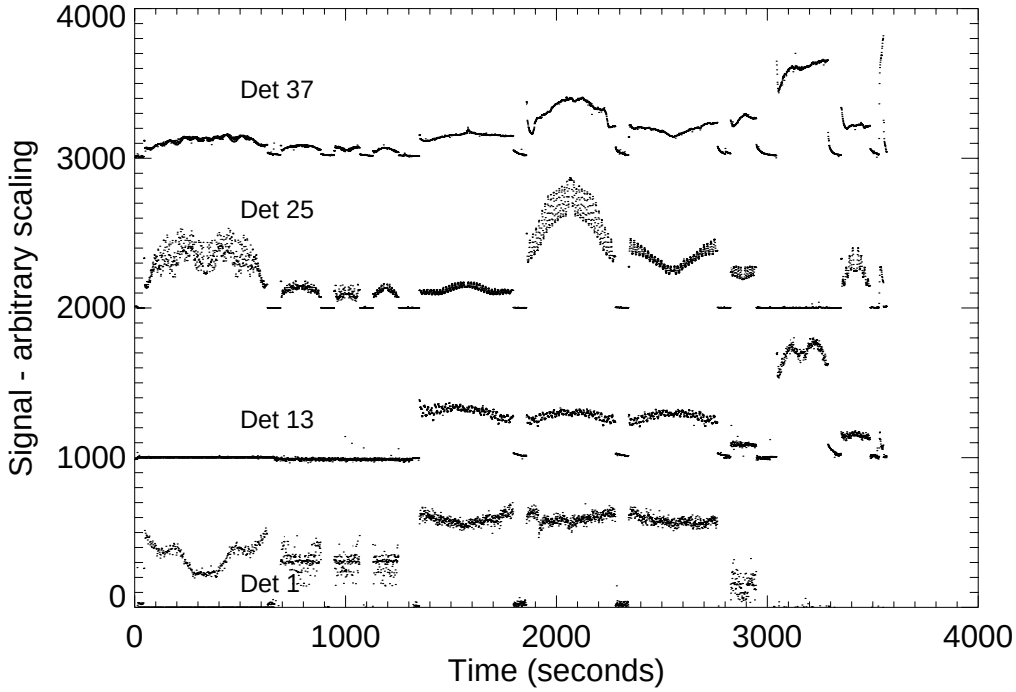

Figure 3.16: *SPD data, in $\mu V/sec$, for the first detector of each band during an AOT 6 observation.*

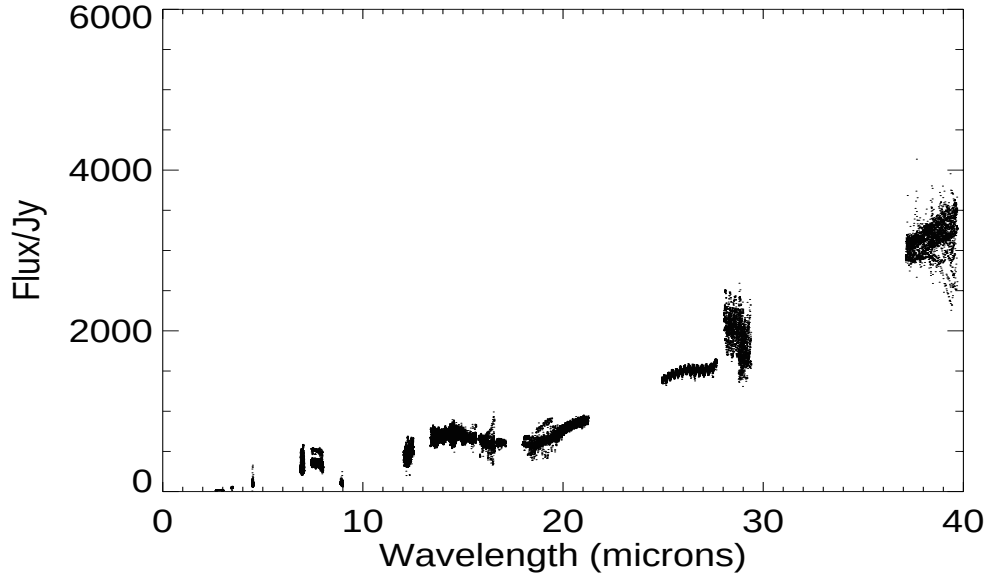

Figure 3.17: *AAR data from all detectors for an AOT 6 observation.*

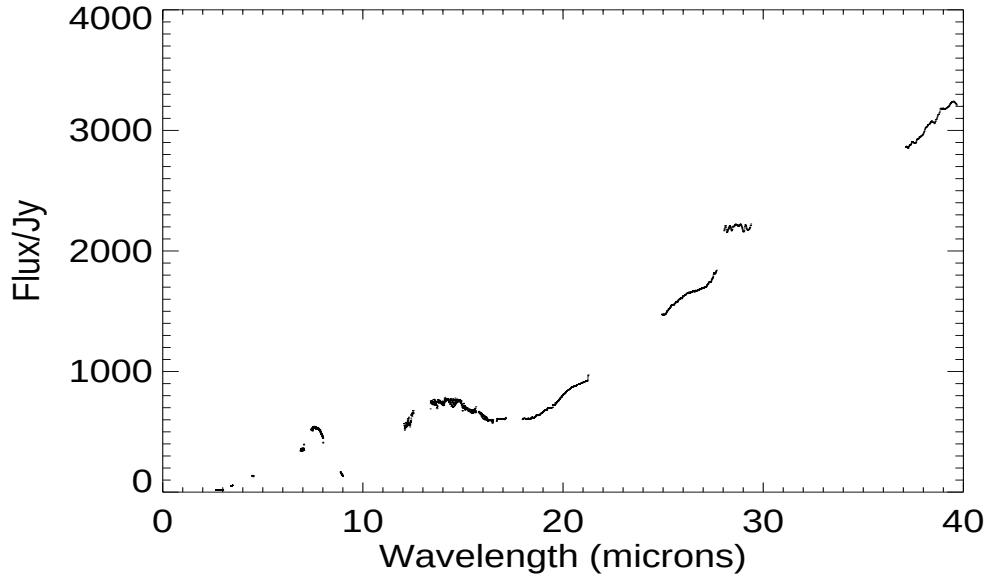

Figure 3.18: *An example of what can be achieved by processing AOT 6 OLP data further in either OSIA or ISAP.*

3.6 AOT 7

The purpose of AOT 7 was to make Fabry-Pérot observations. If requested, Short Wave grating observations were made in parallel.

For the FP the stepsize is always two FP units, about 1/4 of an FP wavelength resolution. Reset intervals are 1 or 2 seconds, with the dwell time equal to the reset interval. The number of scans is greater than, or equal to, three, and only "up" grating scans are commanded.

Any requested SW grating observations were carried out in an identical manner to those of an SWS06 measurement. Users should read section 3.5 for a description of that.

Due to a slight internal misalignment of the Long Wave FP there were problems merging FP observations with grating observations when observing through aperture 3. The 'effective' aperture of the FP was displaced from the center of the grating aperture by approximately $10''$, causing an approximately 40% drop in throughput of the FP when pointing was determined by the grating. The solution decided on was to define a fourth 'effective' aperture, centered on the FP aperture, and carry out all observations through this. This meant the SW grating lost approximately 40% of its throughput. Therefore LW FP observations ($26 - 44\,\mu$m) and SW grating observations ($7.0 - 13.16\,\mu$m) through aperture 3 could not be merged. Any requested aperture 3 grating observations were performed after the FP observations. This change was considered acceptable as the main purpose of AOT 7 was FP observations. Merging was still performed on observations using apertures 1 or 2.

However, some early AOT 7 observations were carried out before this change was implemented, and the archive contains observations containing FP data merged with SW grating observations in the range 7 to $13.16\,\mu$m.

Note that band 2C ends at $13.16\,\mu$m for AOT SWS07 - see table 2.2.

3.6.1 Example AOT 7 timeline

The AOT SWS07 was executed the following way:

- The telescope is pointed to the target position.
- The F-P lines and grating wavelength ranges specified in the AOT are observed. Each FP line is scanned at least three times and each SW wavelength range is scanned at least twice to provide redundancy.
- Dark current checks are performed at regular intervals, at least before and after a set of FP scans on the same line and at least once before the reference wavelength of each SW range.
- F-P scans may have to be broken into segments because the end of the mechanical F-P range is reached and the scan has to be continued in a different F-P order.
- With all F-P scans the LW grating is scanned slowly in coordination with the F-P scan to keep the pre-dispersion tuned to the actual wavelength.
- The phasing of the measurements is essentially independent for the two spectrometer sections, at the cost of increased overheads but giving flexibility in combination.
- If the line list contains wavelengths corresponding to different SWS apertures, the aperture is switched accordingly and the satellite re-pointed to bring the source to the center of the new aperture.
- At regular intervals, between observations, photometric checks are performed, at least once per AOT.

AOT 7 is achieved by using combinations of ICS's 9 and 4. After the instrument has been set up ICS 9 is used to make a dark-current measurement. Another ICS 9 is then used to start the FP. While the FP is operating ICS 4 is used to make SW grating scans, if any are requested. More than one of these may be uplinked while the FP scan is continuing. To observe more lines with the FP more ICS 9's are uplinked. Again ICS 4's could be uplinked to observe with the SW grating section. After all observations have concluded a final ICS 9 is used to make a dark measurement.

3.6.2 Example AOT 7 data

Figure 3.19 shows ERD, SPD and aperture data for part of an AOT 7. The ERD is shown as signal in bit values against time (ITK), and the SPD as signal (in $\mu V/sec$) against time (seconds). While the line is hard to see in the ERD, it can easily be seen in the SPD.

Figure 3.20 shows the LW grating position, the FP position and the resulting wavelength of light falling on detector during the part of an AOT 7.

Figure 3.21 shows SPD signal (in $\mu V/sec$) and AAR flux (in Jy), both against wavelength, for the same period of the example AOT 7. Note the wavelength shift in the location of the peak between the SPD and AAR. This is because the SPD wavelength scale is 'ISOcentric', whereas the AAR is corrected to be heliocentric.

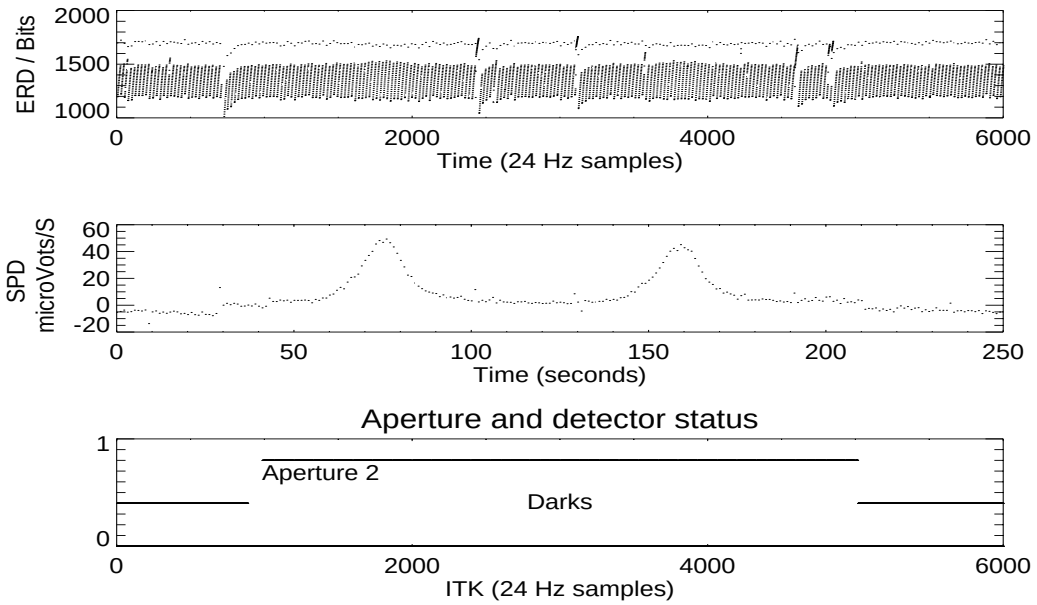

Figure 3.19: *ERD, SPD and aperture data for part of an AOT 7 observation. The FP is scanning across the line twice, going down in wavelength both times as can be seen from figure 3.20.*

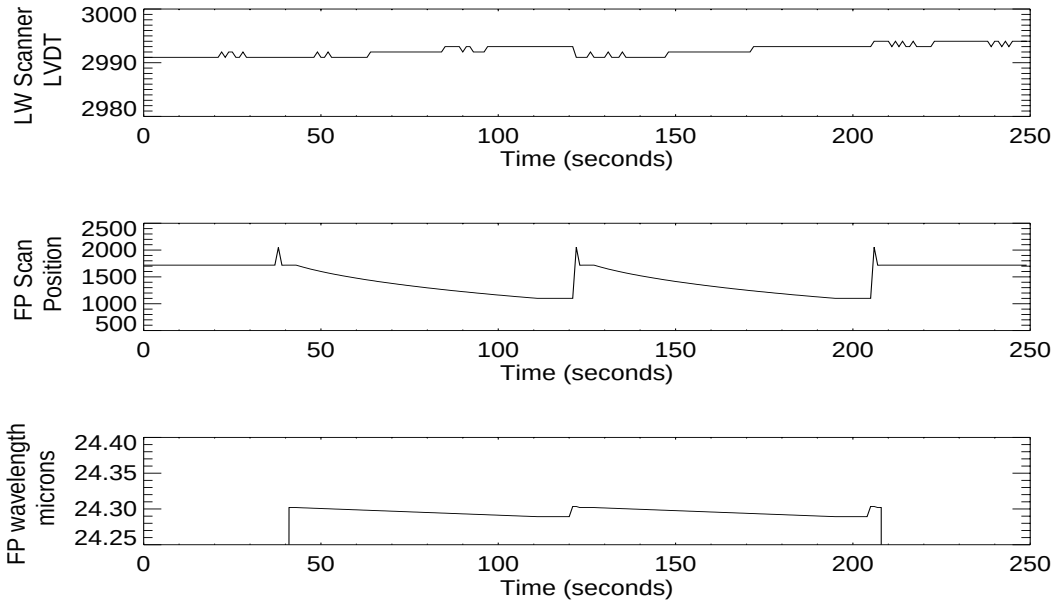

Figure 3.20: *LW grating position, FP position and resulting wavelength for the part of an AOT 7 observation shown above.*

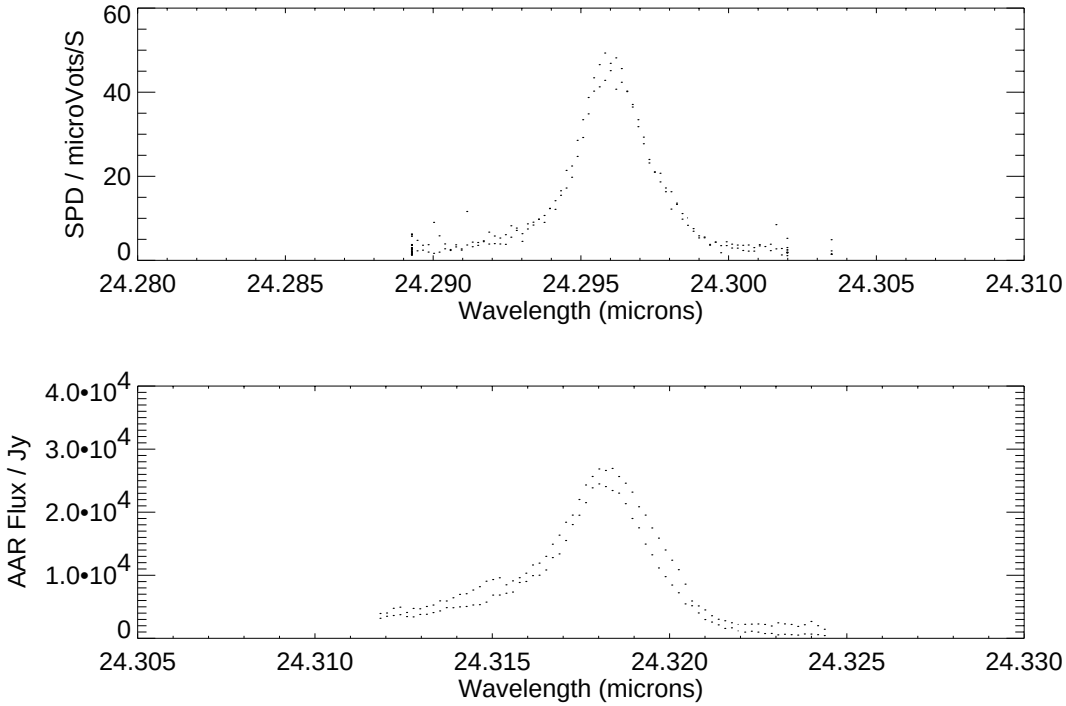

Figure 3.21: *SPD and AAR data for part of an AOT 7 observation.*

3.7 AOT 99 – Post-He Observations

After the liquid Helium depletion of the Infrared Space Observatory, the InSb band 1 detectors of the Short-Wavelength Spectrometer were operated in some timeslots available during the engineering test programme. This time was used to record spectra of stars between 2.36 and 4.05 μm at a resolution as in SWS AOT 1 speed 4 observations. Because they are not standard AOT 1 observations they are available in the archive as AOT 99 observations (under 'non-standard data') and were not processed using the standard pipeline.

As of OLP Version 9.5, a correct wavelength calibration is applied to the post-Helium observations. However, the standard flux calibration steps as available in e.g. OSIA are not applicable to these data. The correct post-Helium flux calibration steps (both absolute and relative within one AOT band) will be made available in future releases of OSIA.

3.7.0.1 Operation mode

The post-Helium observations are obtained in an operation mode similar to the AOT 1 speed 4 observation mode. Differences are:

- scan range is limited to the grating positions resulting in fluxes in band 1
- The long wavelength scanner is not moving
- a photometric check at the highest power of the internal grating calibration source is performed at the end of the observation.

3.7.0.2 Wavelength calibration

As the focal plane temperatures of ISO increased after Helium depletion, geometry changes in the grating scanner mechanism induced a shift in the position of spectral features. This is shown in figure 3.22.

To facilitate the wavelength calibration of the SWS, a fixed Fabry-Pérot is mounted in front of the internal calibration source. During the post-Helium operations, a spectrum of the fringes produced by this system was performed at the beginning of every revolution when the SWS was switched on.

Each of these measurements was used to determine a wavelength calibration of the SWS, applicable for the instrument at the time of the calibration measurement. The wavelength calibration for a single post-He observation was then obtained by interpolating the calibration parameters in time. This results in a wavelength calibration better than 1 resolution element (λ / $\delta\lambda$ = 2200) and comparable to the grating wavelength calibration of an observation during the nominal part of the mission.

The spectral resolution as measured from the FWHM of unresolved lines in NGC 6543 varied throughout the post-He mission, but within the scatter of similar measurements during the nominal mission.

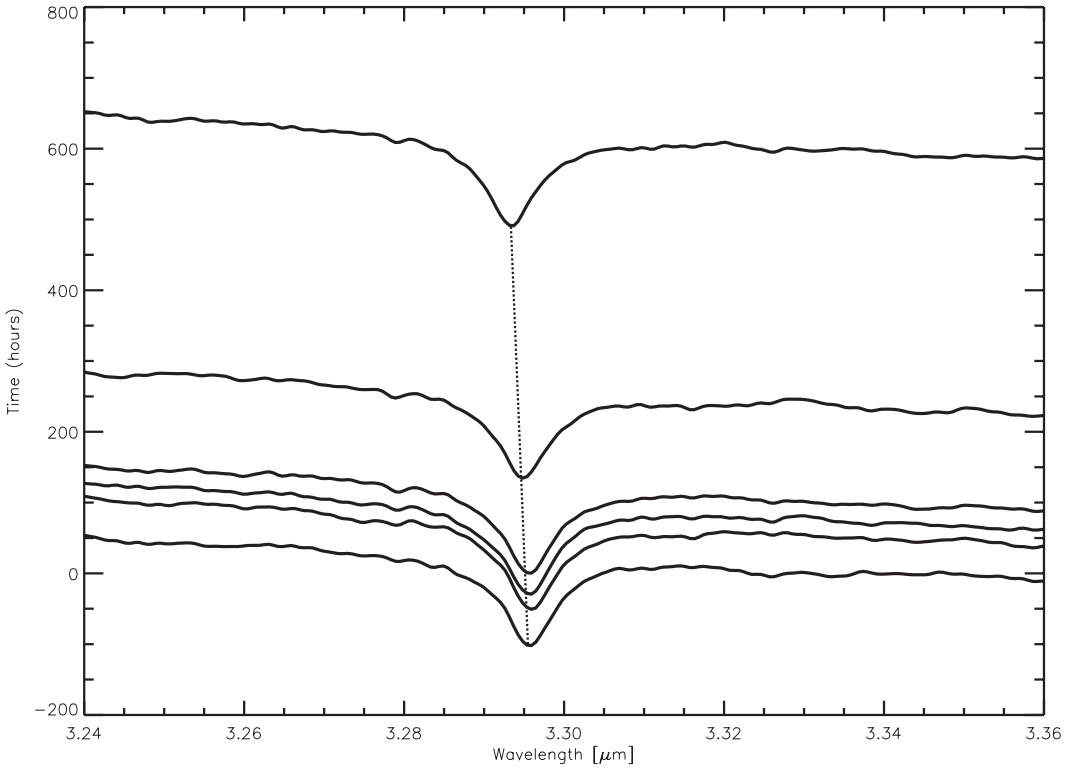

Figure 3.22: *As temperatures increased after Helium depletion, during which post-Helium observations were made, geometry changes in the grating scanner mechanism induced a shift in the position of spectral features. The six spectra shown above were taken at different times during the post-Helium phase and show a clear trend in the wavelength change.*

3.8 AOT S90 – S98 Engineering

S90–S98 were not real AOT's. They were short sequences of commands for activation, de-activation and routine monitoring of the instrument, under direct control of the instrument operators. There are of little interest for observers but are included for completeness.

They were:

- S90 SWS switch-on and complete RAM load. Leave the detector biases switched off.
- S91 Try and cure the detectors by heating the detector substrates to the maximum values (for this purpose electrical heaters were glued on the substrates).
- S92 Switch on the detector biases, put the instrument in its default operational state.
- S93 Try and cure the detectors by irradiating them with photons from the "flashers". For bands 2–6 this would have had no effect without the bias switched on.
- S94 After the instrument has stabilised, or at any other moment, take a dark current measurement and then return the instrument to its default operational state. Introduced at the end of January 1996.
- S95 Never needed
- S96 Never needed
- S97 Never needed
- S98 Switch off.
- S99 Reserved for the CUS.

At the start of a revolution S90 – S94 are executed in sequence to set the instrument up. S98 deactivates the SWS at the end of a revolution.

3.9 AOT behaviour

3.9.1 up-down scans

All grating observations employ what are known as up-down scans. In these, the grating initially scans a wavelength range in one direction, then reverses direction to cover the same wavelength region again. e.g. the scanner may start at 35 μm, scan down to 30 μm and then go back up to 35 μm. Having two scans, in different directions, enables a discrimination to be made between real spectral structure and detector memory effects, as the latter can mimic the former. They are called up-down scans, rather than down-up scans, as it is the LVDT number that increases then decreases, and wavelength is inversely correlated with LVDT. Table 3.1, "Various SWS AOT options", indicates if a particular AOT uses up-down scans.

The SWAASDIR field indicates whether an AAR datapoint is from an up or a down-scan. 1 means the datapoint is part of an up scan, -1 a down scan, and 0 is undefined. Note that 'up-down scans' only refer to what the grating is doing. For FP observations the grating always increased in position (LVDT), hence decreased in wavelength, with time.

An example of an up-down scan is shown in figure 3.23, taken from an SWS01 observation. Plotted are the wavelengths seen by the first detectors in bands 1 and 2 and the SW scanner position. The relationship between the scanner position and wavelength can be seen along with cases of up-down scans where the wavelength seen by a detector decreases then increases. The periods when apertures 1, 2 & 3 are used, times of dark current measurements and photometric checks are indicated.

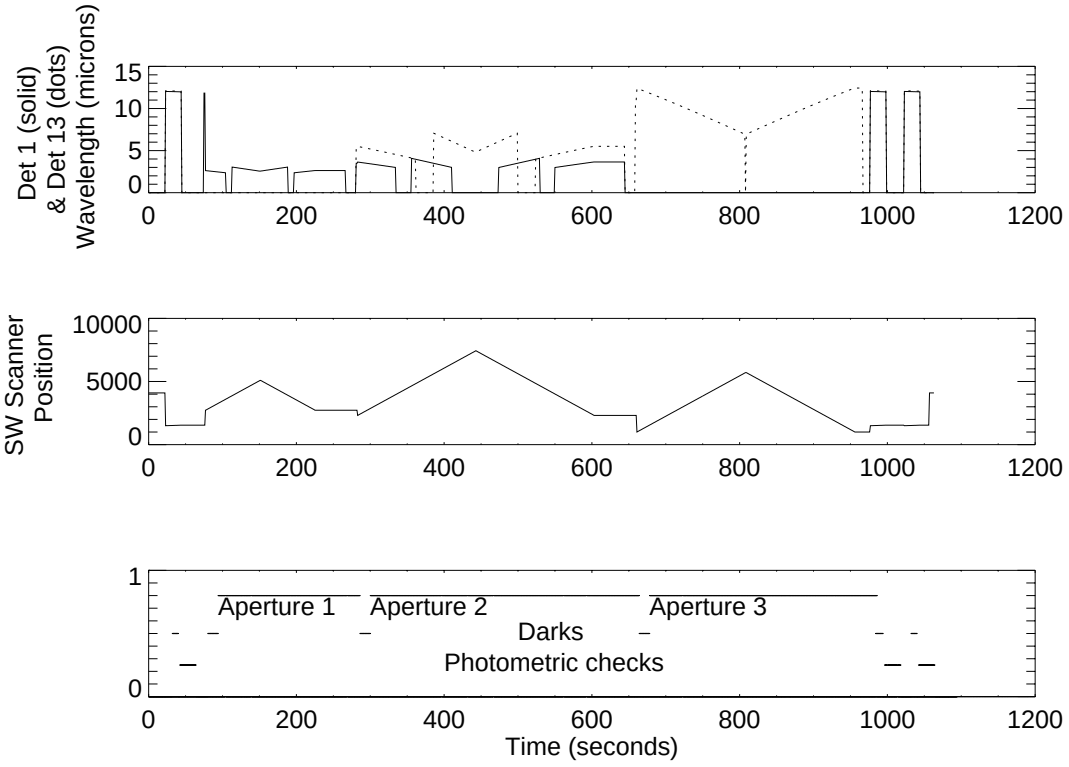

Figure 3.23: *Example of up-down scans. The bottom figure shows which aperture the detectors are looking through over time, the middle shows the SW scanner position and the top shows the wavelength seen by detectors 1 & 13 (bands 1 & 2). As the scanner performs up-down scans over a wavelength range, the detectors see the wavelength decreasing then increasing with time.*

Note that for bright sources (> 1000 Jy) the flux seen in the up-scan can differ by 20% compared to the that seen in the down-scan due to memory effects – see sections 6.8, "Memory Effects" and 5.6, "Flux Calibration Accuracy".

3.9.2 Reference scans

AOT 6 and 7 observations planned before July 10 1997 employed what was known as reference scan calibrations. These were supposed to guard against detector drifts caused by memory effects. The method used was for the grating to occasionally switch back to a set grating position, and hence wavelength. Any changes in the detector response at this wavelength over the timescale of the observation were due to detector memory effects, which could be calibrated out. These reference scans were only present in long AOTs. For example, the interval between reference measurements with detector band 3 was 1000 seconds – band 3 is extremely sensitive to detector drifts because of the strong fringing in the detector spectral response function would change the flux incident on the detector by large (approximately 50 %) amounts, see the diagrams showing band 3 in Vandenbussche 1999, [23].

However, because of a problem in the pipeline module handling reference scan data any such data was unused from OLP V6 onwards. Furthermore, it was found that including such reference scans actually harmed observations due to the interplay of reference scans and memory effects, described in section 6.9, and the reference scans were therefore deleted from observations planned from July 10 1997. Figure 3.24 shows the problems caused by reference scans where there is a difference in the flux level caused by a reference scan.

More information on this can be found in Leech & Morris, 1997, [17].

Users who obtain observations planned before July 10 1997 can recognise scans at the reference wavelengths through the "R" flag in the SWAASTAT or SWSPSTAT fields in the AAR or SPD. It is also present in TDATA. TDATA, or Transparent Data (so called because its contents are not seen by the uplink/downlink system), not only flags the reference scans, but also indicates to which measurements the reference scans (and the normal scans) belong. TDATA is kept in the EOHIMSG1 field in the EOHI, Executed Observation History Per ICS, file. This file is described in the ISO Handbook Volume 2.

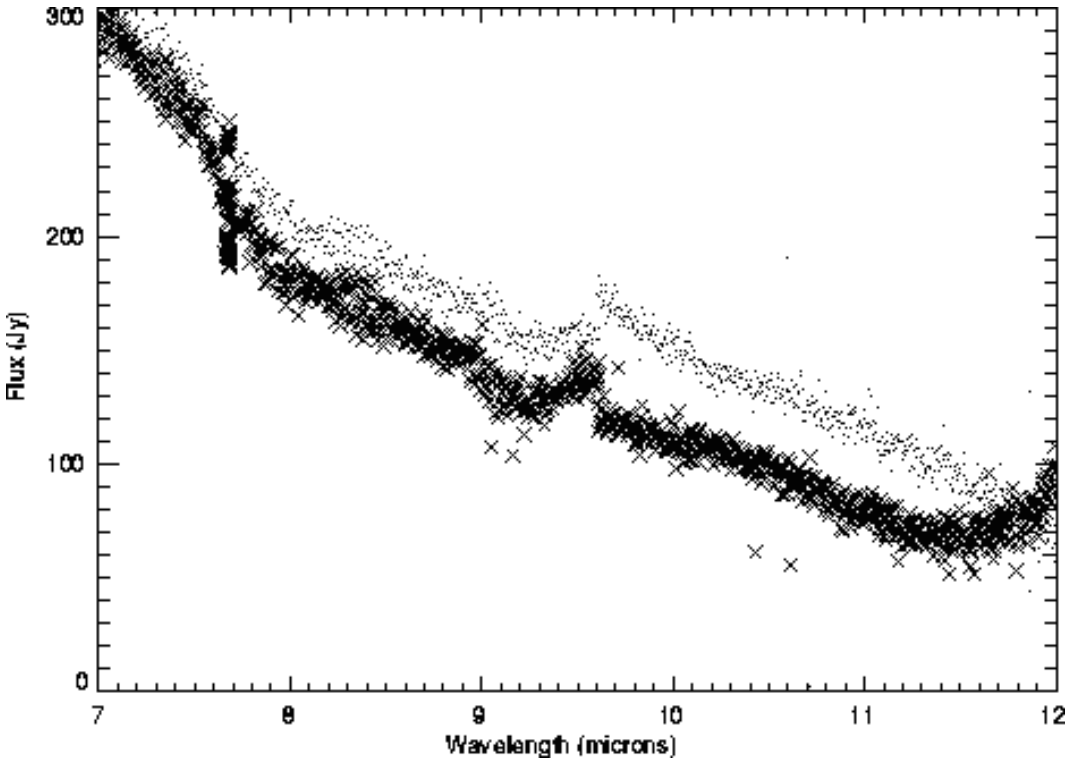

Figure 3.24: *An example of the problems that can be caused by reference scans. The reference scan wavelength is approximately 7.7 μm, which is why there are many datapoints at that wavelength. The up- and down-scans are quite different, caused by a combination of the reference scans and memory effects.*

3.9.3 Recognising the start of an AOT

If you look at ERD data you will want to know when the AOT actually starts. This can be determined by looking at the runflags (byte 13 of frame 8) in the GEHK file, which indicates when ICS's start. The GEHK UTK timekey where changes occur can be correlated with the ERD ITK. Refer to the ISO Handbook Volume 2 for a discussion of the GEHK file.

All ICSs, Instantiated Command Sequences, except the reset ICSs SS0007 and SS0008 start with a preamble to set up the instrument, then initiate the real action by setting one or more run flags (bits) described in Table 3.11.

Table 3.11: *Run flags in frame 8*

ICS	Meaning	Bits set
SS0001	(diffuse calibrator)	4
SS0002	(grating calibrator)	4, 5 and 6
SS0004	(SW scan in AOT7)	5
SS0005	(grating scan)	5 and/or 6
SS0009	(FP)	5, 6 and 7

In all these cases the indicated run flags simultaneously change from 0 to 1. In the AOTs, setting run flags 4-7 does not occur anywhere else. From a practical point of view, the execution of an ICS starts when these flags are set. The only detector data of interest with these flags not set are dark-current measurements at the start of ICSs SS0001 or SS0002 (all AOTs) and SS0005 (AOTs 1 and 2).

Setting run flags 4-7 happens always a few seconds after the start of the ICS execution. At that moment the TDATA for the running ICS is valid. After the run flag goes up, the ICS always lasts at least another 8 seconds (the run flag itself remains set at least 4 secs), to which may be added the uplink time for the next ICS, so that the TDATA for the next ICS is not valid yet.

Interpret a change from 0 to 1 of any of the run flags 4, 5, 6, or 7 as the start of an ICS, and expect the latest arrived TDATA to be applicable. Run flags 0 to 3 must be ignored for this purpose.

Chapter 4

The Pipeline and its effects

4.1 Introduction

The Off-Line Processing (OLP) Pipeline processes the raw data telemetered down from ISO (in terms of bits) into more conventional astronomical units of flux against wavelength. This chapter describes the Pipeline, the error propagation through it and any side-effects noted on the processed data.

The Pipeline is composed of three parts:

• Extracting from the raw data stream the instrument data and placing it into Edited Raw Data (ERD) files. This process is a reformatting only and will not be discussed further.

• ERD to Standard Processed Data (SPD) stage, known as Derive-SPD. This involves removing all instrumental effects on timescales of less than 1 reset interval, converting detector readouts (bits) into slopes (μV/sec) and assigning, where possible, wavelengths with detectors.

• SPD to Auto-Analysis Results (AAR) stage, known as Auto-Analysis. This further processes the SPD removing instrumental effects on timescales of greater than 1 reset interval and converts slopes to fluxes (Jy).

In the course of Derive-SPD and Auto-Analysis several files are used that describe the behaviour of the instrument and its performance. These files are known, for historical reasons, as Cal-G files. They contain such things as the conversion between scanner position and wavelength, the relationship between voltages per second and fluxes, etc.

Examples of the data produced by these steps are given throughout this manual. Sections 3.3 to 3.6 show ERD, SPD and AAR examples for each AOT. Sections 3.9.2, 3.9.1 and 6.8 give examples of short stretches of observations to highlight certain features.

4.2 ERD to SPD (Derive-SPD)

Derive-SPDs main input is Edited Raw Data (ERD), 24 Hz data containing detector readout (in bits) of the target's flux, of internal calibration exposures, of wavelength calibration exposures, of dark currents and of housekeeping data. Derive-SPD also reads in pointing and instrument status files.

For each detector, all data for one full reset interval are combined to a single current estimate at single wavelength and are then saved in the Standard Processed Data (SPD) file for that AOT. No attempt is made within Derive-SPD to average measurements of the same type (e.g. dark current measurements) or to do processing on any time scale longer than one reset interval.

Each measurement for one reset interval of a given AOT is saved separately inside the same SPD product in chronological order of acquisition. The motivation for this is to offer to the observer the possibility of judging the stability and repeatability of SWS measurements. There is an one-to-one correspondence between AOT's and SPD files. That is, one AOT produces one SPD file.

A basic overview of the Derive-SPD processing is given in figure 4.1, the ERD and SPD files are described in sections A.2.1 and A.3.1, and each step in the processing is described in the following sections.

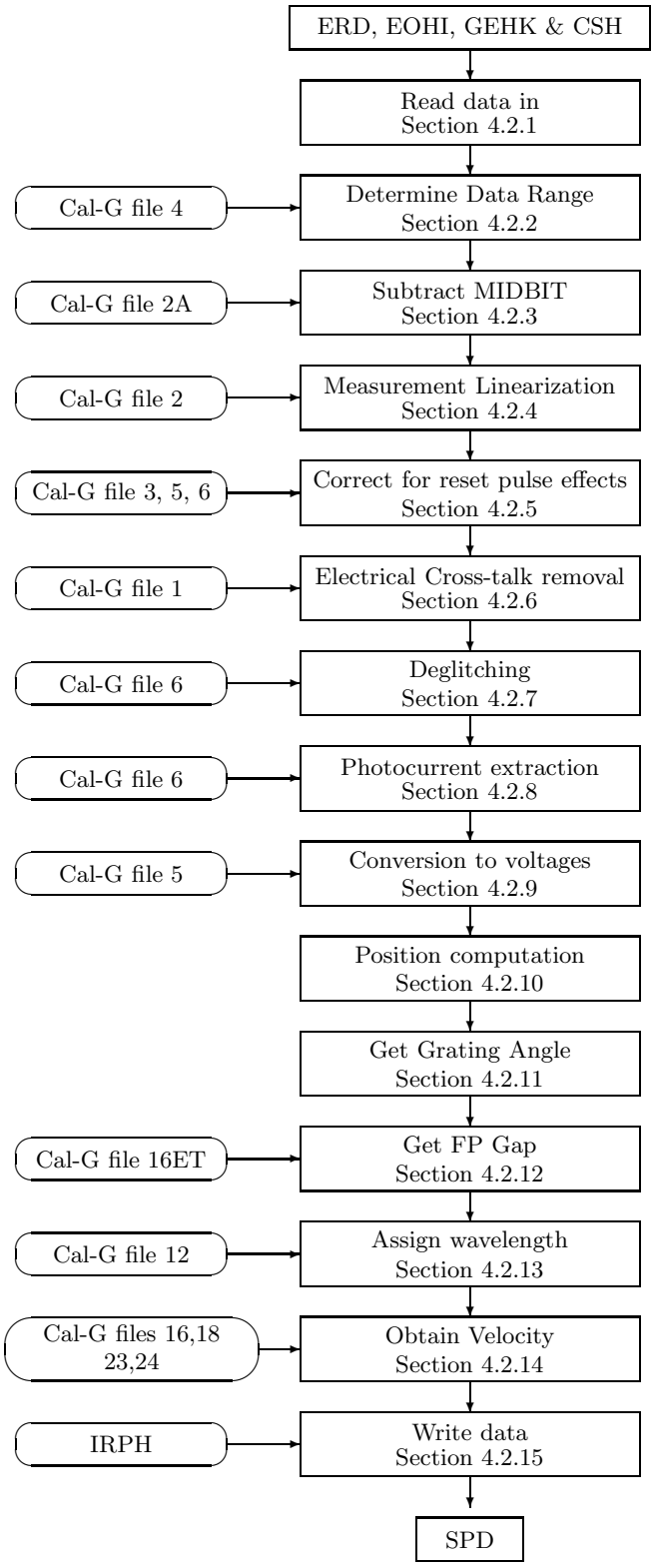

Figure 4.1: *The SWS Derive-SPD process.*

4.2.1 Read ERD

The ERD data for the observation is read in. As discussed above, each AOT generates different types of data: astronomical measurements from the source, measurements from the spectral reference sources (grating and FP), measurements with the calibrators and dark currents. Each of these different types of data has a different physical meaning and serves a different purpose. Hence, the data must be flagged according to their type.

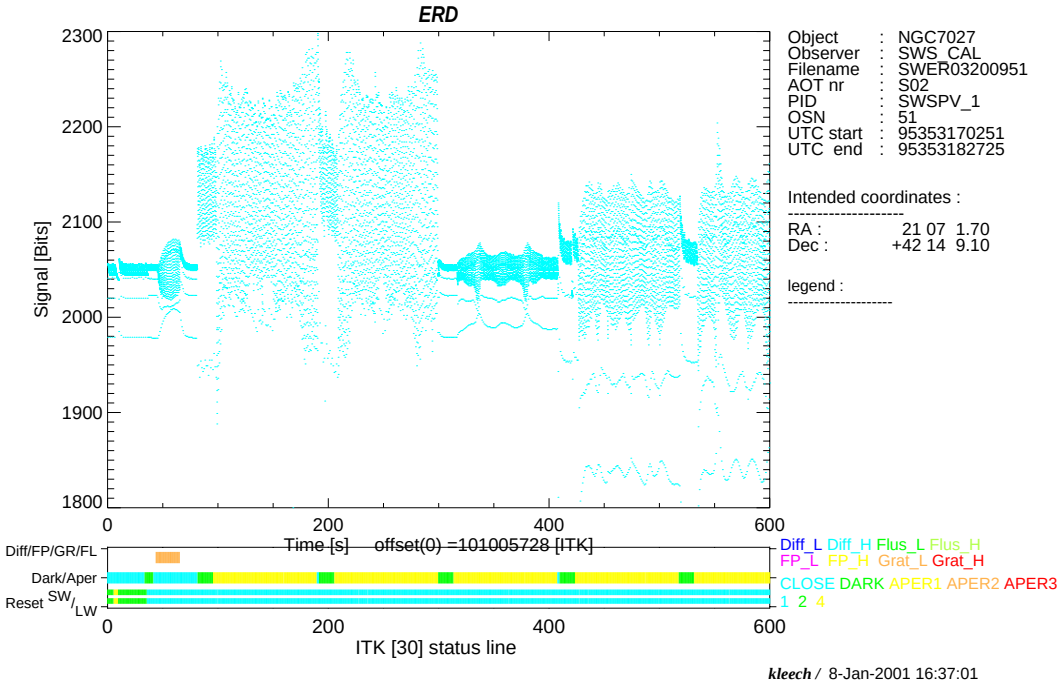

Figure 4.2: *Example ERD data from the first 500 seconds of an AOT 2 before any processing. The instrument status is also plotted showing showing the reset interval used, aperture status etc.*

Each ERD data record is tagged with a Instrument Time Key (ITK) which points toward a unique record in the SSTA Compact Status History (CSH) file (see section A.2.2). Cross-correlating the ERD ITK with the CSH, Executed Observation History per ICS (EOHI) and General Housekeeping (GEHK) files (both described in the ISO Handbook Volume 2) allows a determination of the status of the SWS instrument at the time of the measurement and therefore of the type of the data recorded and the actual wavelength range covered (to be verified during the wavelength check stages).

Figure 4.2 shows the first 500 seconds of ERD of an AOT 2 observation after reading in. This is the same AOT 2 shown in section 3.4. Also plotted are the status values to indicate where darks occur, which aperture is open etc.

4.2.2 Determine Data Range

This marks data out of limits by using Cal-G file 4.

4.2.3 Subtract MIDBIT Values

The detector readouts voltages of between -10 and +10 V are converted into a bit number ranging from 0 to 4095. The midbit is the bit value that corresponds to 0 Volts. While this should be approximately

2048 and different for each detector, it is currently set to exactly half of 4095, i.e. 2047.5, for all detectors. This data is stored in Cal-G file 2A.

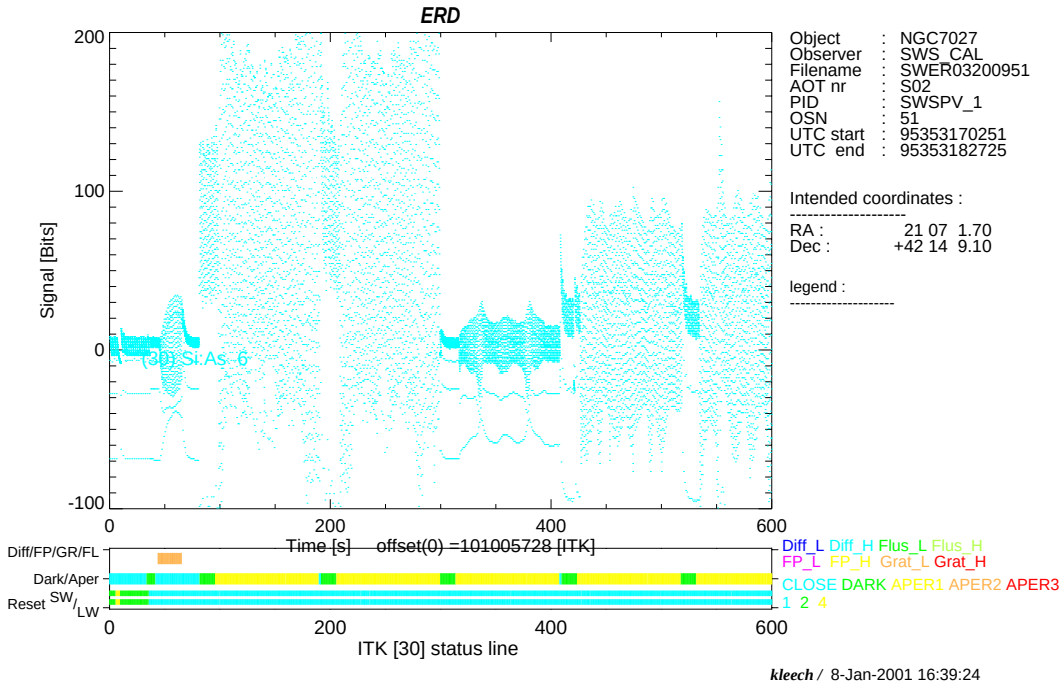

Figure 4.3: *The example ERD data after MIDBIT values have been subtracted. Note that the plot is scaled such that resets are not visible, and this convention will be used in the rest of the plots.*

Figure 4.3 shows the first 500 seconds of ERD from an AOT 2 observation after subtraction of the MIDBIT values. Effectively the values have been shifted down by 2047.5.

4.2.4 Correction of the integration ramp for the RC time constant

The amplifier chain contains a high pass filter. For a constant voltage gradient input the response of the amplifier is to asymptotically approach a constant value, i.e.

$$\frac{dV(t)}{dt} + \frac{V(t)}{t_0} = \frac{dV_o(t)}{dt} \tag{4.1}$$

where $V(t)$ is the output voltage at time t, V_o the input voltage across the capacitor due to the accumulation of charges on the detector, and t_o the detector time constant. In order to later reconstruct the true photo-current, it is first necessary to linearize the ramps, i.e. determine the actual input voltages $V_o(t)$ applied on the detector.

Knowing the RC time constant t_o, it is straightforward to invert the above formula and derive the input voltage. Each detector i has its own time constant $t_o(i)$, stored in Cal-G 2.

Figures 4.4 shows the ERD sample after AC correction. Figures 4.5 and 4.6 show the effects of this stage on a short sample of ERD. This is band 1 detector 1 data where the effect is more visible than the band 3 data shown earlier.

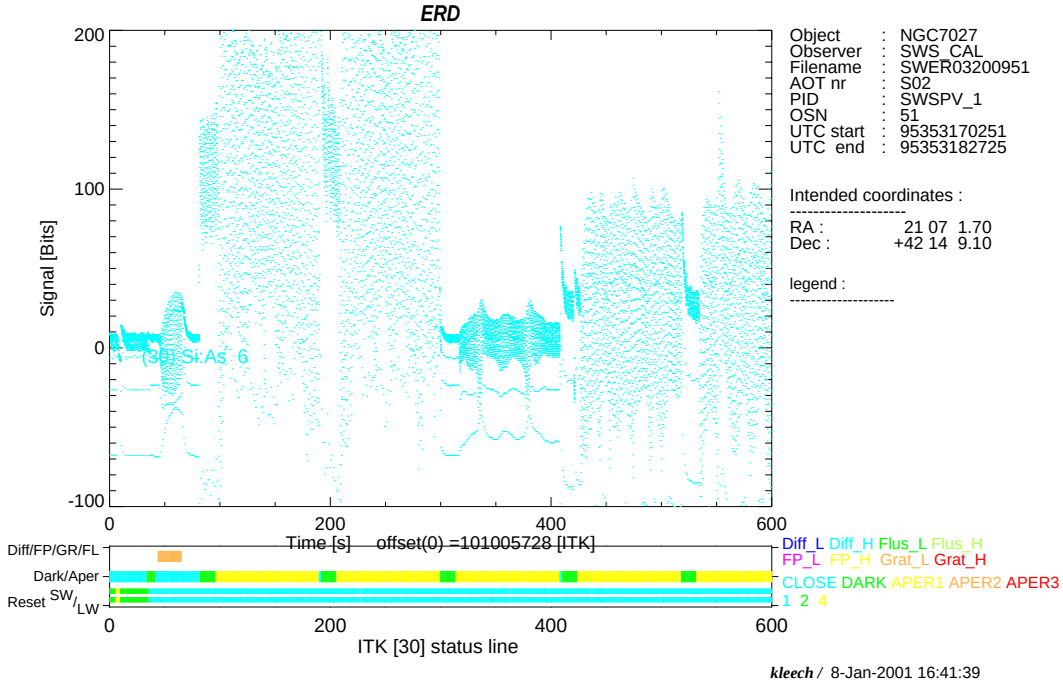

Figure 4.4: *The example ERD data after AC correction. Changes are not apparent on this scale.*

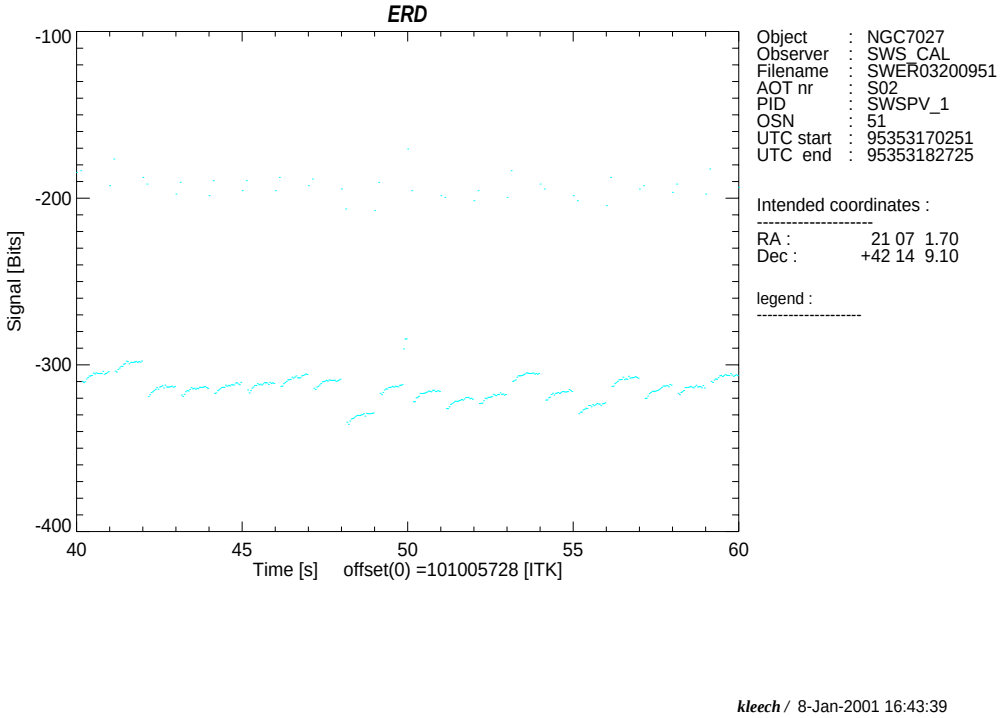

Figure 4.5: *Zoom in on a section of ERD data before AC correction.*

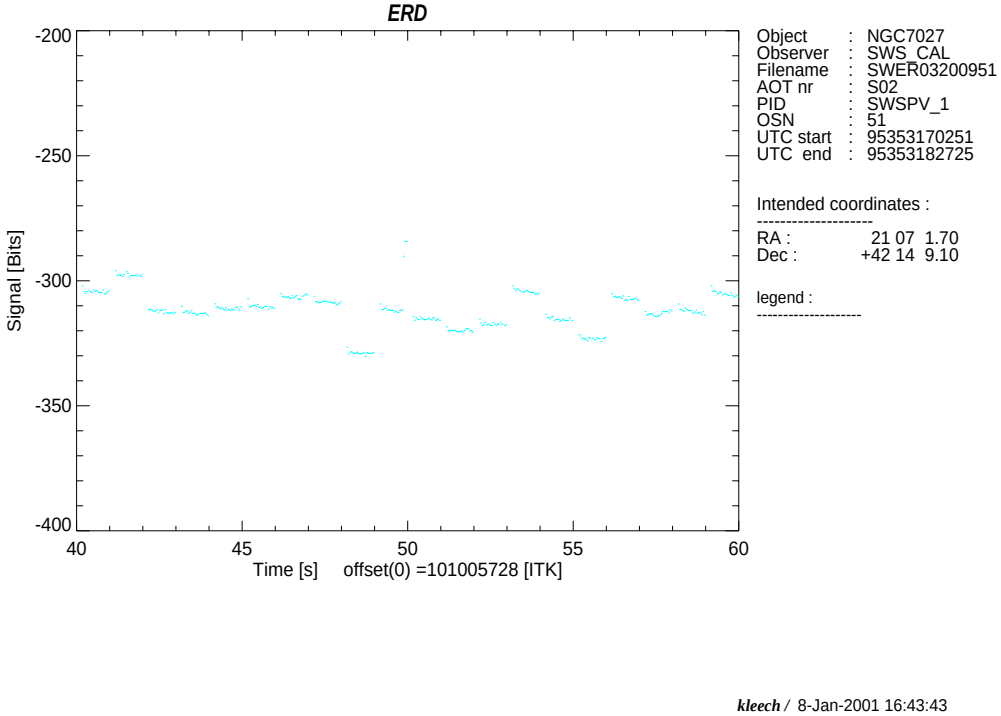

Figure 4.6: *Zoom in on a section of ERD data after AC correction.*

4.2.5 Correct for reset pulse effects

SWS define the pulse-shape as the after-effect of the reset-pulse applied after each reset interval. It manifests itself as an exponential curve with typical decay times of 0.25 – 0.5 seconds and a typical amplitude of 20 – 50 μV. The pulse-shape is an additive component to the integrated signal of the detector, while the impact on the observed slope depends on the gain setting of the instrument.

The correction itself is a plain subtraction of the pulse-shape. However, the difficulty here is to find the right pulse-shape.

It was first believed that the pulse-shape could be corrected for with a single set of pulse-shapes (one for each detector), assuming that the the effect of the after-reset pulse was constant. This correction was implemented for OLP Version 4.3 using calfile 02B, but deactivated for later versions as we learnt that the effect of the after-reset pulse is not constant. The pulse-shape can change from observation to observation and sometimes even within one observation.

OLP Version 9.5 corrects for the pulse-shape on an observation to observation basis and in some cases also on individual parts within one observations. Consequently we do not rely on a fixed type of calibration but use the data itself to do the calibration.

4.2.6 Removal of Electrical Cross-talk

Due to parasitic capacitance between neighbouring detectors any signal in one grating detector will 'leak' to other detectors (primarily the adjacent ones) in the same array. This 'leak' to the adjacent detector is of the order of 10%.

Assuming the detector response is a linear function of the intensity of the signal, a set of cross-talk matrices can be determined with constant correction factors. The read-outs D of each individual detector j in the detector array may then be corrected by applying the following formula:

$$D_j^{corr} = D_j - \sum_{i \neq j} F_{i,j} * D_i \tag{4.2}$$

The sum is over all detectors of index i different from j, where i goes from 1 to M. M being the number of detectors in the array (12 for the gratings and 2 for the FP). This cross-talk correction matrix is held in Cal-G file 1.

There is little effect on the data at this stage so a plot is not shown.

4.2.7 Deglitching

Glitches (ref section 6.7) are recognized in the differentiated voltages. The differential voltages are sorted and the median and the half of the interquartile range around the median are calculated. The higher value of the product of the alpha factor held in CAL-G file 6 and this half of the interquartile range and the width factor (also given in CAL-G file 6) is used as limit to check the voltage differences for glitches. If a glitch was detected the effected difference is marked and skipped.

If any differentiated 24Hz bit values are flagged as glitches the samples around it are checked and, if affected, also marked. If the glitch is so strong that the detector gets saturated all measurements up to the end of the ramp will already have been discarded at the determine data range stage.

If the glitch is not too strong the following measurement do not have to be discarded. In the case of one or two glitches in a slope the software tries to average the partial slopes between the glitches to one slope. One has to be aware, however, that the slope after a glitch is generally higher than the slope before a glitch (especially for a large glitch). See section 4.2.8 for how this is done.

If glitches are detected during a reset this is noted in the flag word. An additional possibility to identify problematic ramps is the offset tag in the SPD/AAR product. This tag contains the actual number of samples contributing to the slope calculation.

The accuracy of deglitching depends not only on how well a glitch can be identified, but also on the effects of the glitch with time (the so called glitch-tails). Studies of slope variations after glitches are ongoing

The SWS Glitch History (SWGH) file contains a list of all glitches detected during processing along with a short characterisation, such as glitch height, skipped samples, etc. For a description of this file see section A.3.2. It is closely related to the SPD and therefore gives a third possibility to identify glitches at the SPD level.

Figures 4.7 and 4.8 show the effect of the deglitching software. Figure 4.7 is of a portion of ERD affected by glitches – glitches occur where the ramps have sudden jumps. Figure 4.8 shows this ERD processed to SPD both with and without the deglitching software. Where it has not been used the glitches in the ERD cause the slope in the SPD to vary rapidly in time. Where the software has been used it has identified where the glitches occur, allowing them to be taken into account when calculating the slopes. The resultant SPD is much smoother.

For a further discussion of glitches and their correction, see Wieprecht *et al* 2000, [24].

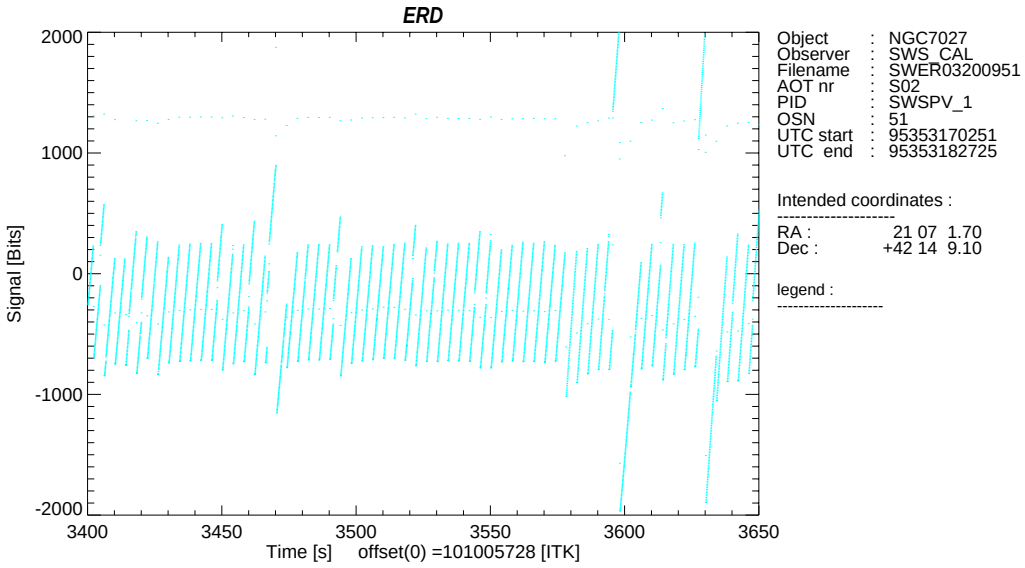

Figure 4.7: *Portion of the example ERD showing glitches. Glitches are present when there are discontinuities in the straight slopes.*

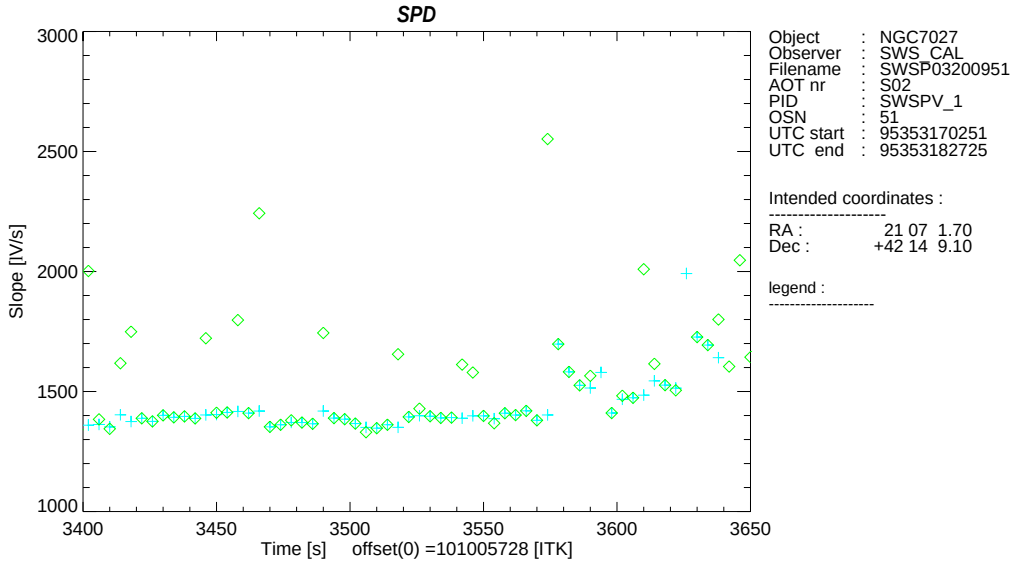

Figure 4.8: *SPD processed with and without deglitching software. The '+' are from ERD processed to SPD with the deglitching software, and the diamonds are from ERD processed to SPD without the deglitching software. The effect or removing the glitches can clearly be seen.*

4.2.8 Extraction of the photo-currents and their uncertainties

A least-square fit is applied to the data taken over one reset interval in order to estimate its slope S. Conceptually this is:

$$V = S \times t + O \tag{4.3}$$

$$S = I \times k \tag{4.4}$$

where,

k is a constant which depends on the internal capacitance, put explicitly to be a constant 1. This implies that I has units of Amp per Farad. It does not need to be explicitly measured as it cancels out when the relative flux calibration is applied.

O is the charge offset at the zero-point of each ramp.

The time t is counted in samples (24 per second) since the start of the ramp.

The slopes, offsets and variances are calculated for continuous stretches of data per reset interval, i.e. stretches not affected by glitches. The returned slope and standard deviation is the average over all stretches of the reset interval. The returned offset is the last valid one and is defined w.r.t. sample 0. This module uses the glitch information generated by the deglitching algorithm above to raise a flag when the slopes are affected by 1, 2 or more glitches, are saturated or when there is no data (see SWSPFLAG in Table A.8 for details). Because of this the routine uses Cal-G file 6.

This program multiplies band 3 data (slope) by -1, as the slopes for this band are inverted compared to the other bands due to the read-out electronics.

In normal data frames all samples in a reset interval are used. For a 1 second integration this time is 17/24 seconds – the first 7 samples are thrown away as being affected by the reset, leaving 17 samples that

can be used. For a two second integration the time is $(17 + 23)/24$ seconds, as 1 sample is thrown away in the last second due to the reset pulse. For an integration lasting K seconds the effective integration time is $\sim (K - 2) + (17 + 23)/24$ seconds.

The accuracy is directly estimated from the fit residuals which allow the computation of the standard deviation of the derived photo-current. Obviously, the accuracy depends not only on the intensity of the source (I), but also on how well the ramps have been previously linearized and therefore on the measurement error of the RC time constants. A statistical weight is computed which is inversely proportional to the error on I and proportional to the number of measurements between two detector resets. This weight will be used by Auto-Analysis to compute the average photo-current for each ramp. It is expected that this error will dominate all previously described ones.

Where glitches are found the slope calculation works differently. Assuming an interval where a glitch is found at sample number j. The software applies a model to fit:

$$y_k = a + b.t_k + s.H[j]_k \tag{4.5}$$

$H[j]_k$ is the unit step function which steps at sample number j from 0 to 1, and as such it is a function of k.

χ^2 can be written as :

$$\chi^2 = \sum_k (y_k - d_k)^2 \tag{4.6}$$

where d_k is the data. It is possible to compute the minimum in χ^2 by differentiating it wrt to each of the parameters and equating them to 0.

$$d\chi^2/da = a.N + b.st + s.sh = sd \tag{4.7}$$
$$d\chi^2/db = a.st + b.st2 + s.sth = std \tag{4.8}$$
$$d\chi^2/ds = a.sh + b.sth + s.sh2 = shd \tag{4.9}$$
$$\tag{4.10}$$

where $st = \sum_k t_k$, $st2 = \sum_k t_k^2$, $sth = \sum_k t_k.h_k$, etc.

The set of equations above is a set of linear equation which can readily be solved with a number of procedures, i.e. Gauss-Jordan elimination, LU decomposition.

OLP Versions 9.5 is not that much different from previous versions, except that there is one extra parameter to be solved. And with two glitches present in the interval, there are two extra parameters to be solved etc. The standard deviations are derived in a similar way to previous OLP versions.

The effect of this stage is to convert the data from a set of 24 samples per second to 1 point per reset interval.

4.2.9 Conversion of digitized read-out's to output voltages

The electronics amplify the detector read-out voltages with a commandable gain factor before the analog to digital (AD) conversion. Each detector can be operated at three different gains of the amplifier chain. The output voltage must be reconstructed from the digitized read-out's and corrected for the gain factor.

The input to the AD converter is related to the voltage across the detector by

$$V_{In} = V_{Det} \times G \tag{4.11}$$

where G is the gain which can be set to one of three values. The slope in V/s is related to the output of the AD converter, in $Bits/sample$, by

$$Slope = Digital\_value * conversion\_factor \tag{4.12}$$

The conversion factor is given by

$$conversion\_factor = \frac{V_{range}}{bits_{max}} * \frac{sample}{s} = \frac{-20}{4095} * \frac{24}{1} \tag{4.13}$$

The numerical values originate from the fact the A/D converter has a maximum input range of 20 V which are converted into 4095 steps, with the input voltage inverted, and that there are 24 samples per second.

Once we have calculated the slope from the digital output we can divide by the gain factor to get the detector voltage.

Values for this are held in Cal-G file 5.

Figure 4.9 shows the effective output from this and the previous stage.

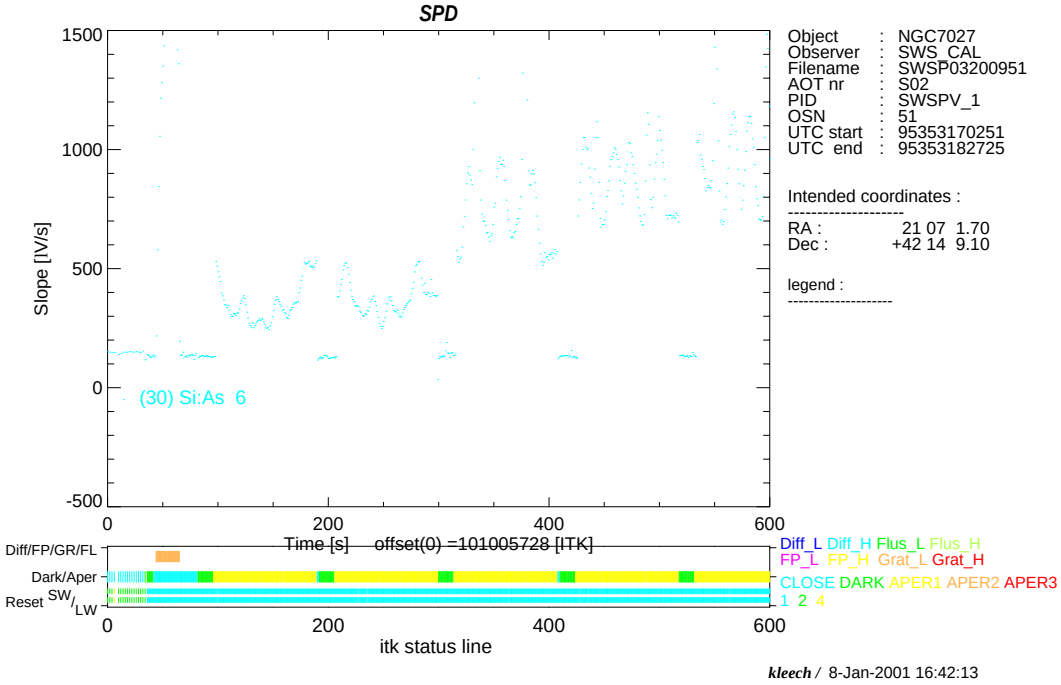

Figure 4.9: *The example data after the slope calculation stage. This stage calculates the slope every reset interval of all valid 24Hz datapoints in that reset interval.*

4.2.10 Position computation

This computes the grating and FP positions.

4.2.11 Get Grating angle

This module converts the grating position to a grating angle, which is then used to calculate the wavelength of the light falling on the detectors. See section 5.7.

It uses Cal-G file 16ET.

4.2.12 Get Fabry-Pérot gap

This module determines the Fabry-Pérot gap from the telemetered currents. See section 5.7.

It uses Cal-G file 12.

4.2.13 Assign wavelength for grating and FP

This module calculates the wavelength of light falling on the detectors. Refer to sections 5.7 and 5.8 for a discussion of the philosophy behind this and the likely accuracy.

For the grating, this involves applying equation 5.4. The grating angle, calculated in section 4.2.11 is used along with various calibration files to determine the wavelength of light falling on each detector. Only bands with an unique order falling on their detectors are assigned a wavelength, all others are flagged as confused. It should be noted that all bands with an unique order falling on their detectors are assigned a wavelength, even if the band was not requested or contains useless data (although for non-FP observations the FP data is not transferred to the AAR).

For an AOT 01 measurement, where the grating moves during a reset interval, the grating position in the SPD is set to the grating position of the first sample in the reset interval. The wavelength in the SPD, however, is the average of the wavelengths for all valid samples. As samples are thrown away due to the reset pulse (see section 6.6, operation described in section 4.2.2), the wavelength is that from sample (24 - Cal-G file 3) / 2 (assuming no glitches).

For the Fabry-Pérot, once the grating wavelength is calculated the mechanical gap width (calculated in section 4.2.12) is corrected to get the optical gap width (calibration file 18). The wavelength which passes through the FP is the one of which a whole multiple fits exactly in two times the optical gap width.

4.2.14 Obtain Velocity from IRPH

The velocity of the spacecraft is obtained from the IRPH file. It is written into the SPD file and used in the Derive-AAR processing stage.

4.2.15 Writing data out

The data produced by the processing chain above is written out to the SPD and glitch list SWGH files. Each AOT results in one SPD file. For a definition of the SPD file see section A.3.1. Note that the SPD file, like an ERD file, contains science data interleaved with calibration data.

A SPD record is produced for every reset interval. Complexities arise when the reset intervals for the SW and LW gratings are different. In this case there will be one SPD record (containing data for all detectors) for each of the shorter reset interval, with the SPD for the longer reset interval having its flag word set to ‘No data’ for the records when it did not contain a reset (see table A.8) and contains ‘0’ in the flux — this sometimes confuses plotting programs. As an example, if the SW grating had a reset interval of 1 second and the LW one of 2 seconds, a SPD record would be produced every second. Every SPD record for the SW detectors (1–24) would contain valid data, while only every other record for the LW detectors would contain valid data, the others being marked as ‘No data’.

Figures 4.10 and 4.11 show the final output of the Derive-SPD stage. The first is detector output against time, the second against the wavelength.

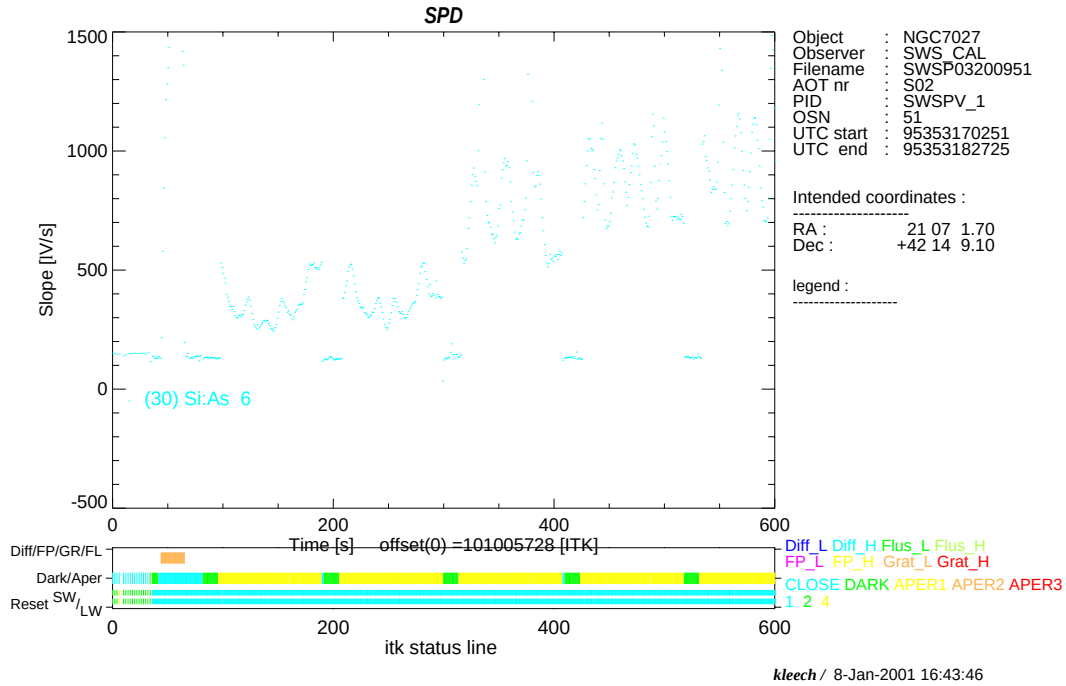

Figure 4.10: *Final SPD data (against time) for the example input ERD data.*

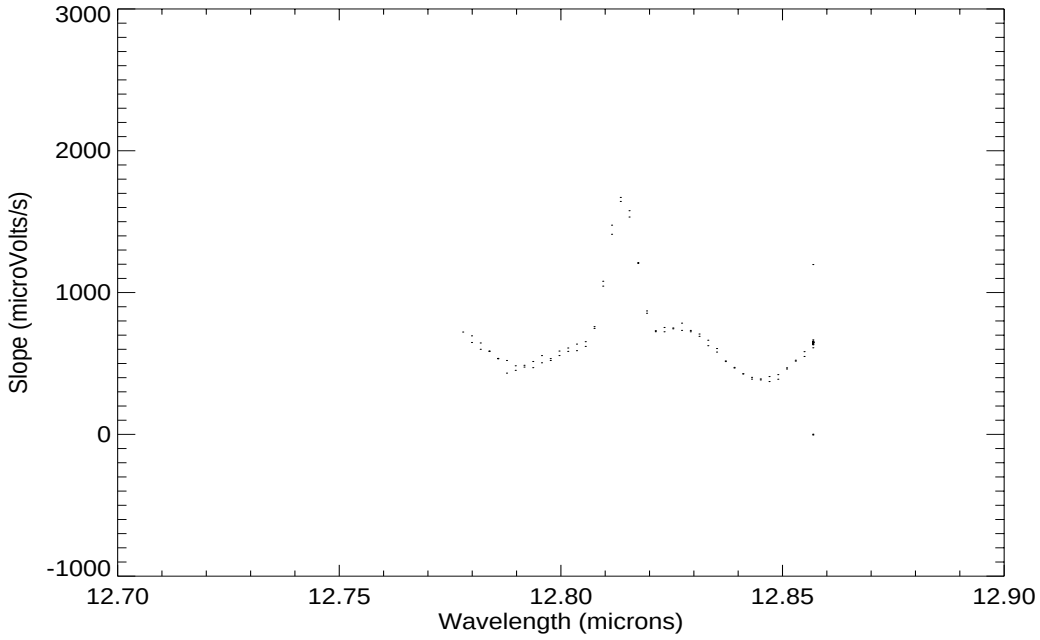

Figure 4.11: *A portion of the SPD data against wavelength for detector 30. The continuum is not at a constant level due to fringes – see Section 5.4.*

4.3 SPD to AAR (Auto-Analysis)

Auto-Analysis (AA) is the processing stage that starts from SPD, corrects for all instrumental effects lasting longer than one reset interval and generates sets of spectra, fluxes (in Jy) against wavelength (in μm). These spectra are generated irrespective of the observation specifications. Figure 4.12 gives an overview of AA processing. Most of the SWS AA processing steps are independent of AOT number as most of the special options (e.g. reference scans, see table 3.1) are used in several different AOT's and thus are implemented as part of the main processing flow.

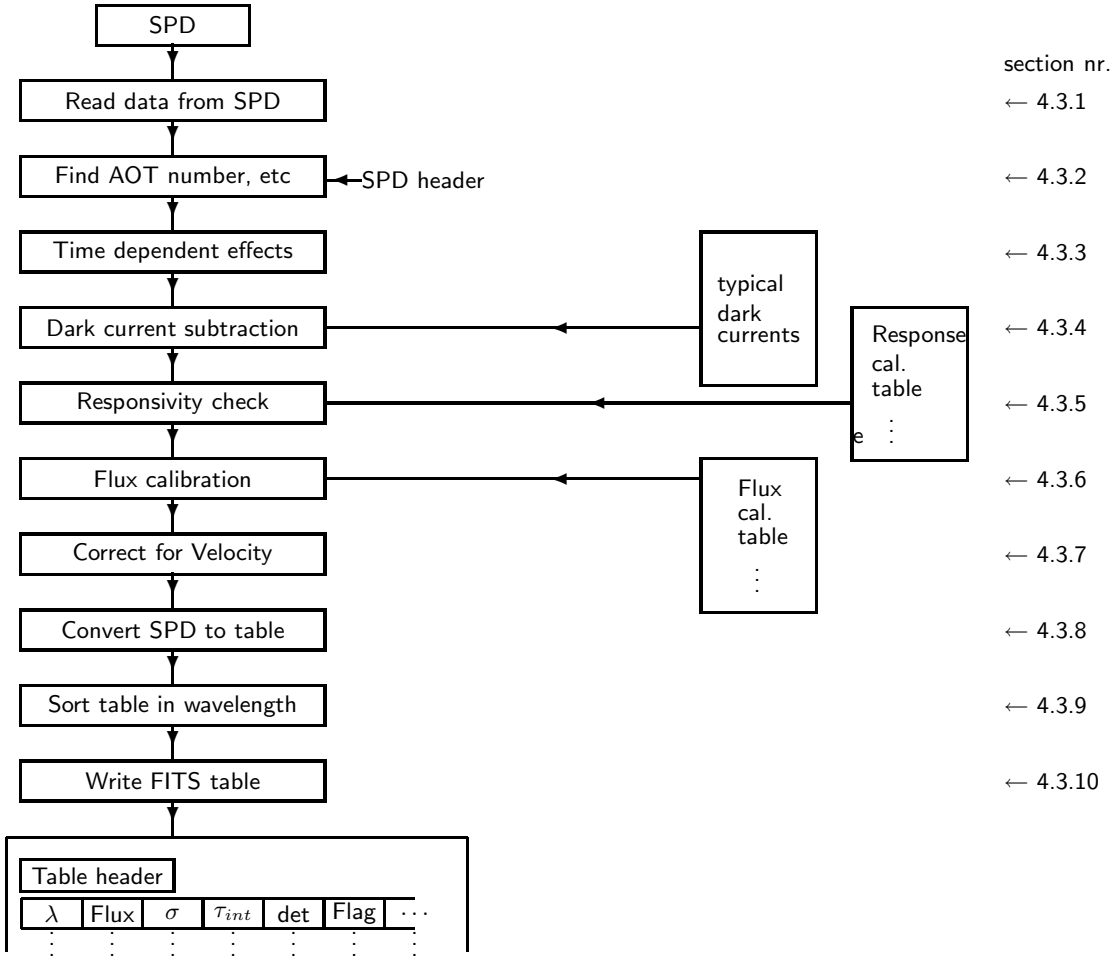

Figure 4.12: *Auto-Analysis flow-diagram*

These steps are described in more detail in the following pages.

4.3.1 Read all data from SPD

The data and header information are read from the input SPD.

4.3.2 Determine AOT and Velocity correction

The AOT number, needed for the further processing of the data, is determined from the `EOHAAOTN` keyword in the SPD FITS header. The velocity of the spacecraft with respect to heliocentric is similarly obtained, and for AOT SWS01 the speed is also obtained.

4.3.3 Correction for time dependent detector behaviour

The detector data may need to be corrected for time dependant effects such as detector hysteresis.

Currently, only a number of readouts at the beginning of dark currents are rejected.

4.3.4 Subtraction of dark currents

Whenever possible dark currents are subtracted from each observation. For every block of dark current data, the median of valid dark current data is calculated for each detector. A (linearly) interpolated dark current block with the same gain and reset length is subtracted from each non-dark current scan. The interpolation is done over the dark current directly preceding the scan and the nearest dark current following the scan. The interpolation is performed in time and the beginning and end of the interpolation are taken as the last frame of the first dark current and the first frame of the second dark current.

If there is no dark current preceding a scan, the dark current after the scan is subtracted or the mean of all dark current in the SPD with the same reset and gain as the scan. If there is no valid dark current point in a block, either the next useful dark current is used or the mean value of all dark dark current in the AOT with the same gain and reset. If there is no valid dark current at all with the same gain and reset length the block is flagged as having no data.

For the PHOTOMETRIC CHECKS only the dark current preceding the measurement is subtracted. No interpolation is done.

The calculated dark current values are also subtracted from the dark current frames themselves.

Each calculated dark current is compared against the value in the calibration file (CAL21_*) and the limits for the dark current therein. If the calculated dark current is outside the defined limits a warning is issued. The calculated dark current is however subtracted.

If no dark current can be found for a specific detector, the data are flagged invalid.

It is (most likely incorrectly) implicitly assumed that the dark current data have not been affected by (or are completely corrected for) detector memory effects.

4.3.5 Responsivity check

For each AOT band the wavelength dependent responsivities are normalized with respect to the key wavelength. This is done per detector and stored in the Cal-G files 25_x. The signals that belong to a certain AOT band are then divided by the normalized responsivities for that AOT band.

Additionally, for an AOT 1 the responsivities are smooth by doing a flux conserving interpolation using wavelength dependent factors which determine the range of wavelengths over which the smoothing has to be done. These factors depend both on AOT speed and on the AOT band as well as on wavelength. This factors are stored in Cal-G file 19.

4.3.6 Flux calibration

The conversion from signal to flux is carried out by normalizing the signal of the photometric check, where data obtained with the internal stimulator are collected and averaged, by that in the Cal-G file 13 from pre-flight measurements. This value is multiplied by the ratio of flux over signal of an external calibration source. Finally the obtained conversion factors are applied to the data.

In case the data does not contain a valid photometric check (such as e.g. in detector band 1, for which photometric checks were taken out of the AOT logic) the values are taken straight from Cal-G file 13. I.e. the normalized signal of the photometric check is assumed to be one.

4.3.7 Velocity Correction

The velocity component (V) in the line of sight towards the target, due to the combined motions of the spacecraft and of the earth is corrected for in this module. This then ensures that the AAR wavelength is heliocentric.

4.3.8 Extracting data from the SPD

All good data (wavelength, fluxes etc.) are transferred to internal arrays. Data for which no wavelength was assigned in Derive-SPD are skipped.

Prior to OLP V6 dark current and photometric check data were transferred into the internal arrays and are therefore present in the AAR. From OLP V6 this is not the case.

4.3.9 Sort the internal table in wavelength

The internal table of wavelengths, fluxes etc. is sorted by wavelength using an appropriate sort algorithm.

4.3.10 Output table files

The table containing wavelength and flux calibrated data is written to a FITS AAR file. For a definition of this file see section A.4.1.

4.4 The Error Propagation of the SWS Pipeline

This section is based on Wieprecht & Feuchtgruber 1999, [25], which summarises the error propagation of the SWS OLP version 8.4. It is also applicable to OLP 9.5. The approach described separates pure statistical errors from systematic errors. It is now possible to get an indication of the accuracy of an SWS product from the product itself.

Error handling in Calibration Procedures (CAPs), are used to derive calibration files and their error values, are not discussed in this note.

Of course, some sources of error (e.g. fringes/indexfringes) will always depend on what sort of and how careful, data reduction has been done outside the automatic PIPELINE.

4.4.1 Statistical Errors

Within the PIPELINE chain there are few sources providing information about statistical errors. The main statistical error is contained in the flag SWSPFLAG of the individual slope. NODATA-, GLITCH-, OOL- flags and the TINT tag (which gives the actual number of samples used to compute a ramp) provide rather reliable information about the quality of an individual slopes. Since this information is directly passed into the AAR, it is a good starting point (of course NODATA = 1 means that these points get a weight = 0 and are not passed into the AAR) for determining the statistical error for a single data entry.

The other statistical error, the one propagated currently in the PIPELINE is contained in the STDEV tag of the SPD. It is just the standard deviation of the slope of the fit of a 1st order polynomial to the integration ramp. In case of a perfect linear ramp this is a reasonable way of characterizing the quality of an individual slope. It provides additional information about the noise during the integration, which can be affected by instrumental effects or still some small glitches, not reflected in the GLITCH flag. From OLP version 8.4 on this value is also passed straight to the AAR product without any conversion, therefore the units are in μV/second.

4.4.2 Systematic Errors

In order to treat systematic errors within the DAAR process and pass the STDEV straight to the AAR product, the AAR tag SWAASPAR, see sectionA.4.1.2, is (mis-)used to store systematic errors in a byte code. The first array tag contains the “offset” error, the second array tag holds the “gain” error. As a baseline, both “offset” and “gain” errors are zero on entry of the DAAR stage.

4.4.3 DERIVE SPD

To calculate the slope in the SWS detector data, the AC-corrected detector outputs for every reset interval, y, versus time, t, are used. While the AC-corrected slope should be linear, uncertainties in the AC-constants of every detector usually result in the slope being slightly curved.

The computed error is therefore not suited for detector-detector comparison, moreover it represents the relative error of one detector.

$$y = a + bt \tag{4.14}$$

where a is the offset and b is the slope of one reset interval. As usual the χ^2-equation is written as

$$\chi^2 = \sum (a + bt - y)^2 \tag{4.15}$$

We want to find a minimum in χ^2. To this end we differentiate the equation to a and b and put both equations to 0: the normal equations.

$$\frac{\partial \chi^2}{\partial a} = 2(aN + b\sum t - \sum y) = 0 \quad (4.16)$$

$$\frac{\partial \chi^2}{\partial b} = 2(a\sum t + b\sum t^2 - \sum ty) = 0 \quad (4.17)$$

The solutions to this set of equations is

$$\Delta \equiv N\sum t^2 - \sum t \sum t \quad (4.18)$$

$$a = \frac{\sum t^2 \sum y - \sum t \sum ty}{\Delta} \quad (4.19)$$

$$b = \frac{N\sum ty - \sum t \sum y}{\Delta} \quad (4.20)$$

When we also form along with the other sums, the sum over y^2, $\sum y^2$, it can be shown that

$$\chi^2 = \sum y^2 - a\sum y - b\sum ty. \quad (4.21)$$

The variance of the solution equals to $\chi^2/(N-2)$ and hence the standard deviation is

$$\sigma = \sqrt{\chi^2/(N-2)} \quad (4.22)$$

N : number of samples

The formal errors in the offset and the slope are resp.

$$\sigma_a = \sigma\sqrt{\sum t^2/\Delta} \quad (4.23)$$

$$\sigma_b = \sigma\sqrt{N/\Delta} \quad (4.24)$$

The "standard deviation of the slope", σ_b is passed into the SPD product and copied to the Auto Analysis product during the DAAR processing step.

4.4.4 DERIVE AAR

To understand the error handling of this part of the s/w it is we discuss the relevant parts of the DERIVE AAR s/w.

4.4.4.1 Dark Current subtraction

See section 4.3.4 for a description of how the dark-current subtraction is carried out.
For every dark current block a number which is used for error calculation is computed :

$$lo = index((total\_number + 1) * 1/4) \quad (4.25)$$

$$hi = index((total\_number + 1) * 3/4) \quad (4.26)$$

$$error = (dark(hi) - dark(lo))/2.0 \quad (4.27)$$

total_number : total number of valid data points during dark block
index : ordered indices of dark current data block
dark : ordered array of slopes during dark current measurement
error : a width value which is used for error propagation (error of the MEDIAN)
: - median dark error

The DARK error for an individual scan can then be expressed as:

$$SWAASPAR(0) = \sqrt{error1^2 + error2^2 + \left(\frac{dark1 - dark2}{2}\right)^2} \tag{4.28}$$

with: $dark1$ = dark current before scan; $dark2$ = dark current after scan; $error1$ = median dark error of dark1; $error2$ = median dark error of dark2; units: [μV/s]

In case of only one valid dark current Bit 22 is set in the flag tag of the SPD/AAR to indicate an uncertainty of the dark subtraction and the result would be instead:

$$SWAASPAR(0) = error \tag{4.29}$$

with: $error$ = median dark error of the valid dark current

4.4.4.2 Responsivity calculation

See section 4.3.5 for a description of how the responsivity calculation is carried out.

The key information during this step is contained in CAL25. These calibration files contain an "error curve" (units: [%]) representing the accuracy of the RSRF, see section 5.4, including known spectral features.

Two error quantities have to be handled within RESPCAL per detector and scan. The DARK offset error and the error curve contained in CAL25. Division of DARK offset error by RSRF gives normalized absolute offset error:

$$SWAASPAR(0) = \frac{SWAASPAR(0)}{CAL25.DATA.RESPONSxx * (1 - CAL25.DATA.SIGMAxx)} \tag{4.30}$$

and SWAASPAR(1) gets a copy of the CAL25 error:

$$SWAASPAR(1) = CAL25.DATA.SIGMAxx \tag{4.31}$$

with:
$CAL25.DATA.RESPONSxx$ = CALFILE 25 response value linear interpolated conserving the flux
$CAL25.DATA.SIGMAxx$ = resulting error from linear interpolation conserving the flux. It is assumed the error follows the same integration formulae (trapezoid rule) as the fluxes, except that the error is divided by the square root of a dilution factor being the ratio between FWHM and the local step size in wavelength. Integrating over more wavelengths yields a smaller error while interpolating over a small part wavelength interval a larger error.

xx = number of detector within the selected CAL25; SWAASPAR(0) contains now already normalized fluxes and SWAASPAR(1) is still in (%).

Part of the uncertainty in the key wavelength numbers is caused by the RSRF uncertainty, however this is very difficult to disentangle. In order to get back the right key wavelength accuracies, the RSRF uncertainty at the key wavelength is subtracted first.

The errors can be written now as:

$$SWAASPAR(1) = SWAASPAR(1) - SWAASPAR(1)_{at\ keywavelength} \tag{4.32}$$

This error computation is only applied for periods where a valid wavelength is associated. Therefore errors during dark current and photometric checks are passed through without any modification. This is important for the next processing step.

4.4.4.3 Flux calibration

See section 4.3.6 for a description of how the responsivity calculation is carried out.

The important information to be included in the PIPELINE are the quoted accuracies of the SWS flux calibration at the key wavelengths for the respective PIPELINE version – see section 5.6.

The REL_FLUX_ERRx tag of CAL13 contains the key wavelength accuracies (further on called "CAL13-error"). We know that for some AOT bands (especially for Si:Ga bands) we have even flux dependent errors (larger errors in the high flux regime). Therefore the calfile 13 structure contains error for low, median and high flux regimes. The boundaries of these regimes are determined by comparing any individual data point against limits given in the calfile 13 header (Keyword: ERRLOW and ERRMED).

Two more sources of error have to be handled within FLUXCON, the DARK error of the photometric check and the noise of the photometric check. The later one has been derived already in the current PIPELINE, the error due to the dark current in front of the photometric check has been neglected so far.

$$SWAASPAR(1) = \sqrt{(SWAASPAR(1) + CAL13error)^2 + photerrnoise^2 + photerrdark^2} \tag{4.33}$$

with:
$photerrnoise$ = noise of the photometric check data. Calfile 41 contains the representative shape of photometric checks. The actual photometric check is mapped onto the representative photometric check data using the relation of the MEANs as multiplication factor. The square root of the difference of actual photometric check data and representative photometric check data divided by the number of points is used to get the noise of the photometric check data.

$photerrdark$ = uncertainty originating from dark current of photometric check converted to relative units :

$$signal = MEDIAN3(photdata) \tag{4.34}$$
$$sigerr = MEDIAN3(photdata + darkdata) \tag{4.35}$$
$$photerrdark = MEDIAN(signal)/MEDIAN(sigerr) \tag{4.36}$$

with:
$MEDIAN3$ = 3 sample MEDIAN FILTER
$photdata$ = data of photometric check
$darkdata$ = dark current values of dark current preceeding the photometric check

The SWAASPAR(0) value has to be converted first from normalized to absolute (Jy) in the same way the fluxes are by running through FLUXCON. Then:

$$SWAASPAR(0) = SWAASPAR(0) * (1 + CAL13error) \tag{4.37}$$

4.4.5 Decoding of SWAASPAR

SWAASPAR(1) contains the GAIN error in % ranging from 0 to 255.
SWAASPAR(0) contains the OFFSET value in Jy using a lookup table :

```
BYTE VALUE     Error       Function
-------------------------------------
  0    -     0.        byte * 0.1
  1    -     0.1
  .    .      .
 10    -     1.0
-------------------------------------
 11    -     2.0       byte - 9.
 12    -     3.0
  .    .      .
109    -   100.0
------------------------------
110    -   110.0       (byte-109)*10.+100.
111    -   120.0
112    -   130.0
  .    .      .
199    -  1000.0
------------------------------
200    -  1200.0       (byte-199)*200. + 1000.
201    -  1400.0
  .    .      .
255    - 11200.0   --> MAX value
------------------------------
```

For convenient decoding of errors it is possible to use *DECODE_AA_ERROR* of the SWS IA system or OSIA.

4.5 Glitch removal effects in fast speed AOT 1 observations

4.5.1 Introduction

It was noted that the glitch removal process in Derive-SPD had an impact on the fluxes of spectral lines when observing with fast speed AOT 1. The glitch removal process incorrectly marked datapoints within a line as glitched, leading to non-gaussian spectral line shapes and, where the lines are fitted with a gaussian, a resultant underestimate of flux. This effect can be seen in figure 4.14.

4.5.2 Verification

In order to quantify this effect, the spectra of three Planetary Nebulae with strong emission lines were examined in the following manner:

1. Check the AAR derived with the OLP (V5.2) to see if there are points belonging to the spectral line which are flagged as glitched.
2. Derive a new SPD and AAR in which glitch detection is disabled by setting the parameter alpha in CAL06 to a very high value.
3. Compare those lines in which some points are identified as glitched in the standard AAR, to the corresponding ones in the non-deglitched AAR.
4. Flatfield/Rebin both AARs and fit a Gaussian to the lines of interest to calculate the line fluxes.

4.5.3 Results

Figures 4.13 and 4.14 show several examples of the comparison between the standard AAR product (crosses) and the non-deglitched AAR (asterisks).

Table 4.1 displays the results of the line flux calculation after a Gaussian fit, for all those lines in the three observations in which points flagged as glitched were found.

Table 4.1: *Comparison between different processing methods*

Source	Line (μm)	Line flux standard AAR (W cm^{-2})	Line flux non-deglitched AAR (W cm^{-2})	% discrepancy
1	24.31	4.70×10^{-17}	5.31×10^{-17}	11.5
	25.88	7.79×10^{-17}	8.78×10^{-17}	11.3
2	15.55	4.81×10^{-17}	6.11×10^{-17}	21.3
3	10.51	3.01×10^{-18}	5.48×10^{-18}	45.1
	15.55	3.88×10^{-18}	1.10×10^{-17}	64.7
	25.88	3.38×10^{-18}	4.77×10^{-18}	29.1

The results of the analysis are:

1. Most spectral lines are either not, or only slightly, affected by glitch removal.
2. In few lines, some points at the wings of the line are flagged as glitched, causing the line profile in this region to deviate from the non-deglitched one.

3. In few lines, many points belonging to the line are flagged as glitched. Glitch removal applied to these points introduces a substantial error in the line profile and in the line flux.

4. For those cases described above, the non-deglitched line profiles can be fitted by a Gaussian function much better than the deglitched ones.

4.5.4 Conclusions

Generally the spectrum resulting from a fast speed AOT 1 observation is improved after glitch removal. However, when points belonging to spectral lines are flagged as glitched, one must be cautious about the line profiles and fluxes (except for band 4) because the line profile may be significantly distorted by glitch removal.

If a user wants to derive line fluxes from fast AOT 1's it will be necessary to check the datapoints around a line to see if they are flagged as glitched. If they are it may be necessary to visit one of the data centers so that additional data processing can occur.

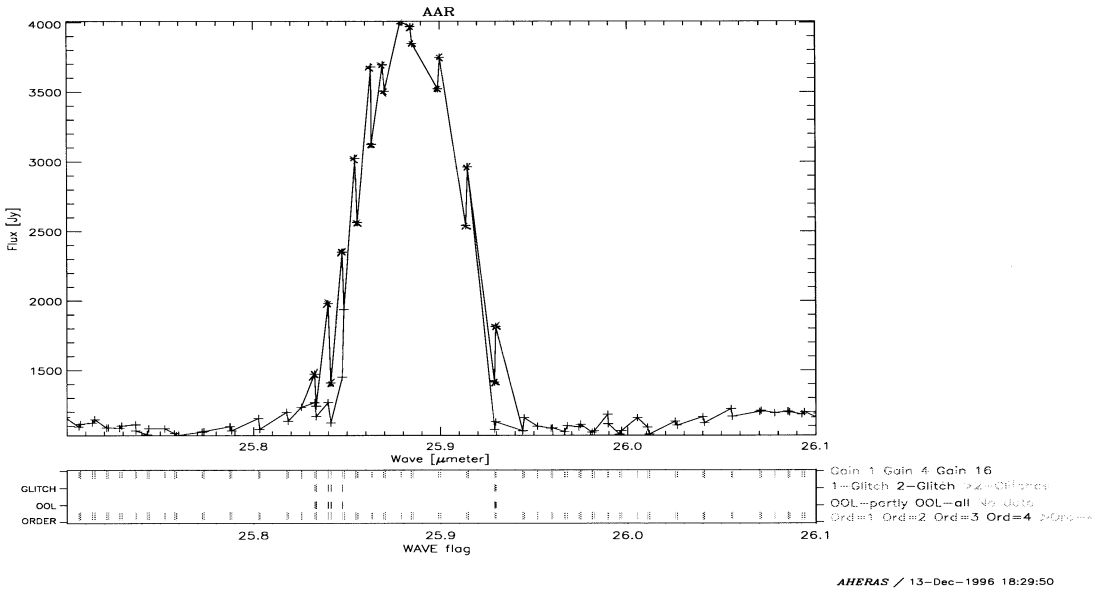

Figure 4.13: *Good AOT 1 line fitting. This is a case where the Derive-SPD glitch process has not misidentified any datapoints. The standard processing (crosses) and the processing without glitch recognition (asterisks) are similar.*

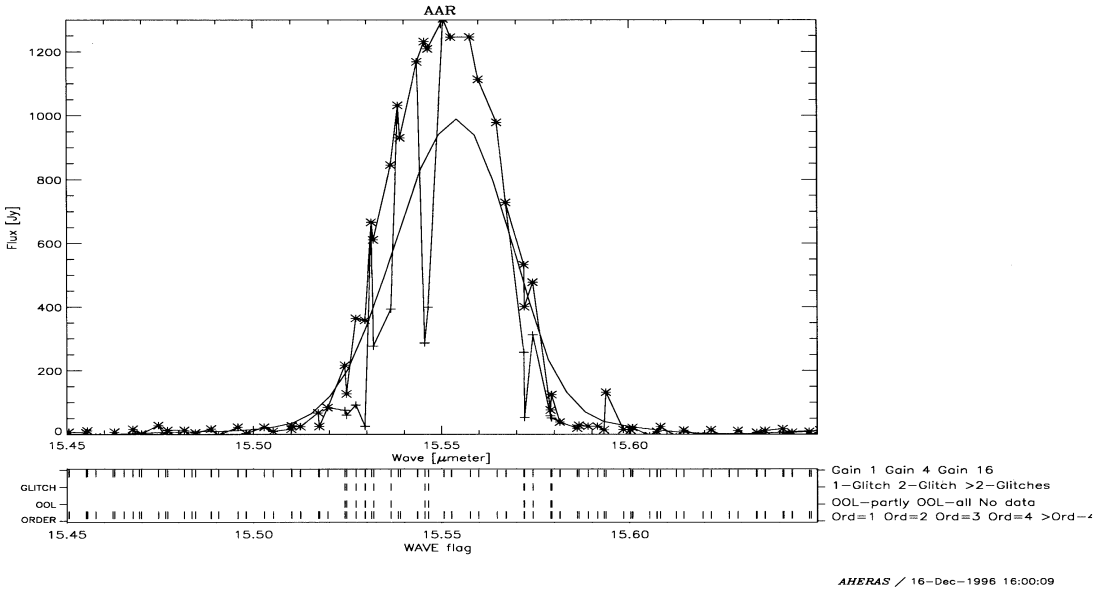

Figure 4.14: *Bad AOT 1 line fitting. This is a case where the Derive-SPD glitch process has mis-identified datapoints. The standard processing (crosses) is different to the processing without glitch recognition (asterisks). A gaussian fit to the standard processing is shown, and underestimates the line flux.*

4.6 Version history of the OLP Pipeline

The OLP pipeline went through several revisions during the ISO mission. From OLP version 5.0 all SWS products were declared scientifically valid. Prior to that version only the ERD had been declared valid.

To find out which version of the OLP software produced a FITS product look at the header field OLPVERS.

The history of the OLP pipeline is as follows:

V2.3 - released from 27 Oct 95

V2.3.1 - released from 13 Nov 95

V2.3.2 - released from 21 Nov 95

V2.3.3 - released from 8 Dec 95

V2.3.4 - released from 18 Dec 95

V2.3.5 - released from 26 Dec 95

V2.3.6 - released from 8 Jan 96

V2.3.7 - released from 10 Jan 96

V2.4 - released from 24 Jan 96

V2.4.1 - released from 5 Feb 96

V2.4.2 - released from 12 Feb 96

V2.4.3 - released from 19 Feb 96

V3.0 - released from 11 Mar 96

V3.1 - released from 18 Mar 96

V3.2 - released from 25 Mar 96

V3.3 - released from 2 Apr 96

No changes relevant to SWS.

V4.0 - active from 13 May 1996.

Often does not produce (proper) LW output and the wavelengths are incorrect for fast AOT 1 (speed 1,2,3).

V4.1 - active as of about 21 May 1996.

LW output (in terms of flux level) is corrected again, wavelengths for fast AOT 1's still bad.

V4.2.1 - active as of 11 June 1996.

SWS AC correction improved and standard deviation in SWS SPD now calculated correctly.

V4.3 - active 19 June 1996.

Column SWAALINE in SWS AA now filled properly.

V5.0 - active as of 19 August 1996

Scientifically validated pipeline.

V5.1 - active as of 1 October 1996

The system was changed so that when reprocessing data from a revolution the Cal-G files pertaining to that revolution would be used, instead of the latest ones. This is in case, e.g. the wavelength calibration changed during the mission leading to several wavelength calibration files each relevant for a portion of the entire mission. This was a transparent modification as far as users are concerned.

V5.2 - released as of 19 November 1996

No changes relevant to SWS.

V5.3 - released as of 13 December 1996

No changes relevant to SWS.

V6.0 - released as of 5 May 1997

Many changes. They can be found by looking through this document for the words 'OLP V6'. The most important are a better flux and wavelength calibration, the filling of the standard deviation field in the output (SWSPSTDV) with valid information, the extracting into the AAR only the science data rather than all data for which a valid wavelength could be assigned and the removal of several bugs.

V6.1 - released as of 1 Aug 1997

Cal-G files 13 and 25_x used by OLP 6.0 were derived with calibration analysis software inconsistent with the OLP V6.0 software (this was noted only after the deadline for OLP V6.0). Cal-G files 13 and 25_x were therefore re-derived to be consistent. The opportunity was also taken to re-derive some of the Cal-G 25_x files using observations of standard stars.

V7.0 - released as of 1 May 1998

This was the first post-mission pipeline released by the IDC. Prior to this there was no proper error calculation.

V8.4 - released as of August 1999

This added off-band data in the SPD and had updated error and wavelength calculation.

V8.6 - released as of 18 November 1999

This ensured Y2K compatability.

V9.5 - released as of 28 November 2000

The Derive-SPD part of the software was re-written in IDL, and many changes made. Derive-AAR was only changed slightly.

Chapter 5

SWS Calibration

5.1 Introduction

This chapter discusses the expected accuracy of the data obtained by SWS, the products derived from them and indicates where the main sources of error lie. The overall strategy is discussed in the SWS Calibration papers "The Photometric Calibration of the ISO Short Wavelength Spectrometer", by S.G. Schaeidt *et al*, [20], "The Wavelength Calibration and Resolution of the Short Wavelength Spectrometer" by E. Valentijn *et al*, [22], and the general paper on SWS by de Graauw *et al*, [7], in the A&A special issue (November 1996 Vol 315) devoted to ISO. In summary, internal calibration sources were used to tie together extensive ground based calibrations with in-flight observations of astronomical calibration sources.

The focal plane geometry and detector alignments are discussed in section 5.2. Flux calibration, and the calibration of the Relative Spectral Response Function, are discussed in sections 5.3 and 5.4, while the resultant accuracies are discussed in section 5.6. Sections 5.7 and 5.8 discuss the wavelength calibration and its accuracy.

5.2 Determination of focal plane geometry, array geometry and alignment

The relative positions of the various entrance apertures and detectors need to be known to ensure that one grating wavelength calibration can be applied to all combinations of entrance slit and detector. The respective offsets have been calibrated in instrument level tests on the ground. Beam profile measurements and wavelength calibrations on astronomical sources were used for in-orbit checks.

5.3 Flux calibration

The photometric sensitivity was determined on ground by scanning the spectrum of a calibrated blackbody source within the test cryostat. These tests resulted both in detailed spectral response functions for the various AOT bands and in a first calibration of the signal created by the internal stimulators. The signal from the stimulators was used to monitor variations in the broad band sensitivity of the detectors, e.g. due to memory effects.

In orbit, an extensive observing program on astronomical sources was executed to determine the correct conversion from signal (as measured from the detectors) to flux (emitted from the astronomical sources). It was started during PV and carried on at a lower level during the mission. The dark current measurements carried out on ground and in orbit were done with SWS shutter closed.

Flux calibration involves (1) fitting a slope to the 24Hz voltage detector samples for each reset interval and (2) converting this to a flux. This is complicated by the presence of non-linearities in the system, glitches, and how well the conversion of voltage/sec to fluxes is known. Parts 1 and 2 are handled by Derive-SPD and AA separately and are discussed in sections 4.2.8 and 4.3.6 respectively, with errors discussed in section 4.4.

At constant illumination the corrected output (see section 4.2.8) of the SWS detectors can be approximated as a voltage changing linearly with time;

$$V(t_{int}) = S \cdot t_{int} + O \tag{5.1}$$

Where t_{int} is the time within one integration.

The rate of increase of this voltage (i.e. the slope S) is a linear combination of the source flux incident on the detectors, the physical quantity of interest, for the relevant wavelength λ, instrumental gain G (dependant on observation time, detector block, detector number, aotband, λ), the dark current $D(t)$ (μV/sec) and the Flux conversion factor, F_{conv}, that relates the corrected signal to a flux value in astronomical units. The dark current $D(t)$ is determined by the gain and the detectors used for observing, and is a measurement on the observation.

The flux calibration involves converting the slope (S) in the above equation to a flux:

$$\begin{aligned} I(\lambda) &= G(t, detectorblock, detectornumber, aotband, \lambda, RSRF) \\ &\quad \cdot F_{conv} \cdot (S(t,\lambda) - D(t)) \end{aligned} \tag{5.2}$$

Note that in this equation it is implicitly assumed that *all* memory effects (see section 6.8) can be neglected or have been removed.

With the instrumental gain split into several orthogonal components:

$$\begin{aligned} G(t, block, detector, aotband, \lambda, RSRF) &= G_{photmetric}(t, block) \cdot \\ &\quad G_{flatfield}(detector, aotband) \cdot \\ &\quad G_{RSRF}(detector, \lambda, RSRF, aotband) \end{aligned} \tag{5.3}$$

$G_{photometric}$ accounts for time variations in the detectors response at the time of observation. This correction brings the measurement to a standard time determined by the Cal-G file 41, and is calculated from the internal grating calibrator.

$G_{flatfield}$ is a gain correcting for an individual detectors response relative to the average of the detectors. This gain brings all the detectors (within an AOT band) response to that of one average detector.

G_{RSRF} Corrects for the response of a detector at wavelength λ (anywhere within the AOT band) relative to the response of that detector at the key wavelength of the AOT band. This information is held in Cal-G files 25_x.

Following equation 5.2 the actual source flux $I(\lambda)$ is reconstructed by first subtracting the dark current from the measured slopes, and subsequently applying the instrumental gain and the flux conversion to convert the signal at a key wavelength of an AOT band to flux in Jy.

5.4 The RSRF and Effect of Fringes

The Relative Spectral Response Function (RSRF) is the total throughput of the system (telescope, grating, optics, detectors etc) as a function of the wavelength. It arises from the convolution of the detector response as a function of wavelength, the filter response as a function of wavelength and takes such effects as geometrical considerations (e.g. slit width, source structure) into account.

Fringes are a modulation with wavelength of the light falling on the detectors. The fringes arise due to constructive/destructive interference in either in the detector material itself (between the front and back of the detector) or similarly in the filter material. To some extent all detector bands suffer from fringes. Bands 1, 2 & 4 are only lightly affected, whereas the fringes are more pronounced in band 3. An example of fringes in the band 3D spectrum of a star can be seen in figure 5.1.

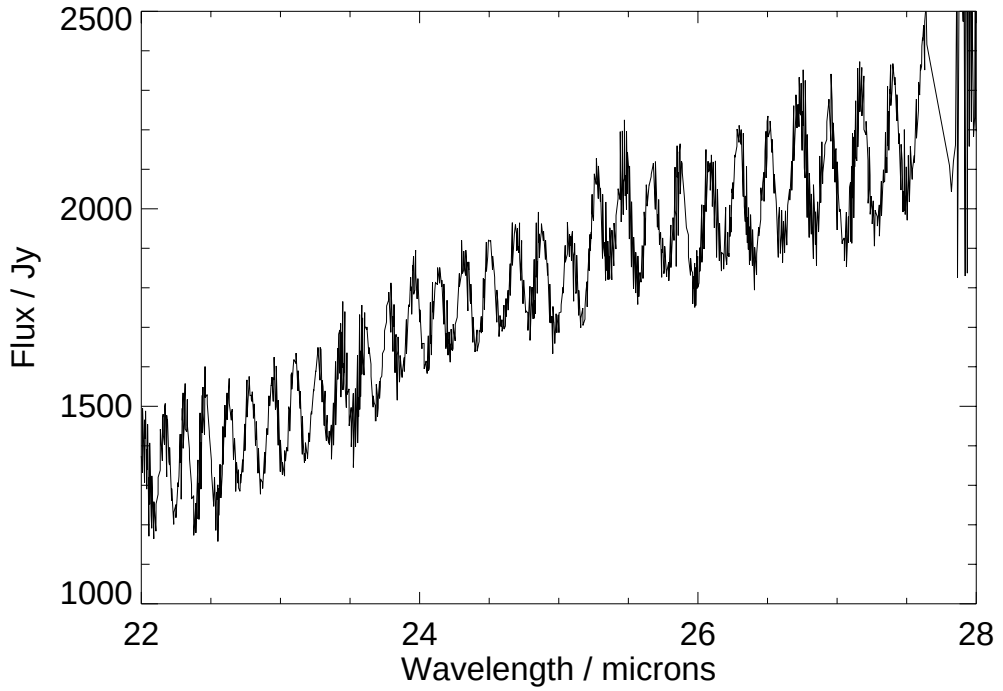

Figure 5.1: *Example of fringe effects in band 3.*

An attempt is made to remove fringes during the OLP processing pipeline. However, because the fringes may shift in wavelength space depending on where the source is in the slit (especially in the dispersion direction) and whether the objects being observed is a point source or extended, fringe removal may not be perfect. This may cause problems for observations of faint sources. Any faint features should always be checked against the relevant Relative Spectral Responsivity File, SWS Cal-G 25_x, to ensure they are not artifacts.

5.4.1 The RSRF calibration

The RSRF of the SWS Flight Model was intensively measured in the laboratory prior to launch. The calibration source used was a cryogenic black-body source with temperatures between 30 and 300K. After the launch of ISO, the recalibration of the RSRF was performed on standard stars and asteroids using

calibration uplink procedures. These scan more than the allowed wavelength range for each AOT band and ensure each scanner position is scanned.

The in-flight RSRFs are derived using the SWS Interactive Analysis package. The measurements are processed as in the standard pipeline up until the flux conversion steps. The RSRF is then obtained by dividing this 'raw' spectrum by a model of the observed source. For stellar sources containing spectral features, small inaccuracies in the model can introduce false features in the RSRF, and thus in every spectrum processed with this RSRF. Therefore, extreme care has to be taken before 'correcting' the RSRF.

5.4.2 RSRF Calibration sources and model sources

A full description of the calibration of the Relative Spectral Response Function is given in document [23]. This document should be consulted if it is necessary to understand the history of the calibration or for details of the models used.

5.4.3 Accuracies of the RSRFs

Two problems affect the RSRF: instrumental features introduced either via the laboratory RSRF measurements or the in-orbit calibration sources; and problems introduced in the data processing stage by poor dark current estimation and subtraction. Both of these are discussed in the following sections.

While users should check these sections before claiming the existence of any features, they usually only affect objects at the few percent level.

5.4.3.1 RSRF Artifacts

Features found in SWS spectra and attributed to the RSRF are:

- Band 2C: 9-9.3 μm : possible residue of the correction for the instrumental absorption feature.
- Band 2C: 10.1 μm : possible residue of the correction for the instrumental emission feature.
- Band 2C: 11.0 μm : possible residue of the correction for the instrumental emission feature.
- Band 3A: 12.3 μm : possible residue of the correction for the instrumental emission feature.
- Band 3A, 3C, 3D, 3E : the fringes in bands 3 were also observed during the instrument level tests, so they are also present in the RSRF and will be divided out. However, the fringes in the RSRF are less resolved than in high resolution observations on point sources since the blackbody in the lab was extended to the SWS slit. Slight pointing errors will also result in a wavelength shift of the spectrum observed, so that the fringes can be slightly shifted wrt to the fringes in the RSRF, and this will result in fringe residues in the spectra.
- Band 3D: the red side of band 3D shows leakage from the wavelength region around 14 μm. Since the RSRF was corrected based on observations of stars that have a relatively high flux at 14 μm, no proper correction of the RSRF in the leakage region was applied. In spectra of cold sources a false drop at the end of band 3D can be seen.
- Band 4 : no in-orbit correction has been applied due to lack of suitable observations/sources. It is now known that the lab measurements show a strong debiasing effect, and it can thus be expected that the shape of the current band 4 RSRF has a global inaccuracy of about 10%.

5.4.3.2 RSRF features propagated to the spectra after wrong dark subtraction

The effect on the final spectrum of subtracting a wrong dark-current value depends on the RSRF in the wavelength region affected. The SWS RSRFS are not flat – they show steep slopes at the ends of the bands, and various bands show distinct features in their RSRF. The RSRF correction has to be applied on data for which a proper offset correction is done, i.e. the dark current subtraction has to be done correctly. If the dark current subtraction is not done properly, dividing the data by the RSRF will induce false shapes in regions where the RSRF shows features or where the RSRF has a steep slope. Poor matches between different AOT-bands can often be understood (and corrected for) from such a combination of dark current uncertainties and a steep RSRF in the overlap region. An example can be seen in figure 5.2. Shown is the original spectrum in band 3A (black, lower curve) and the spectrum in band 3c (blue). There is a clear discrepancy between the flux level and the slope of the spectrum in the overlap region. If we vary the dark current levels in the data with 10 % before applying the RSRF, we obtain the green spectrum for band 3A. The continuity of the spectrum at the band borders is much better now. 10 % is typically the difference between two dark current measurements in an observation, so it is not unreasonable to assume that the dark current measured for the 3A scan in this observation is off by 10 %.

The figures in Vandenbussche 1999, [23], show where the RSRF is steep or show features and thus where the risk for these artifacts exists. If the signal level of a scan is of similar strength to the dark currents for that band, it is wise to check if discontinuities at band overlaps or features whose position coincides with RSRF features are real or artifacts.

5.4.4 Overview of the RSRF curves

RSRF curves for one representative detector in every AOT-band are plotted in document [23], which should be referred to when checking against any possible false features due to incorrect RSRF correction.

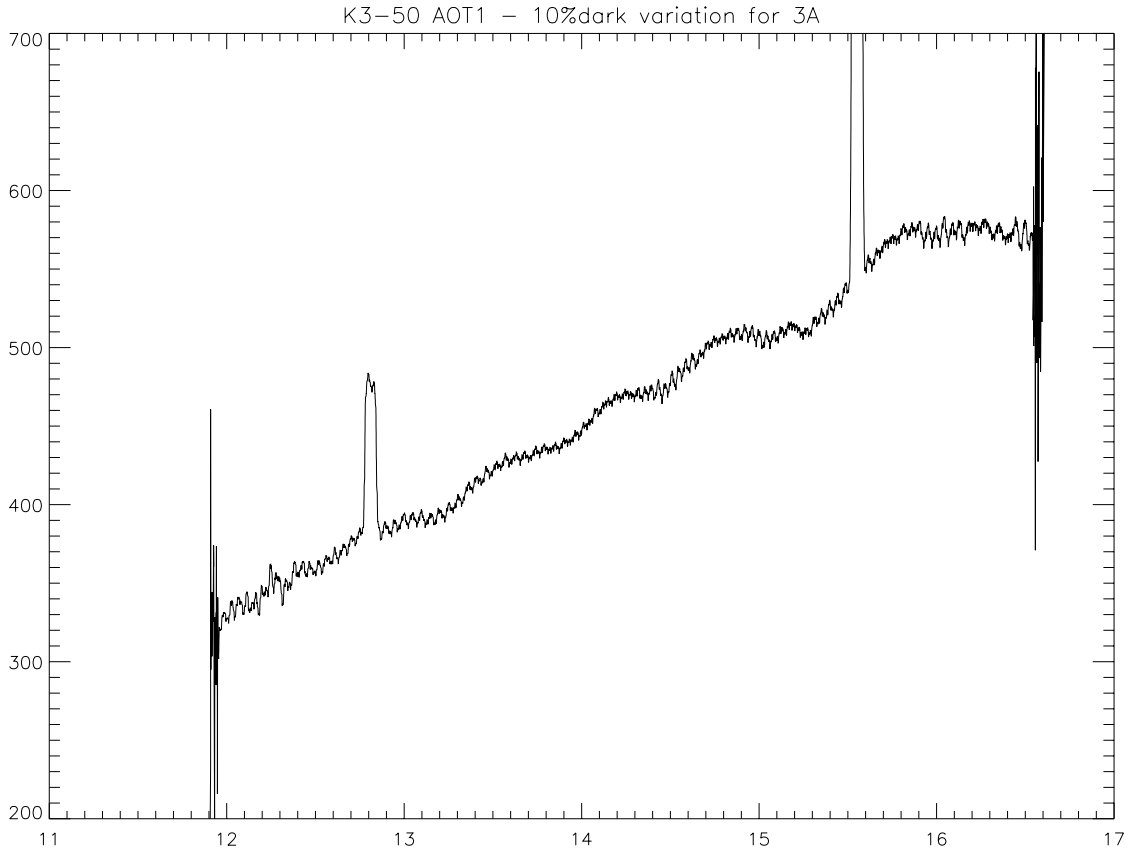
K3−50 AOT1 − 10%dark variation for 3A
700
600
500
400
300
200
11
12
13
14
15
16
17

additional corrections were equivalent to 0.8 LVDT for the wavelength calibration source angle and 0.3 LVDT for aperture 1. For the SW section, the correction was 6.5 LVDT for detector band 1.

Also used were observations towards η Car with the FP in a fixed position and the grating scanning. The wavelength calibration of the FP for the peaks of the fringes from the strong continuum was used to update the wavelength calibration for wavelengths above 35 μm where suitable emission lines in PN are lacking. This relied on the (ground based) calibration of the FP.

Table 5.3: *Lines used for grating wavelength calibration*

Ion	Wavelength μm
[Mg IV]	4.488
[Ar VI]	4.527
[Mg V]	5.608
[Ar II]	6.895
[Ar III]	8.991
[Si IV]	10.510
[Ne II]	12.814
[Mg V]	13.521
[Ar V]	13.102
[Ne III]	15.555
[S III]	18.712
[Ne V]	24.318
[O IV]	25.890
[S III]	33.481
[Ne III]	36.014
plus H recombination lines	

For the FPs the situation was different. Here the internal wavelength calibration source was a fixed, stable FP, providing a series of very narrow transmission peaks. The in-orbit wavelength calibration of the two FPs relied mainly on the ground calibration of these peaks which was assumed to be unchanged in-orbit. Line observations towards astronomical sources were used for confirmation only.

5.8 Wavelength calibration accuracy

The goal of wavelength calibration was to achieve an accuracy of between 10 and 20% of a resolution element for the two gratings. An accuracy of 10% was hoped for the LW grating as this is used by the FP wavelength calibration.

5.8.1 SW & LW Grating

The errors expected on the wavelength calibration of the grating are shown in Table 5.4. It lists the requirements on ISO, what has been achieved in ground tests and during operations.

Table 5.4: *Grating Wavelength calibration errors.*

	SW	LW	
		$< 40\mu$m	$> 40\mu$m
Requirements	$< \lambda/10000$	$< \lambda/10000$	$< \lambda/10000$
Obtained on	< 1 LVDT	$< 0.5 - 1.0$ LVDT	2.0 LVDT
ground	$\lambda/10000$	$\lambda/12000 - \lambda/20000$	$\lambda/6000$
Flight Achieved	1 LVDT	0.5 - 1 LVDT	
	$\lambda/5000 - \lambda/12000$	$\lambda/8000 - \lambda/16000$	

The limitations on the grating wavelength calibration accuracy appear to come from pointing, see section 6.10.

Overall the wavelength calibration stabilisation was kept accurate to within 1 LVDT during the mission. This was achieved by updating the calibration files at irregular intervals. After about one year of operations it became clear from the biweekly quick grating wavelength check that the calibration was shifting slightly. In revolution 356 and 370 full grating scans were therefore performed to check on this, and the shift was corrected by an update of the calibration files. Three more full grating scans were performed in revolutions 475/479, 669/670, and in the last month before He-boiloff. They were analysed and again resulted in updates to the grating polynome.

As it became apparent that regular updates of the grating polynome would be necessary, it was also decided to have a regular look at some external source with strong emission lines. Between revolution 360 and 800 27 of these observations were performed on NGC6543, observing 8 lines in the SW section and 5 in the LW section. The lines were analysed, and one noticeable effect was discerned, a slowly increasing trend in LVDT against time. This indicated that a more precise wavelength calibration would be possible by linear interpolation of the calibration files, and this was inserted into V8.4 of the OLP.

5.8.2 Fabry-Pérot

For the two FPs relevant information concerning wavelength calibration accuracies is shown in Table 5.5. Throughout the mission no wavelength shifts of more than 1 FP scan step were found, within the requirements listed in the table. More information on this can be found in Feuchtgruber 1998, [4].

The accuracy of the internal wavelength calibration was, as expected, about 1 FP scanner step at $24\,\mu$m, which corresponds to about 10^{-4} μm. However, the effective FP gap is slightly dependent on wavelength, because shorter wavelengths penetrate deeper into the reflecting meshes. During the ILT's, vapour absorption lines were measured to determine this gap correction, which had a maximum of about one FP resolution element over the full wavelength range of the FPs. Remaining uncertainties of this correction and the memory effects of the Si:Sb detector material used in the shortwave FP section cause a final uncertainty in the wavelength calibration of 2 FP scanner steps between 11.4 and 26 μm, and 1 FP

Table 5.5: *FP Wavelength calibration errors.*

	SW-FP1	LW-FP1
Requirements	$< \lambda/100000$	$< \lambda/100000$
Obtained on ground	$\lambda/125000$	$< \lambda/125000 - \lambda/200000$
Flight Achieved	$\lambda/100000$	$\lambda/100000$

scanner step between 26 and 44.5 μm. Regular checks of the internal calibration during PV and routine phase indicate excellent stability.

The verification of the wavelength calibration by observations of external spectral lines suffered from the lack of accurate wavelength standards and radial velocities. However, a few lines could be used to verify the internal calibration and the resulting accuracy was 1/3 of a resolution element or better.

Chapter 6

Instrumental Characteristics

6.1 Introduction

This section discusses the behaviour of the instrument, detectors etc as determined from in-orbit measurements.

6.2 Grating Performance Overview

The SWS instrumental signal-level unit is $\mu\mathrm{Vs}^{-1}$, the average rise of the voltage of the ramp during one second of time (see section 2.4 for an explanation of this). It is found that the signal response of the instrument is a linear function of the illumination over a very large range of input signals (0.5–100,000 Jy), when hysteresis effects are ignored. Therefore this unit is fully qualified for simple linear calculations backwards and forwards relating source flux density, instrument signal level, instrument noise level and noise equivalent flux density (*NEFD*, *i.e.*, the input flux density which gives an output signal with a signal-to-noise ratio $SNR = 1$). The SWS grating sections produce a $\sim$1.3-3 $\mu\mathrm{Vs}^{-1}$ signal on a single detector element for a source flux density of 1 Jy.

Both the response and the noise of the detectors have been characterized as function of signal strength. Table 6.1 summarizes the overall properties of the detectors.

For sensitivity calculations, the noise per reset interval may be summarized as

$$N[\mu V/s] = \frac{\sqrt{N_R^2 + (N_D^2 + N_S^2 S)t_r}}{t_r} \tag{6.1}$$

with S the signal in μV/s and t_r dimensionless (happens to be equal to the reset interval in seconds). The empirically determined noise parameters N_R (read noise, in μV/s) N_D (dark current noise, in μV/s), and N_S (signal shot noise, $\mu\mathrm{V}^{0.5}/\mathrm{s}^{0.5}$) have been obtained by forcing a fit through this function, and are summarized in Table 6.2. For the SW grating and the FP detectors the function works well up to a $t_r \approx 8$ sec (although 8 second resets were only used for a short period at the start of the mission). For the LW grating detectors the function does not work well in describing the t_r dependency, and the resulting values are not necessarily directly to be associated with read noise and dark noise. Parameter values are chosen in such a way that they give the best description for the short reset intervals.

For Band 4, test measurements show consistently a very poor increase of *SNR* for $t_r > 2$ sec. The parameters listed in table 6.1 for band 4 apply to $t_r = 1$ sec and $t_r = 2$ sec.

Table 6.1: *Summary of SWS detector properties for a reset interval $t_r = 2$ sec*

detector	T (K)	bias (V)	minimum system noise[3] (μV/s) gain=16	minimum system noise[3] (electrons)	int.[4] (μV/s)	average response (μV/s/Jy)[5]
Gr–InSb	3	-	0.7	35	0.32	3.0
Gr–Si:Ga	3	12	1.5	75	0.32	1.6
Gr–Si:As	4.5	3.0	3.0	150	0.40[2]	1.5
Gr–Ge:Be	2	0.6	2.0	100	1.00	1.3
F-P–Si:Sb	10	1.1	1.1[1]	70	0.40	0.007
F-P–Ge:Be	2	0.6	3.0	200	0.40	0.0037

Notes:

1. values listed for element 2; noise = 0.7 μV/s for element 1

2. this is the excess photon noise measured at Signal levels $> 1000\mu$V/s

3. measured at a signal power at which photon noise is negligible; except FP-Ge:Be where still some photon-noise is suspected; estimated photon-noise free $NEP_2 = 1.05 \times 10^{-16}$ W/$\sqrt{Hz}$

4. int. is intercept: photon noise at signal = 10 μV/s

5. 1 Jy = 10^{-26} WHz$^{-1}m^{-2}$, ISO telescope area taken as 0.28 m^2

Table 6.2: Grating noise parameters

	Units	Band Material range (μm)	1 InSb 2.38–4.05	2 Si:Ga 4.05–12.0	3 Si:As 12.0–29.5	4 Ge:Be 29.5-45.2
N_R	$\mu V/s$		0.75	0.75	1.00	1.56
N_D	$\mu V/s$		0.70	1.50	3.00	2.00
N_S	$sqrt\mu V/s$		0.10	0.13	0.14	0.32

6.3 Fabry-Pérot Overview

The SWS Fabry-Pérot section may be used for wavelengths between 11.4 and 44.5 μm. Instrument level tests showed that performance in the extended wavelength range outside the nominal design wavelength range of 15–35 μm was good enough to make the extended range available. A few remaining peculiarities of the extended range are discussed together with the following performance description. Results throughout this section refer to use of the Fabry-Pérot AOT bands of Table 2.2 that have been selected to give the best tradeoff between the various design goals (high sensitivity, low leakage etc.).

6.3.1 Spectral Resolution

The Fabry-Pérot spectral resolution was measured in laboratory tests at a few discrete wavelengths using solid state laser sources. Figure 6.1 shows the spectral resolution as a function of wavelength, interpolated between these measurements. The spectral resolution decreases towards the short wavelength ends of the wavelength ranges covered by the two Fabry-Pérots, where the wavelengths corresponding to the resonances of the reflective meshes are approached. The Fabry-Pérot spectral resolution depends on precisely parallel F-P plates.

Measurements of the Fabry-Pérot spectral resolution in-orbit suffered from the lack of bright, narrow lines. Three lines were measured and lower limits found to the spectral resolution that were very close to expectations. This is reported in Valentijn et al. 1999, [22]. The lower limits are plotted in figure 6.1.

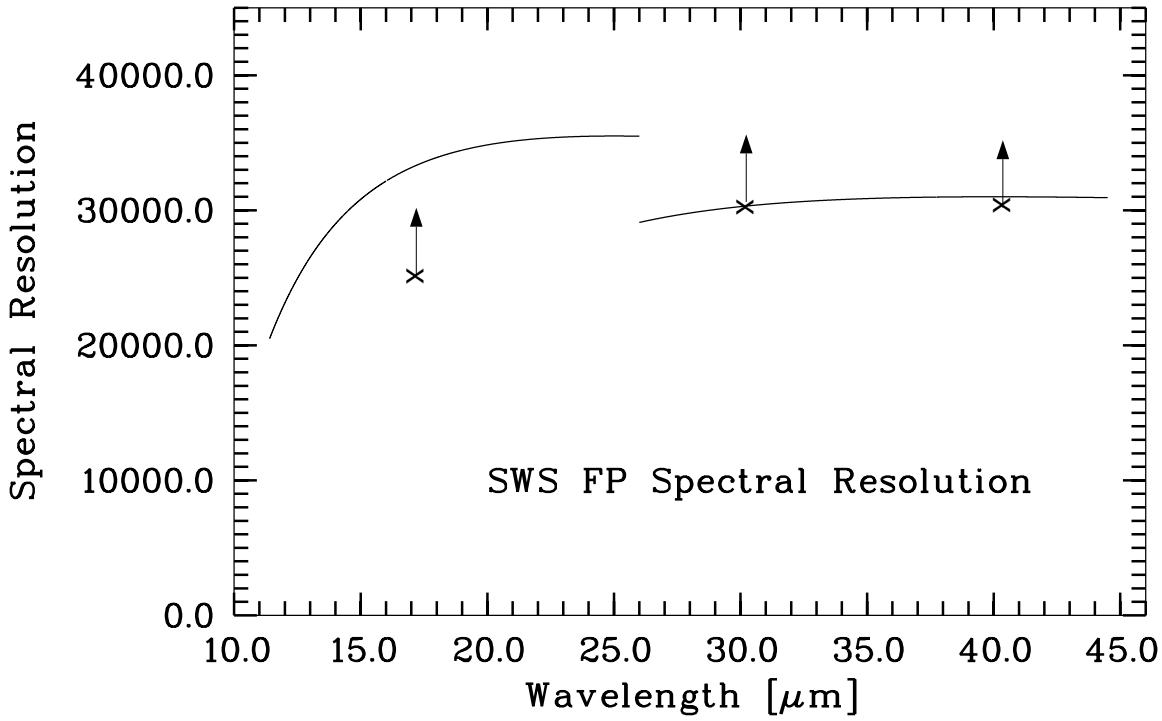

Figure 6.1: *SWS Fabry-Pérot spectral resolution as a function of wavelength, computed from measured mesh properties and confirmed by checks at three wavelengths, as shown by lower limits.*

6.3.2 Sensitivity

The F-P sensitivity was characterized in instrument levels tests by doing measurements on a calibrated blackbody source within the test cryostat. Figure 6.2 shows the SWS Fabry-Pérot spectral response. The conversion between units applicable to astronomical sources (Flux density of a point source in Jy) and the resulting instrumental signal (μV/s) is given as a function of wavelength. Diffraction losses caused by the fact that the aperture is comparable in size to the ISO diffraction disk have been taken into account; the flux used to derive figure 6.2 is the true point source flux. The effect of these diffraction losses is however not large (figure 6.3).

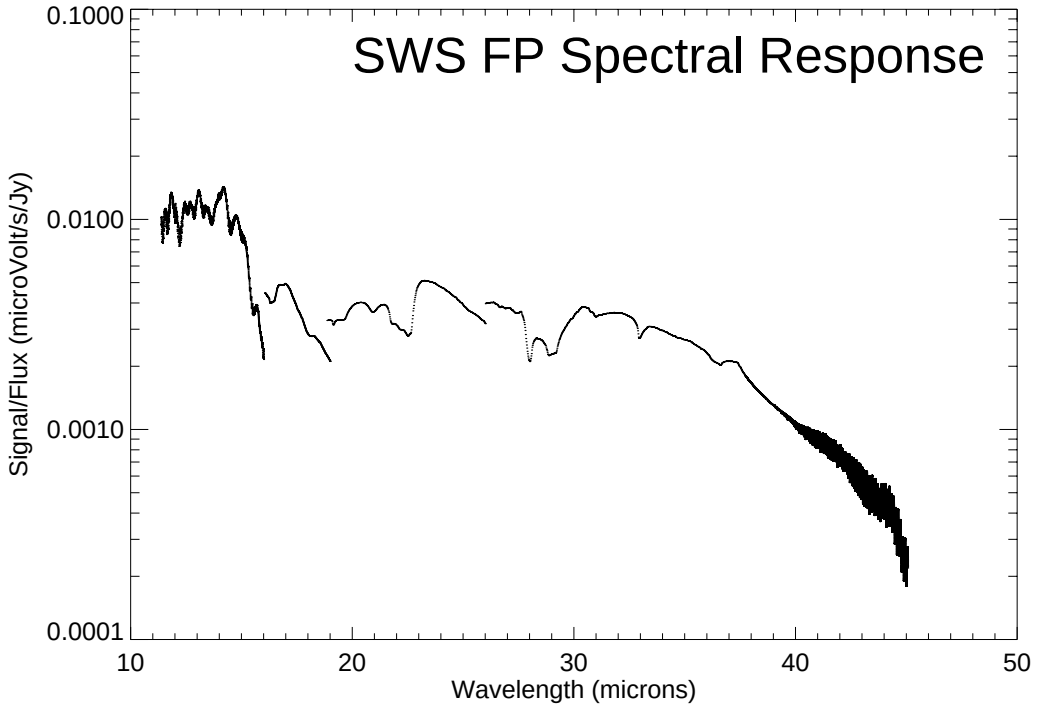

Figure 6.2: *SWS Fabry-Pérot spectral response. The flux scale corresponds to a point source, diffraction losses at the aperture have been taken into account.*

The spectral response curve has structure on various wavelength scales. Large scale trends are determined by the counteracting effects of detector spectral response increasing with wavelength until close to the detector cut-off wavelength, and decreasing transmission of the Fabry-Pérot interferometer. Structures on scales of microns or tenths of microns can be traced to the detector spectral response curves and filter transmission curves. A rapid low-amplitude modulation in the 11.4–16 μm range (not resolved in figure 6.2) is caused by reflections between the surfaces of the transmission filter used behind slit 1 in the long-wavelength section of SWS. This 'parasitic Fabry-Pérot' effect is also observed for grating data using the same slit. The stronger modulation detected at $\lambda \geq 40\,\mu$m in the long-wavelength extended range is again caused by a parasitic Fabry-Pérot effect, this time in a reflecting CaF_2 filter. The nearby reststrahlen resonance of CaF_2 causes strong variations with wavelength of the indices of refraction and absorption, leading to the observed modulation pattern. The modulations were characterized with sufficient accuracy to allow good flux calibration in the extended wavelength ranges.

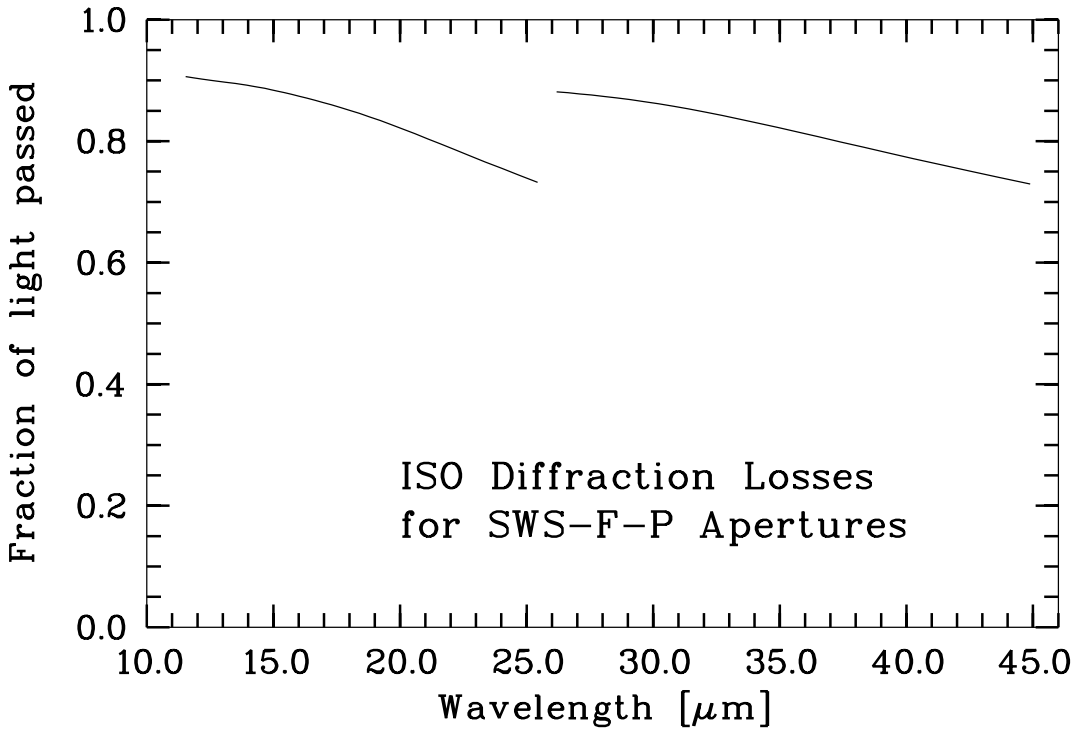

Figure 6.3: *Computed ISO diffraction losses for the SWS F-P channels. The fraction of the ISO diffraction disk accepted by the effective SWS F-P aperture is shown as a function of wavelength.*

6.3.3 Noise

Measurements of noise for various reset intervals and signal levels during the SWS instrument level tests resulted in the following characterization of the noise behaviour of the F-P detector and integrating preamplifier system:

- Noise at low signal levels is independent of signal. Here, noise as a function of reset interval can be approximately modelled as the quadratic sum of a constant read noise term and a dark current noise term increasing with time. Deviations from this model exist but may be ignored for simple sensitivity estimates
- At higher signal, *SNR* improves only with the root of the signal, indicating dominance of shot noise.

For sensitivity calculations, this may be summarized as

$$N[\mu V/s] = \frac{\sqrt{N_R^2 + (N_D^2 + N_S^2 S)t_r}}{t_r}$$

with S the signal in μV/s and t_r dimensionless (happens to be equal to the reset interval in seconds). The empirically determined noise parameters N_R (read noise, in μV/s) N_D (dark current noise, in μV/s), and N_S (signal shot noise, $\mu V^{0.5}/s^{0.5}$) for the two F-P detector materials are summarized in Table 6.3.

6.3.4 Saturation

No saturation problems are expected for the SWS Fabry-Pérot detectors. The saturation limit is given by the fact that the integration ramp for 1s detector reset interval does not hit the saturation level

Table 6.3: *Fabry-Pérot noise parameters*

Band	5	6
detector	FP-Si:Sb	FP-Ge:Be
range (μm)	11.4-26	26-44.5
N_R	0.63	0.89
N_D	1.00	3.00
N_S	0.18	0.13

of the warm electronics for signals less than about 20,000 μV/s. Although not foreseen in the current design of the offline data processing, it is in principle possible to obtain data for signals about seven times stronger by analysis of partial integration ramps. It is assumed here that the expected strong flux has been correctly specified in the AOT input, since only then the gain and reset time are set properly. Taking typical values from figure 6.1 and figure 6.2, the 20,000 μV/s limit corresponds to a saturating flux density of about 2×10^6 Jy, or a saturating flux in an unresolved line of about 10^{-11} Wm^{-2}.

6.3.5 Leakage

The Fabry-Pérot section uses the grating as an order selector that suppresses unwanted F-P orders. This suppression is not complete for part of the SWS wavelength range. Neighbouring F-P orders 'leak' through the wings of the grating instrumental profile, contributing significantly to the total measured signal (See Figure 6.4). For observations of a single line superposed on a smooth continuum, the only drawback of leakage is a more complicated flux calibration, since leakage will increase the observed continuum but not the line. More serious effects occur in crowded spectra, where strong lines seen in the 'wrong' F-P order may significantly distort the observed spectrum, requiring observations of wider wavelength ranges in order to determine the severity of this effect and 'clean' the spectrum.

Leakage has been quantified by analysis of the grating instrumental profile as seen by the F-P detectors in scans of solid state laser lines. Figure 6.5 shows the leakage as a function of wavelength. It must be considered preliminary, since it is based on extrapolating the grating instrumental profile from measurements only at a few wavelengths of laser lines.

Figure 6.6 shows the effect of leakage on a observation of a single line specially planned to observe the leakage. Because the observation was carried out over a large wavelength interval two 'ghost' lines appear either side of the real line. Usually these 'ghost' lines would not appear in observations, as they cover a much smaller wavelength range. The observed NeIII line is very strong and, as the FP scans from longer to shorter wavelengths, the line appears non-symmetric because of memory effects in the Si:Sb detector. The 2 leaking orders do not have the same intensity because the grating instrumental profile is not centered on the main order. This slight deficiency in the grating wavelength calibration, although within specifications, translates into this non-symmetric pattern compared to the ideal case shown in figure 6.4 where the leaking orders have the same height.

The spectral response data in section 6.3.2 have not been corrected for the effects of leakage, i.e. they refer to the total signal.

6.3.6 Tracking Noise

The coordination between Fabry-Pérot scans and the movement of the grating that tracks the F-P scan is a source of signature (or, loosely, 'noise') that ultimately limits the quality of F-P spectra on bright sources. For all but very short F-P scans, the wavelength sampled by the F-P would soon be no longer tuned to the transmission peak of the grating if there were no tracking. The discrete steps of the grating's

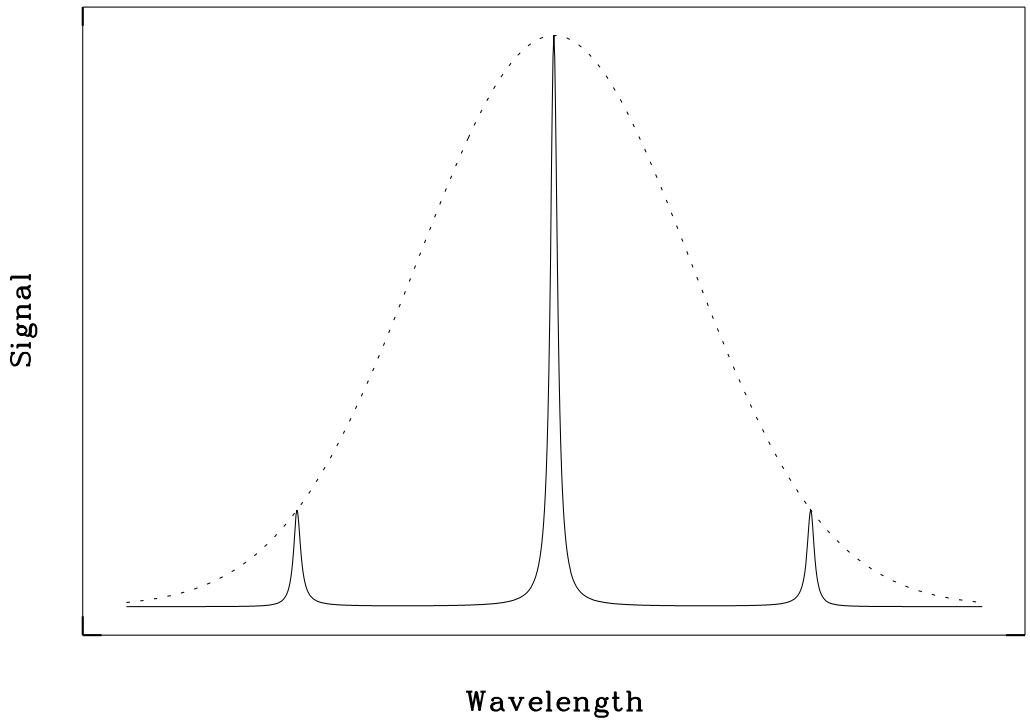

Figure 6.4: *Basics of leakage in F-P spectra. The instrumental profile of the combination of F-P and grating is given by the solid line. Residual transmission from neighbouring F-P orders occurs if the instrumental profile of the grating alone (dashed line) is too wide.*

tracking movement result in the final F-P scan of a pure continuum source looking like a repetition of a small section of the grating instrumental profile.

The amplitude of this 'noise' depends on various factors like quality of grating wavelength calibration, ratio between grating stepsize and line profile FWHM, pointing stability. It is hence difficult to predict for an observation at a certain wavelength. Instrument level tests with optimized grating wavelength calibration showed 'signal-to-noise' around 200. In the case of an observation of a single line on a smooth continuum, part of the 'noise' could be calibrated out by observing a larger region of continuum around the line, provided the non-systematic contribution of pointing jitter is not too large.

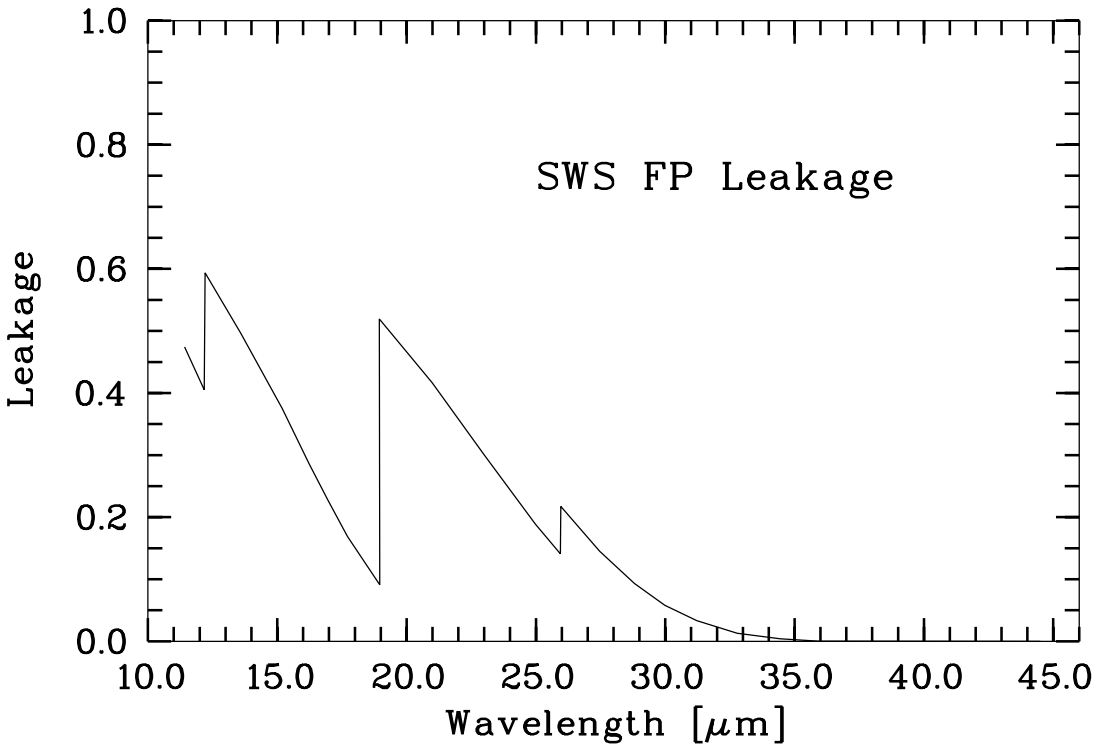

Figure 6.5: *SWS Fabry-Pérot leakage. Leakage is defined here as the fraction of the total detected signal that originates in unwanted Fabry-Pérot orders. The data shown here are based on extrapolation from measurements at a few wavelengths.*

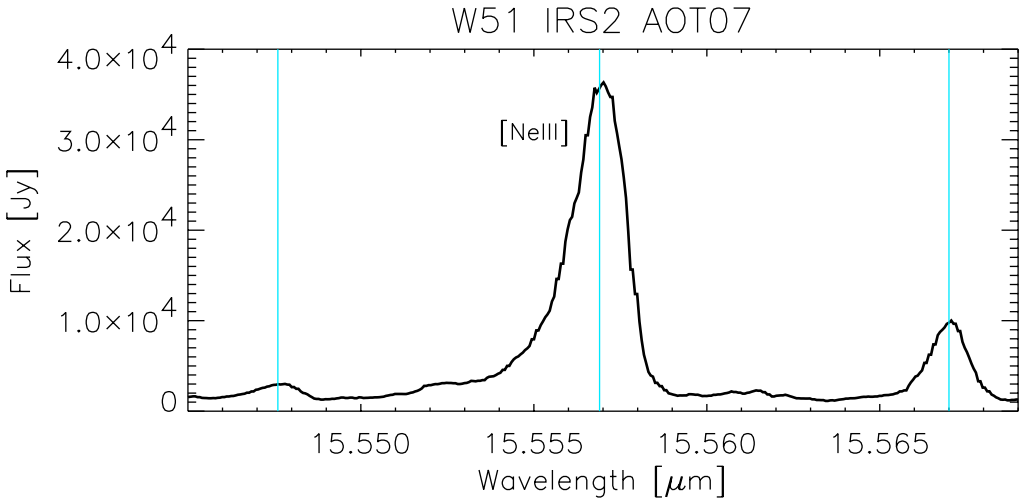

Figure 6.6: *Example of FP leakage on a single line. A large wavelength range was scanned for this measurement, resulting in two 'ghost' lines at approximately 15.548 and 15.567 μm from leakage of the real line at 15.557μm.*

6.4 Detector Noise & Dark Current

Tables 6.2 and 6.3 give average detector dark noise for an entire band for a one second reset interval in column N_D. The detector noise given is that if some processing has been carried out on the data, namely throwing away samples affected by glitches. For comparison, the pre-launch values of detector noise were 0.6 μV/s for bands 1, 2, 3 & 5 and 0.9 μV/s for bands 4 and 6.

Detector dark noise and dark current values for individual detectors are stored in calibration G files 21_1, 21_2, 21_4 and 21_8, corresponding to the 1, 2, 4 and 8 second reset interval. Units are μV/s. Note that 4 and 8 second resets were only used early in the mission for calibration measurements.

Checks were made at the start of every revolution for the purpose of characterising the dark current and noise throughout the mission. It was found that they were stable for all bands except band 3. Here, the dark currents increased by up to a factor of three during the mission, while the dark noise hardly increased for most detectors. In most cases the increase in dark currents was gradual, but occasionally it was from a sudden jump, e.g. detector 36 (band 3 detector 12) on rev 150. Dark currents also decreased - after 250 revolution of high dark currents, those in detector 36 dropped to one-fifth of their high value.

Which detectors in a band are or are not good can change. For example, at the start of the mission band 3 detector 34 was poor. After PV, when its bias voltage was changed, detectors 30, 31 and 36 were the worst in that band. In general a bad detector has either a high dark current or/and a high noise.

The dark currents were higher at the start of a revolution for all bands, decaying with time so that after about four hours they had reached their nominal values. This was especially the case for bands 2, 4 and 6, with darks currents between 15% and 100% higher than nominal at the start of a revolution. This effect was less important for bands 3 and 5, while for band 1 it was only observed in a few detectors.

The dark noise showed no variation throughout a revolution.

Normally all changes in dark current will be automatically corrected during the OLP processing, see section 4.3.4. Cases where the continuum is weak can cause problems for dark current subtraction in the OLP pipeline, especially when memory effects are included. When the amount of flux falling on the detector is small, there may be cases where the output of the detector from (incident flux plus dark current plus noise) is less than the output from (dark current plus noise), the end result being negative fluxes in the AAR product. The limiting flux for this is of the order of a few Jy for band 2.

6.5 Detector Response

The variation in the detector response throughout the mission, as determined from photometric checks, was below 5%. While for bands 1 and 2 this change was of a random nature, the band 3 responses showed a slight anti-correlation with dark currents, and the band 4 response increased by a small amount.

During a revolution, the band 1 response was stable to within 2%, whereas for band 2 the response was higher by 40% at the start of a revolution, decreasing with time. For bands 3 & 4 this effect was only at the 10% level.

Again, normally all detector response changes will be automatically corrected during the OLP processing, see section 4.3.5

6.6 Behaviour around a reset

As was discussed in section 2.4, "SWS Detectors and operation", the destructive readouts that occur every 1, 2 or 4 seconds affect the readout electronics, which then take some time to return to normal. An example of this can be seen in figure 6.7 (an example of a glitch). It shows the ERD output of detector against time. A reset interval of 1s is used, therefore there are twenty-four samples per reset.

In this example, the first sample read out from the amplifier after a reset is the one located at a bit value of about 2800. The second is at about 2700 and the third is at 2000 – due to the rate at which the capacitor is charging the third sample appears to be an extrapolation of the previous ramp. When a slope is fit to the 24 Hz readouts the first few readouts are ignored, because they are affected by the destructive readout. The number of detector samples to ignore is given in Cal-G file 3. During PV it was found that the default number of samples to ignore after a reset was different from that thought pre-launch, so the contents of this calibration file was changed.

After the third sample the output of the amplifier seems to have stabilised and the capacitor seems to be charging up linearly, resulting in the increase of the bit value against sample (or time). This is not quite true however. If you look carefully at the figure you can see that each of the ramps has a slight curve in it. This causes errors when trying to fit a slope to the ramps.

During PV it was also noted that the RC-corrected slopes, which should be straight, had a curvature to them. This was evident from the observation that the first second had a slightly different slope to that of subsequent seconds (for reset intervals of 2 or 4 seconds), and was traced to the pulse shape reset after effects effectively causing different RC constants for the different seconds. It may be corrected in future versions of the OLP software by having different RC constants for the different seconds. These RC constants are held in Cal-G file 2.

6.7 Glitches

Glitches are caused by such events as fast moving electrons and ions inside the earths magnetic field hitting the detectors. Whatever causes a glitch, the effect of one is a sudden change in the output voltage which causes a step (a "glitch") in the affected ramp. Most glitches cause an increase in the output voltage, but some can cause a decrease. For small glitches (the majority) the slopes before and after the glitch are indistinguishable from each other. Figure 6.7 shows an example of a glitch in the 24Hz ERD data. Note that the sets of two points with Bit values of around 2700-2800 are the result of the detector reset every second. The sample immediately after the two high points is also affected but appears okay due to the signal level.

Some glitches, however, are large and have effects that lasts for a long time (they have tails). These tails are especially seen in band 4, due to the detector material and operating conditions, and are probably due to memory effects, see section 6.8. Figure 6.8 shows two examples of band 4 glitches in the SPD. In both cases the detector requires a long time to stabilise. Note that a strong glitch in one detector can affect other detectors in the same detector array.

Derive-SPD attempts to correct for glitches, and for details of how this is acomplished see section 4.2.7.

Another type of detector upset, apparently similar to glitches, has been observed. The symptoms are that each detector in a block suffers a sudden rise in sensitivity, which slowly decays with time. They usually only affect one of an up-down scan pair, and the only solution is to throw the affected scan portion away. As they affect an entire detector block they are given the name 'scan jumps'.

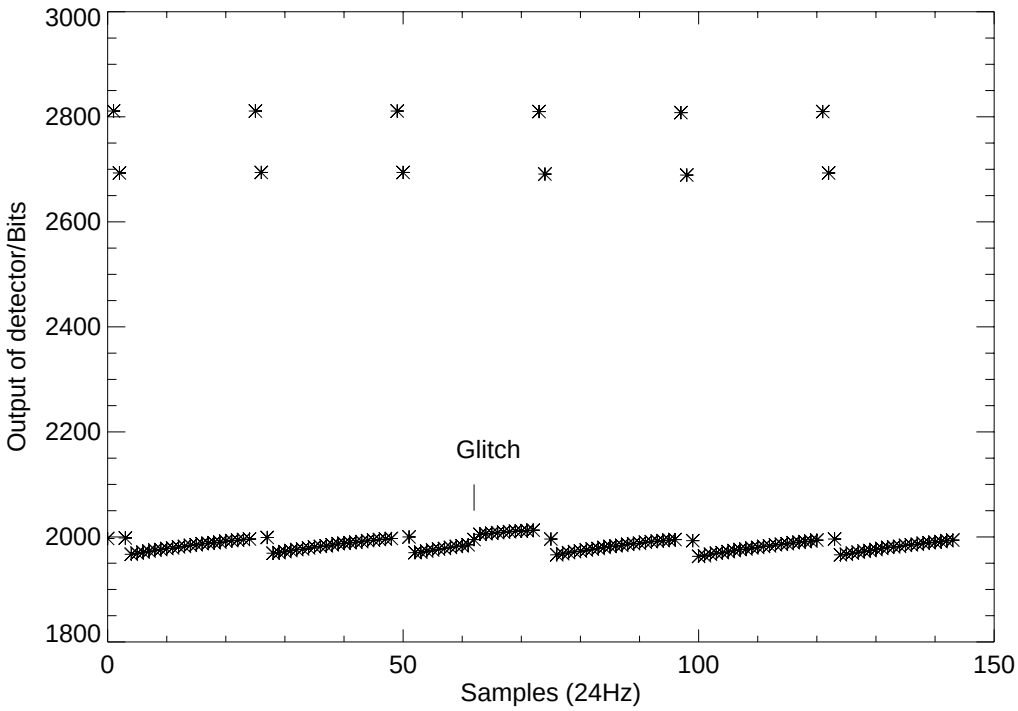

Figure 6.7: *A typical example of a small glitch seen in the ERD. The dots are the 24 Hz sample readouts of voltage across the capacitor (in bits), with the small glitch the sudden rise in the middle ramp. This plot covers several destructive readouts, the effects of which are discussed in section 6.6.*

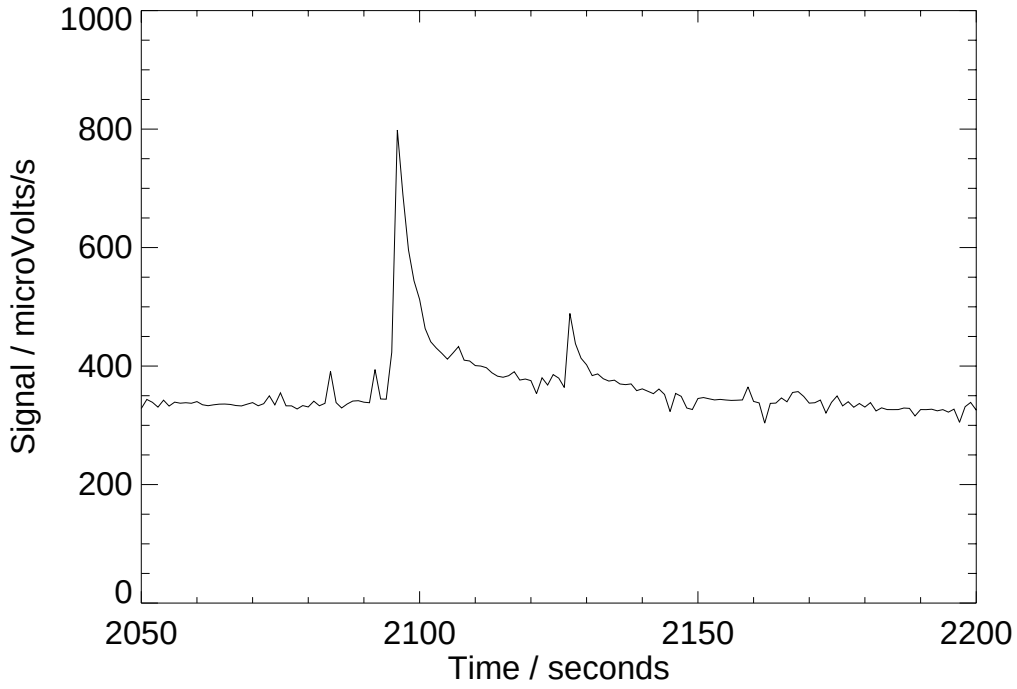

Figure 6.8: *Two examples of less-frequent long lasting glitches. The data shown is SPD from a band 4 detector.*

6.8 Memory effects

The band 2 and 4 detectors used in SWS "remember" their previous illumination history - bands 1 and 3 are not affected by memory effects due to the different detector material used. Going from low illumination to high illumination, or vice-versa, results in the detectors asymptotically reaching their new output value. These are referred to as "memory effects". Currently the only memory effects accounted for in the pipeline are those that affect dark currents – the first few dark current readouts are ignored.

An example of memory effects can be seen in Figure 6.9, which shows ERD data from detector 39 (band 4) as the illumination changes during a dark current check. It can be seen that the detector takes a few resets to stabilise both on light-dark or dark-light illumination changes.

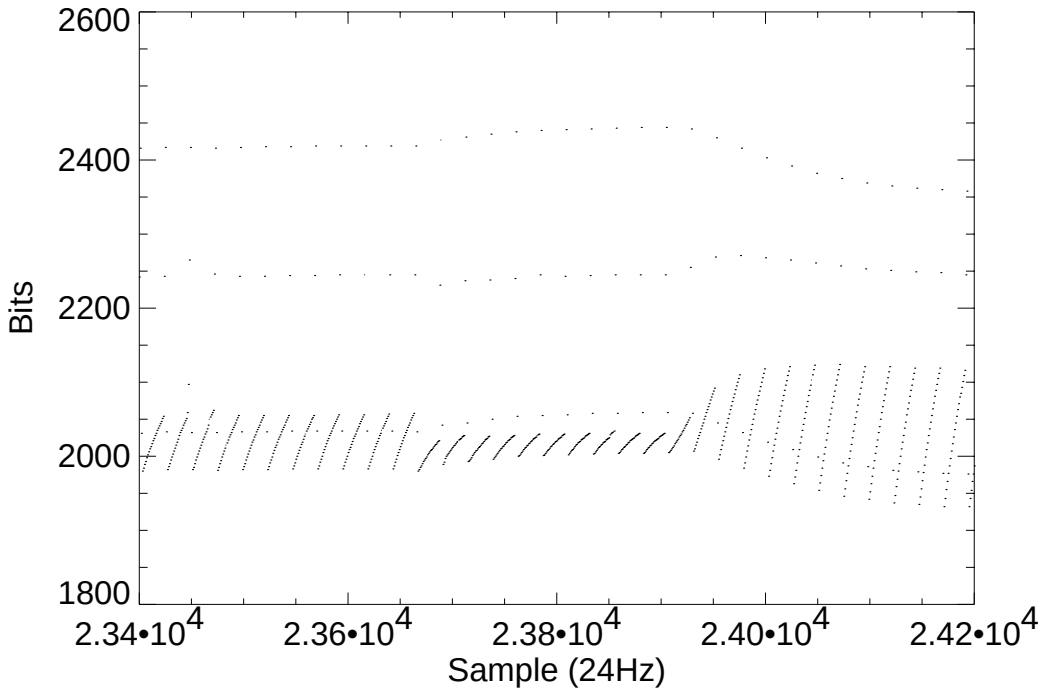

Figure 6.9: *An example of memory effects. The dots are the 24 Hz sample readouts of voltage across the capacitor (in bits). It can be seen that the band 4 detector requires several readouts to stabilise when going from an illuminated to non-illuminated condition, and vice-versa. Small glitches can be seen in the first and second ramps.*

Another example of memory effects is the effect seen in up-down scans of fairly bright sources. For sources with fluxes greater than about 100 Jy memory effects cause the up and down scans to differ in response (and hence flux) by up to 20% in bands 2 and 4. This effect can be seen in figures 6.10 and 6.11. Figure 6.10 shows the output of detector 13 against time along with the wavelength of light falling on the detector. It can be seen that the detector output rises from a low state at the start of the observation, and that it does not fall back to its low level at the end. Figure 6.11 shows the result of this in AAR. The top plot is for the up-scan, the lower for the down-scan – the down scan is shifted down by 500 Jy for clarity and remember that the up-scan actually scans down in wavelength (see section 3.9.1). While the short wavelength data for both scans has approximately the same flux level, the long wavelength data (that taken at the start and end of the observation) has quite different flux levels. In this example, the

first up-scan should not be used to derive the spectrum.

It is important to stress this - if you see your data is affected by memory effects you must decide how much data to use and in extreme cases discard one (or more) scans. In the case of the observation lasting for several up-down scan pairs this does not cause a significant loss in total observing time. For an observation lasting only one up-down scan pair it results in a loss of 50% of the observing time.

Memory effects can also change the shape of line profiles. As an example, as the grating scans across a strong gaussian line the sensitivity of the detectors will change. If this change is large enough it will result in one side of the gaussian having a different shape from the other. As lines are scanned in different directions by the up-down scans, the line will have a different shape in both scans. If the scans are averaged the line will be broader than it actually is. Users should be aware of this effect.

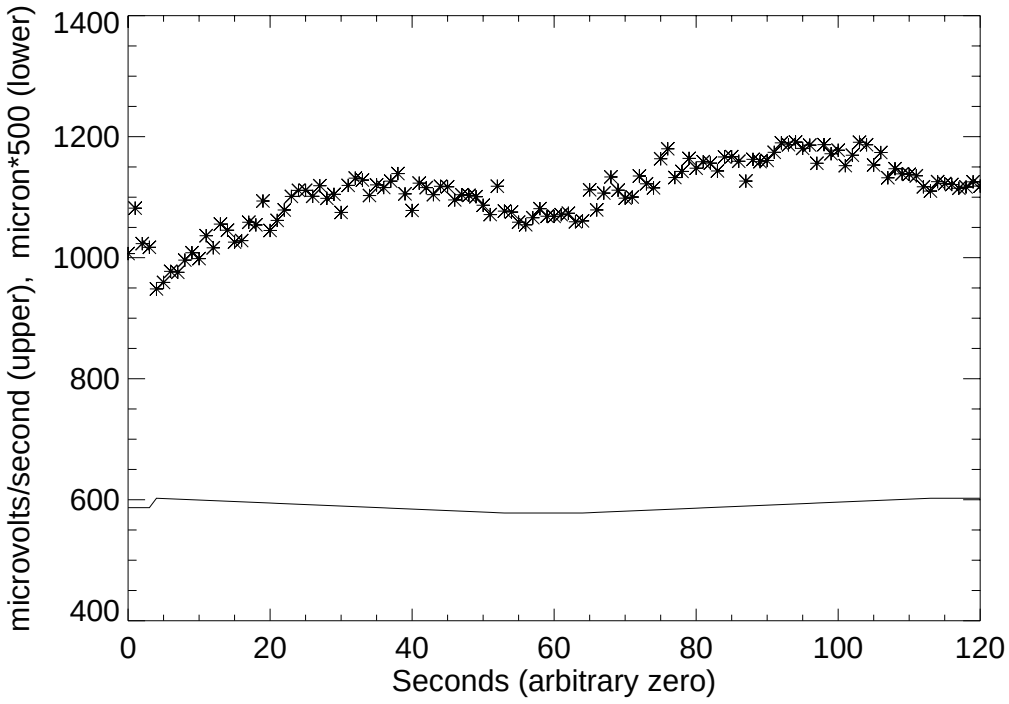

Figure 6.10: *Example of memory effects in band 4 on an up-down scan as seen in the SPD. Top is the detector output, bottom is the wavelength seen by the detector. The up-scan starts at time 5 sec and ends at approximately time 55 sec. The down-scan then occurs from time 65 to 110 sec. Due to memory effects the detectors require a stabilisation time upon an illumination change, resulting in the two parts of the scan having different shapes.*

Table 6.4 (based on ground based tests) gives indications of the errors introduced into flux calibration by memory effects.

Table 6.4: *Errors introduced by memory effects.*

1 InSb	2 Si:Ga	3 Si:As	4 Ge:Be	5 Si:Sb	6 Ge:Be
$<< 1\%$	$6 - 15\%$	$<< 1\%$	$8 - 30\%$	25%	5%

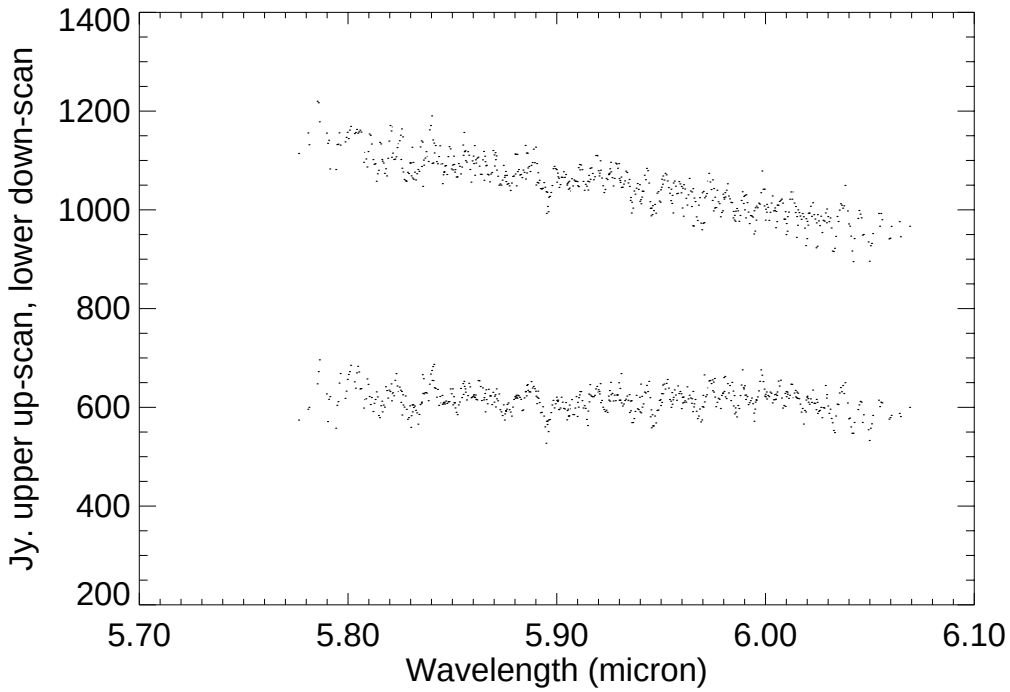

Figure 6.11: *Example of memory effects on up-down scans as seen in AAR. The down scan has been shifted down by 500 Jy for clarity. The up scan is carried out first, starting at high wavelength and progressing to low wavelength. The down part of the scan is then carried out from low to high wavelength. There is a considerable difference in the shape of the observed continuum due to memory effects.*

6.9 Reference Scan Memory Effects

Reference scans, described in section 3.9.2, "Reference scans", and detector memory effects can combine to affect the data produced from band 2 and band 4 detectors during AOT S06 observations.

This possible problem in the flux calibration of S06 science observations is traceable to memory effects left over from reference scans, and was demonstrated in figure 3.24. The intended science objectives may then be compromised in portions of the spectrum.

The document by Leech & Morris 1997, [17], gives examples of such effects and indicates what to do if they occur.

6.10 Pointing Effects

The accuracy of the target input coordinates, and of the pointing, have a large impact on the instrumental throughput, of the point source flux accuracy but only a minor impact on the wavelength accuracy of SWS for point sources. ISO's random pointing error can also introduce effects in the data if the target coordinates are incorrect or if the target is in a crowded field.

Several documents were written covering the effects of pointing accuracy.

Leech & Heras 1997, [16], gives examples of what can go wrong when incorrect target coordinates are used. In summary, a star offset from the center of the aperture by $6''$ in the cross-dispersion direction (y-axis) loses approximately 40% in throughput – this example is taken at $17\,\mu$m. A similar offset in the dispersion direction (z-axis) does not result in as large a flux decrease, due to the beam profile (see 2.3.3). An offset in the dispersion direction does, however, affect the wavelength calibration, with a $4''$ mispointing resulting in a 1 LVDT (1/8 grating resolution) wavelength offset. As the maximum possible offset is about 2 LVDT, or about 1/4 of a grating spectral resolution element, and within the quoted wavelength accuracy, errors introduced into the wavelength scale can usually be ignored.

Also note that problems may occur if there is another object, with a flux similar or greater than the target, $4 - 10''$ away in the z-direction, as can happen in crowded fields.

This study was extended by Heras 1998, [11], which compares the ratio of on- and off-source observations of a star with the pointing jitter. It finds that sudden flux jumps are associated with pointing fluctuations. It also notes that even for nominally on-source observations (defined to be those where the pointing error is less than about $4''$), there is a correlation between noise in an observation and pointing jitter.

During the ISO mission several stars were observed every few weeks for purposes of wavelength and flux calibration. The flux of one of these targets, Gamma Dra, was seen to have a modulation in it that is suspected to be due to pointing errors. The report by Feuchtgruber 1998, [5], can be read for further information on this.

Information on how the spacecraft pointing can affect observations of extended objects can be read in Feuchtgruber 1998 [6]. In this case the observed line fluxes varied by 10% over the course of several months. This was attributed to the spatial extent of NGC 6543, the SWS slit size projected on the sky, see section 2.3.2, and the change in roll angle between the observations.

To derive the position angle of an aperture information on the spacecrafts position on the sky must be used. This can be found in the header keywords INSTRA, INSTDEC, INSTROLL found, for example, in the AAR. Specifically, INSTROLL is the angle, measured anticlockwise, between north and the spacecraft z-axis (ref. the ISO Handbook Volume 2 for a description of these keywords).

6.11 Grating instrumental profile and resolution

The document by van den Ancker, Voors & Leech 1997, [1], discusses investigations of the grating instrumental profile and describes possible instrumental effects on emission lines profiles observed with SWS.

Ground-based tests showed the SWS Instrumental Profiles (IPs) to have a Gaussian shape up to accuracies of a few percent. To verify that this would also be the case in-flight, several objects showing strong, narrow, emission lines (mostly Planetary Nebulae) were observed in ISO's performance verification (PV) phase to investigate the influence of parameters such as the position of the source in the aperture, the size of the target and the SWS AOT band.

The conclusions (based on AOT 2 & 6 observations, should be applicable to AOT 7 SW grating observations but are not applicable to AOT 1 observations) are:

- The SWS grating instrumental profile is very close to Gaussian.
- The only systematic differences from a Gaussian profile are a slight "shoulder" on the blue side of the base of the profile and a depression on the red side as compared to a purely Gaussian profile. The only parameter this seems to depend on is the position of the source in the slit.
- The grating resolving power of SWS for all investigated sources is better than expected for extended sources at all wavelengths. This could either mean that none of line-emitting regions in any of the sources fully filled the SWS aperture, or that the SWS resolving power for extended sources is better than expected.
- In AOT bands 2 to 4 the resolving power for point-like sources is slightly better than predicted from the ground.

6.12 Single Detector Signal Jumps

The document by Heras 1997, [8] summarizes a study made on single detector signal jumps. These effects occur in only one detector at a time and can be generally described as a sudden increase or decrease of the signal, which then remains constant or has a long recovering time ($>>$ 10 s) after the jump. These jumps are normally seen at low signal levels. Examples of such jumps in SPD data are shown in figure 6.12

The signal jumps observed for each detector vary significantly between different cases, and may be negative or positive.

Jumps in band 3 are of different nature from jumps in bands 1 and 2.

The frequency of jumps in bands 1 and 2 is of approximately 5 jumps per hour.

The signal jump is more clearly reflected on the first second of the reset interval than in the second one, indicating a relation between the signal jump and a residual after reset pulse effect. This will be further investigated when working on a possible correction for these jumps.

For bands 1 and 2 and for the measurements with a reset interval of 2 seconds, half of the jumps are associated with the detection of glitches. However, no correlation has been found between the characteristics of these jumps and and those of the glitches.

Users are recommended to examine the SPD from their observations to look for such jumps. If they are present the user can either throw the affected portions of the data away or try to adjust the baseline of the affected portion to the pre- and post-jump baseline.

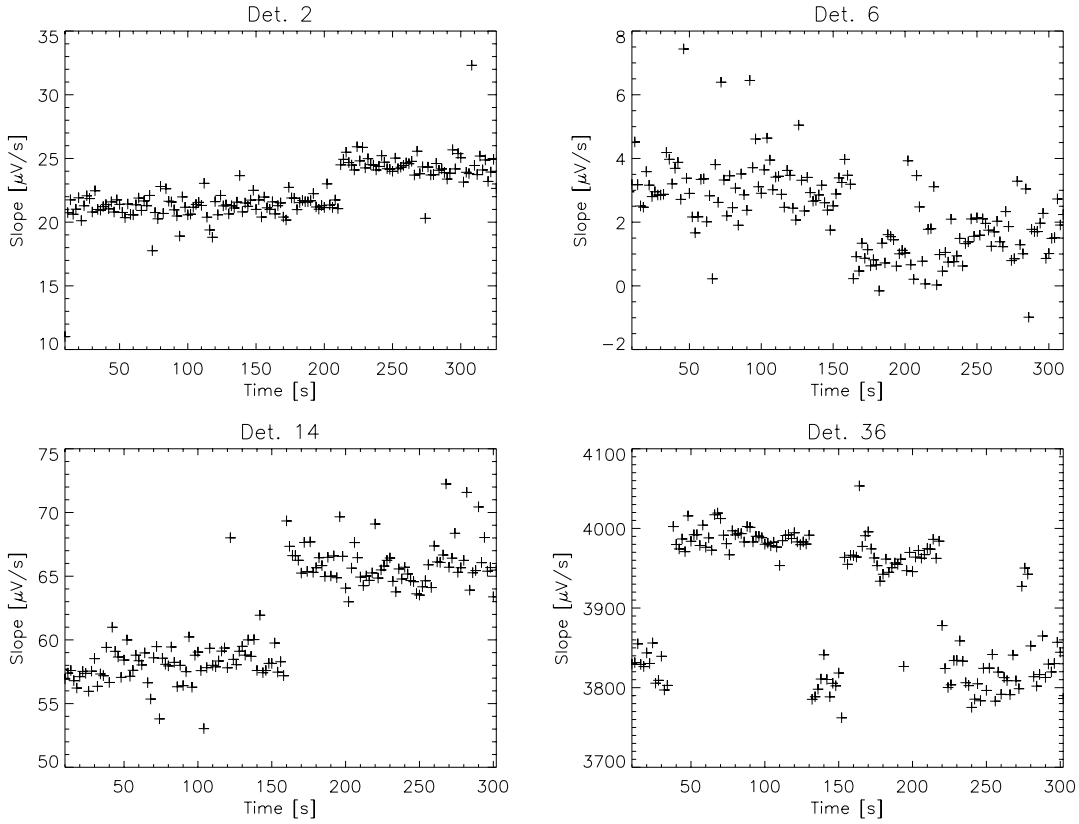

Figure 6.12: *Four examples of single detector signal jumps. In all cases the signal from one detector suddenly jumps to a different value and remains there for a log time.*

6.13 Light leakage in band 3D

Band 3D suffers from leakage around 27 μm. Figure 6.13 shows band 3 data of an object with flux falling towards longer wavelengths. The slight increase in the flux seen in band 3d from about 27 μm onwards is not real but is due to leakage from approximately 13 μm. This leakage is of the order of 10% and will primarily affect objects with flux falling sharply towards long wavelengths.

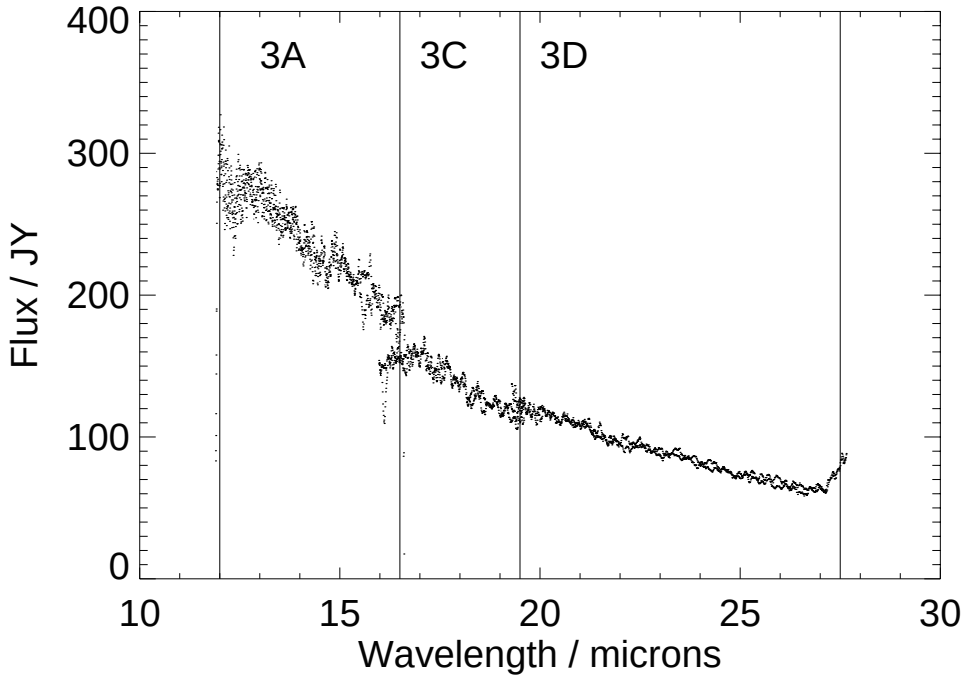

Figure 6.13: *Band 3 data showing the leak around 27 microns.*

6.14 CAM CVF & SWS

In May 1997 cases came to light where the action of a CAM-CVF observation before a SWS observation led to an increased SWS band 3 detector dark current. This increase above the nominal value approached a factor of 100 in some cases. The dark current decreased with time during the SWS observation and reached the nominal dark current less than 30 mins after the CAM-CVF observation. This effect can be seen in affected observations by selecting and plotting all the dark currents from the data (SWSPFLAG bit 27 set) - the dark currents are enhanced and decrease with time. In severe cases this effect can manifest itself in the AAR by band 3 fluxes being negative and in the SPD by the band 3 up and down scans having different shapes.

No correlation between the dark current and the operation of any other instrumental AOT was seen.

This could only affect observations made before June 1997. After this date SWS observations were not scheduled until after 30 minutes of a CAM-CVF observation.

6.15 Diffuse Background Emission

SWS does not use spatial chopping, hence all spectra will contain some contribution by zodiacal light and galactic background. In most cases, this will be negligible compared to the source flux. The zodiacal background component is the most important over the largest part of the SWS wavelength range, with a continuous spectrum corresponding to a dust temperature of about 260K, that does not affect searches for line emission. As an order of magnitude estimate, a typical zodiacal light flux density seen within a SWS aperture will be about 0.3Jy.

Appendix A

Product Description

A.1 Introduction

This appendix describes the products available from the ISO Data Archive (IDA). It is split into five sections describing the Raw data (ERD and CSH) files; the standard processed (SPD) files; the Auto-Analysis Results (AAR) files; the other product files available from IDA; and the Calibration-G files. Note that the format for all these files is binary FITS format and is described in the IDPD.

A.2 Raw data files (ERD and Compact Status)

Two files are described in this section: the SWS Edited Raw Data file) and the SWS Compact Status file.

A.2.1 SWS Edited Raw Data

These files are normally named SWER*.FITS, where '*' is a number generated from the revolution the observation was made, the order the observations were performed in that day and the order it appeared in the proposal.

A.2.1.1 Headers

The ERD files contain primary headers described in Table A.1. In this table example information is used to fill the header.

Most keywords are self explanatory. Those that are not include:

TMRATE The Telemetry Rate can only be 32, indicating 32 kbps.

EOHAAOTN This can take the values S01, S02, S06 or S07, for the appropriate AOT, or S90 to S99 for calibration/post-He observations. This is copied from the field of the same name in the EOHA file for the observation, see the ISO Handbook Volume 2 for an explanation of this file.

EOHAPCAT indicates the proposal category as entered by the user in PGA. The categories were European GT, NASA GT, ISAS GT, OT or Calibration, and these are coded in EOHAPCAT as the ASCII numbers 1 to 5 respectively. This is copied from the field of the same name in the EOHA file for the observation.

EOHATTYP indicates the scientific category as entered by the user in PGA. The categories were Solar System, Interstellar Matter, Stellar Physics, Extragalactic Systems or Cosmology, and these are coded in EOHATTYP as the ASCII numbers 001 to 005 respectively. This is copied from the EOHASCAT field in the EOHA file for the observation.

ATTUTCS should be close in value to EOHAUTCS. If the observation contains micro-slews (e.g. SWS aperture changes) this value will refer to the first pointing.

ATTOTFTH AOT on target flag. When the pointing is within this accuracy of the target the on target flag is set.

ATTTYPE Can be set to "T" for solar system tracking, "P" for fine pointing (single target) or "R" for a raster operation.

Time keys The various time keys, referred to by TREFUTK, TREKITK and TREFITKU, are described in the ISO Handbook Volume 2.

VERSn indicates the version numbers of the various files used to generate this product.

Table A.1: *ERD primary headers*

Header keyword	Contents	Comment
SIMPLE =	T	
BITPIX =	8	
NAXIS =	0	
EXTEND =	T	
ORIGIN =	'ESA '	European Space Agency
TELESCOP=	'ISO '	Infrared Space Observatory
INSTRUME=	'SWS '	Instrument used
COMMENT		SWS Edited Raw Data
FILENAME=	'SWER23300209'	File name in ISO archive
DATE =	'26/09/95'	Creation date 95/269
FILEVERS=	'0377 '	Version ID in ISO archive
OLPVERS =	'LATEST '	SOC OLP system version
CALGVERS=	'CALG_40 '	/ SOC OLP CAL-G files version
USERNAME=	'PIPELINE'	/
VERS1 =	'1411/EOHA282'	/ Version ID of each input file
VERS2 =	'1411/EOHI282'	/ Version ID of each input file
VERS3 =	'0804/APPH282'	/ Version ID of each input file
OBJECT =	'NGC6543 '	Target ID as given by proposer
OBSERVER=	'SWS '	Proposer ID in ISO Mission DB
EQUINOX =	2000.0	Equinox
TMRATE =	32	Telemetry rate in Kbps (Kbits/sec)
EOHAUTCS=	'96130004435'	Approx. UTC of start of observation
EOHAUTCE=	'96130013951'	Approx. UTC of end of observation
EOHAAOTN=	'S06 '	AOT name
EOHAPLID=	'SWS_EE2 '	Proposal ID
EOHAOSN =	'09 '	Observation sequence number
EOHAPSN =	'00 '	Pointing sequence number
EOHAPCAT=	'4 '	Proposal category
EOHACIND=	' '	Calibration indicator
EOHATTYP=	'003 '	Target type
AOTVERS =	'95118180436'	AOT-to-OCT logic version

TREFCOR1=	241288656	/UTC of 1st reference time
TREFPHA1=	282.19191	/Orbital phase at TREFCOR1
TREFCOR2 =	241289612	/UTC of 2nd reference time
TREFPHA2 =	282.20301	/Orbital phase at TREFCOR2
TREFCOR3 =	241290568	/UTC of 3rd reference time
TREFPHA3 =	282.21411	/Orbital phase at TREFCOR3
ATTUTCSL=	'96130004411'	UTC of start time of slew to intended target
ATTUTCS =	'96130004421'	UTC of time of first arrival at intended target
ATTOTFTH=	10.0	On-target flag threshold (arc secs)
ATTRA =	303.56	Intended Right Ascension of instrument viewing, in degrees
ATTDEC =	28.0	Intended DEClination (with ATTRA), in degrees
ATTTYPE =	'R '	Type of attitude operation (P/R/T)
ATTGUIDE=	150002	Guide star reference number
ATTSAANG=	92.6	Solar aspect angle (degrees)
ATTERROR=	0	CONTINGEncy flag(0=success; 1=target not acq'd)
TREFUTC1=	231986675	UTC (whole seconds since 01-01-1989)
TREFUTC2=	4101430	UTC (remaining fraction of second)
TREFUTK =	1781286624	ISO Uniform Time Key (UTK)
TREFITK =	1781286624	ISO INSTRUMENT Time Key (ITK)
TREFITKU=	0.04166666666667	ITK unit length in seconds

A.2.1.2 Records

The ERD file contains records (24 per second) with the fields described in Table A.2.

Table A.2: *Records in the ERD file*

Field name	Number	Format	Comment
GPSCTKEY	1	I*4	Instrument time key
GPSCRPID	2	I*1	Raster point ID
GPSCFILL	1	I*2	Filler
SWERDR5	12	I*2	5-micron array readouts
SWERDR10	12	I*2	10-micron array readouts
SWERDR20	12	I*2	20-micron array readouts
SWERDR35	12	I*2	35-micron array readouts
SWERDRFP	4	I*2	FP detector readouts
SWERHK1	1	I*2	SW scanner - actual position (if mode = 0,1)
SWERHK2	1	I*2	SW scanner - LVDT output (if mode = 0,1)
SWERHK3	1	I*2	SW scanner motor current (if mode=1)
SWERHK4	1	I*2	SW scanner DAC output (if mode=1)
SWERHK5	1	I*2	LW scanner - actual position (if mode = 0,2,3)
SWERHK6	1	I*2	LW scanner - LVDT output (if mode = 0,2,3)
SWERHK7	1	I*2	LW scanner motor current (if mode=2)
SWERHK8	1	I*2	LW scanner DAC output (if mode=2)
SWERHK9	1	I*2	Last received internal command (if mode=3)
SWERHK10	1	I*2	Temp. sensor FP cal. source (if mode=3)
SWERHK11	1	I*2	Fabry-Pérot main current
SWERHK12	1	I*2	Fabry-Pérot correction current 1
SWERHK13	1	I*2	Fabry-Pérot correction current 2
SWERSLHK	1	I*2	Slowly commutated Housekeeping (HK)
SWERIRC	1	I*2	Internal readout counter
SWEREXEC	1	I*2	"Execute" flags

Notes:

1. The five SWERDR fields contain the detector readouts, whereas the thirteen SWERHK fields allow the wavelength falling on each detector to be calculated.

2. The two GPSCRPID fields should always contain '1's for SWS, unless a SSO is being tracked.

3. The selection of which of fields SWERHK1 to SWERHK10 contain valid information is mode-dependent. The "mode" can be 0 (default), 1, 2 or 3. A change in mode implies the start of a new measurement period, and the value of the mode is contained in the corresponding Compact Status field SSTAHKMD.

4. Whereas all other fields repeat at the rate of 24 Hz, SWERSLHK repeats at 0.5 Hz. The meaning of any individual readout depends on the accompanying value of SWERIRC.

5. SWERIRC begins at 1 (for the first readout cycle of a new format), then increments up to 48. It is derived from the "SWS internal frame counter" and indicates the sequence of information in SWERSLHK.

7. SWEREXEC is extracted from the more significant byte of the SWERIRC. They appear only in ERD records for which SWERIRC is a multiple of 2, as the flags are telemetered at a rate of 12 Hz, and are set to zero for the intervening records. The more significant byte of SWEREXEC is always set to zero, e.g. the sign bit for the flags is not extended.

A.2.2 SWS Compact Status

These files are normally named SSTA*.FITS.

A.2.2.1 Headers

The CSH files primary header, filled with example information, is described in Table A.3.
Most keywords are self explanatory, or have been described above.

Table A.3: *CSH primary headers*

Header keyword	Contents	Comment
SIMPLE =	T	/
BITPIX =	8	/
NAXIS =	0	/
EXTEND =	T	/
ORIGIN =	'ESA '	/ European Space Agency
TELESCOP=	'ISO '	/ Infrared Space Observatory
INSTRUME=	'SWS '	/ Instrument used
COMMENT		/ SWS Compact Status
FILENAME=	'SSTA26400248'	/ File name in ISO archive
DATE =	'09/07/95'	/ Creation date 95/190
FILEVERS=	'0298 '	/ Version ID in ISO archive
OLPVERS =	'OLP_21 '	/ SOC OLP system version
CALGVERS=	'CALG_40 '	/ SOC OLP CAL-G files version
USERNAME=	'PIPELINE'	/
VERS1 =	'0298/SCSH264'	/ Version ID of each input file
VERS2 =	'1411/EOHA282'	/ Version ID of each input file
VERS3 =	'1411/EOHI282'	/ Version ID of each input file
EQUINOX =	2000.0	/ Equinox
TMRATE =	32	/ Telemetry rate in Kbps (Kbits/sec)
EOHAUTCS=	'96166223020'	/ Approx. UTC of start of observation
EOHAUTCE=	'96166223818'	/ Approx. UTC of end of observation
EOHAAOTN=	'S07 '	/ AOT name
EOHAPLID=	'MPEWARM1'	/ Proposal ID
EOHAOSN =	'48 '	/ Observation sequence number
EOHAPSN =	'0 '	/ Pointing sequence number
EOHAPCAT=	'1 '	/ Proposal category
EOHACIND=	' '	/ Calibration indicator
EOHATTYP=	'2 '	/ Target type
AOTVERS =	'94350161513'	/ AOT-to-OCT logic version
TREFCOR1=	241288656	/UTC of 1st reference time
TREFPHA1=	282.19191	/Orbital phase at TREFCOR1
TREFCOR2 =	241289612	/UTC of 2nd reference time
TREFPHA2 =	282.20301	/Orbital phase at TREFCOR2
TREFCOR3 =	241290568	/UTC of 3rd reference time
TREFPHA3 =	282.21411	/Orbital phase at TREFCOR3
ATTUTCSL=	'96166222532'	/ UTC of start time of slew to intended target
ATTUTCS =	'96166222627'	/ UTC of time of first arrival at intended target
ATTOTFTH=	10.0	/ On-target flag threshold (arc secs)
ATTRA =	302.66	/ Intended Right Ascension of instrument viewing, in degrees
ATTDEC =	27.8	/ Intended DEClination (with ATTRA), in degrees

```
ATTTYPE =                  'P '  / Type of attitude operation (P/R/T)
ATTGUIDE=                150002  / Guide star reference number
ATTSAANG=                 115.9  / Solar aspect angle (degrees)
ATTERROR=                     0  / CONTINGEncy flag(0=success; 1=target not acq'd)
TREFUTC1=                241288656  / UTC (whole seconds since 01-01-1989)
TREFUTC2=                1428250  / UTC (remaining fraction of second)
TREFUTK =                617295744  / ISO Uniform Time Key (UTK)
TREFITK =                617295744  / ISO INSTRUMENT Time Key (ITK)
TREFITKU=  0.04166666666667  / ITK unit length in seconds
```

A.2.2.2 Records

The Compact Status file contains records with the fields described in Table A.4. The records are defined in the binary header of the FITS file.

Table A.4: *Records in the CSH file*

Field name	Number	Format	Comment
CSGPUKST	1	I*4	UTK start time
CSGPUKEN	1	I*4	UTK end time
CSGPIKST	1	I*4	ITK start time
CSGPIKEN	1	I*4	ITK end time
CSGPUTST	2	I*4	UTC start time
CSGPUTEN	2	I*4	UTC end time
CSGPOSN	1	I*1	Observation Sequence Number
CSGPFILL	15	I*1	Spare
SSTASHUT	1	I*2	Shutter position (0=closed, or 1/2/3)
SSTAGAIN	6	I*2	Nominal gain in each of the bands (1/4/16)
SSTACALS[1]	4	I*2	Calibration source status
SSTARESP	2	I*2	Reset interval in frames (SW/LW)
SSTAHKMD	1	I*2	House keeping mode
SSTAFPS	1	I*2	FP selection (1=FP1, 2=FP2)
SSTASPAR	9	I*2	Spare

1. Note that the four elements of SSTACALS are:

1. Grating calibrator

2. Flusher

3. FP calibrator

4. Diffuse calibrator

A zero in a SSTACALS field indicates that the respective calibrator is off. 1 indicates it is on low, 2 that it is on high.

A.3 Standard processed (SPD) files

There are two files in this section: the SWS Standard Processed Data file, and the SWS Glitch History Data file.

A.3.1 SWS Standard Processed Data

These files are normally named SWSP*.FITS by the IDA.

A.3.1.1 Headers

The SPD files contain primary headers described in Table A.5. In this table example information is used to fill the header.

Most keywords are self explanatory, or have been described above.

Table A.5: *SPD primary headers*

Header keyword	Contents	Comment
SIMPLE =	T	/
BITPIX =	8	/
NAXIS =	0	/
EXTEND =	T	/
ORIGIN =	'ESA '	/ European Space Agency
TELESCOP=	'ISO '	/ Infrared Space Observatory
INSTRUME=	'SWS '	/ Instrument used
COMMENT		SWS Standard Processed Data
FILENAME=	'SWSP26400248'	/ File name in ISO archive
DATE =	'17/10/95'	/ Creation date 95/290
FILEVERS=	'0399 '	/ Version ID in ISO archive
OLPVERS =	'LATEST '	/ SOC OLP system version
CALGVERS=	'CALG_40 '	/ SOC OLP CAL-G files version
USERNAME=	'JSTERNBE'	/ Unofficial data product
OBJECT =	'TEST_OBJ'	/ Target ID as given by proposer
OBSERVER=	'KLEECH'	/ Proposer ID in ISO Mission DB
EQUINOX =	2000.0	/ Equinox
TMRATE =	32	/ Telemetry rate in Kbps (Kbits/sec)
EOHAUTCS=	'96166223020'	/ Approx. UTC of start of observation
EOHAUTCE=	'96166223818'	/ Approx. UTC of end of observation
EOHAAOTN=	'S07 '	/ AOT name
EOHAPLID=	'KLTEST '	/ Proposal ID
EOHAOSN =	'48 '	/ Observation sequence number
EOHAPSN =	'0 '	/ Pointing sequence number
EOHAPCAT=	'1 '	/ Proposal category
EOHACIND=	' '	/ Calibration indicator
EOHATTYP=	'2 '	/ Target type
ATTUTCSL=	'96166222532'	/ UTC of start time of slew to intended target
ATTUTCS =	'96166222627'	/ UTC of time of first arrival at intended target
ATTOTFTH=	10.0	/ On-target flag threshold (arc secs)
ATTRA =	102.66	/ Intended Right Ascension of instrument viewing
ATTDEC =	21.8	/ Intended DEClination (with ATTRA)
ATTTYPE =	'P '	/ Type of attitude operation (P/R/T)

ATTGUIDE=	150002	/ Guide star reference number
ATTSAANG=	115.9	/ Solar aspect angle (degrees)
ATTERROR=	2	/ CONTINGEncy flag(0=success; 1=target not acq'd)
TREFUTC1=	235175420	/ UTC (whole seconds since 01-01-1989)
TREFUTC2=	8505250	/ UTC (remaining fraction of second)
TREFUTK =	1857816480	/ ISO Uniform Time Key (UTK)
TREFITK =	1857816480	/ ISO INSTRUMENT Time Key (ITK)
TREFITKU=	0.04166666666667	/ ITK unit length in seconds
TREFCOR1=	235175420	/ UTC of 1st reference time
TREFPHA1=	282.09099	/Orbital phase at TREFCOR1
TREFHEL1=	-253.41	/ Heliocentric correction +(s) at TREFCOR1
TREFDOP1=	-13.92	/ ISO velocity towards target (km/s) at TREFCOR1
TREFCOR2 =	235175659	/ UTC of 2nd reference time
TREFPHA2 =	282.09430	/Orbital phase at TREFCOR2
TREFHEL2 =	-253.40	/ Heliocentric correction +(s) at TREFCOR2
TREFDOP2 =	-13.93	/ ISO velocity towards target (km/s) at TREFCOR2
TREFCOR3 =	235175898	/ UTC of 3rd reference time
TREFCOR3 =	241280569	/Orbital phase at TREFCOR3
TREFHEL3 =	-253.39	/ Heliocentric correction +(s) at TREFCOR3
TREFDOP3 =	-13.94	/ ISO velocity towards target (km/s) at TREFCOR3
ISRRSEV =	0	/ RTA maximum severity level = OK
ISRQSEV =	1	/ QLA maximum severity level = WA
ISRRWARN=	' '	/ RA-warning flag from IS user
ISRNOOSL=	0	/ No. of out-of-soft-limit errors
ISRNOOHL=	0	/ No. of out-of-hard-limit errors
ISRNMW =	0	/ No. of monitor warnings
ISRNCVW =	0	/ No. of command verification errors
ISRNBTW =	0	/ No. of bad telemetry errors
ISRNMVW =	0	/ No. of memory verification errors
ISRNSQLA=	9	/ No. of severe QLA errors
INSTRA =	102.66474	/Reference instrument J2000 right ascension (deg
INSTDEC =	+21.81240	/Reference instrument J2000 declination (deg)
INSTROLL=	318.89	/Reference instrument J2000 roll angle (deg)
CINSTRA =	188.96338	/Corrected reference instrument J2000 right ascension (deg)
CINSTDEC=	-40.78920	/Corrected reference instrument J2000 declination (deg)
CINSTROL=	319.71	/Corrected reference instrument J2000 roll angle (deg)
VERS1 =	'0298/SSTA26400248'	/ Version ID of each input file
VERS2 =	'0298/GEHK26400248'	/ Version ID of each input file
VERS3 =	'0298/EOHI264'	/ Version ID of each input file
VERS4 =	'0298/SWER26400248'	/ Version ID of each input file
VERS5 =	'0976/SC03_010'	/ Version ID of each input file
VERS6 =	'0976/SC04_010'	/ Version ID of each input file
VERS7 =	'0976/SC02A_010'	/ Version ID of each input file
VERS8 =	'0976/SC02B_010'	/ Version ID of each input file
VERS9 =	'0976/SC05_010'	/ Version ID of each input file
VERS10 =	'0976/SC02_010'	/ Version ID of each input file
VERS11 =	'0976/SC01_010'	/ Version ID of each input file
VERS12 =	'0976/SC06_010'	/ Version ID of each input file
VERS13 =	'0976/SC16E_013'	/ Version ID of each input file
VERS14 =	'0976/SC12_010'	/ Version ID of each input file
VERS15 =	'0976/SC23_010'	/ Version ID of each input file
VERS16 =	'0976/SC24_010'	/ Version ID of each input file

```
VERS17 =              '0976/SC18_010'  / Version ID of each input file
VERS18 =          '1490/IRPH28299000'  / Version ID of each input file
VERS19 =              '1350/ORBIT'     / Version ID of each input file
VERS20 =          '0718/SISR28299000'  / Version ID of each input file
```

A.3.1.2 Records

The SPD file contains records with the fields described in Table A.6. In the FITS file they are defined in the binary header.

Table A.6: *Records in SPD file*

Field name	Number	Format	Unit	Comment
GPSCTKEY	1	I*4		Instrument time key
GPSCRPID	2	I*1		Raster point ID
GPSCFILL	1	I*2		Filler
SWSPSTAT	1	I*4		Status of this record
SWSPGPOS	2	R*4		Average positions for gratings 1/2
SWSPGANG	2	R*4	degrees	Angles for SW & LW gratings
SWSPFPOS	1	I*4		Position of FP
SWSPFCUR	3	R*4		Average main current for FP coils
SWSPFGAP	2	R*4	μm	Gaps for FP
SWSPWAVE	52	R*4	μm	Detector wavelength
SWSPFLUX	52	R*4	$\mu V/sec$	Detector slopes
SWSPOFFS	52	R*4		Number of 24 Hz samples used to calculate the slope
SWSPSTDV	52	R*4	$\mu V/sec$	Standard deviation of the detector slope
SWSPFLAG	52	I*4		Flags per detector

Notes:

1. One record is generated every reset interval (1, 2 or 4 seconds).

2. Because SWS has no raster AOTs, the raster point IDs will always be set to 1 EXCEPT when tracking a Solar System Object.

3. The I*4 status number SWSPSTAT, one per measurement, can be decoded by referring to Table A.7.

4. The I*4 status number SWSPFLAG, one per detector, can be decoded by referring to Table A.8.

Table A.7: *Decoding of Status word SWSPSTAT*

Meaning	Bits set	
dark	00000000000000000000000000000000	0
aperture 1	00000000000000000000000000000001	1
aperture 2	00000000000000000000000000000010	2
aperture 3	00000000000000000000000000000011	3
reset band 1 & 2	00000000000000000000000000000100	4
reset other bands	00000000000000000000000000001000	8
reset all bands	00000000000000000000000000001100	12
diffuse cal normal	00000000000000000000000000010000	16
diffuse cal high	00000000000000000000000000110000	48
fp check normal	00000000000000000000000001000000	64
fp check high	00000000000000000000000011000000	192
flusher normal	00000000000000000000000100000000	256
flusher high	00000000000000000000001100000000	768
grating check normal	00000000000000000000010000000000	1024
grating check high	00000000000000000000110000000000	3072
fp nr 2 active	00000000000000000001000000000000	4096
BAND1 requested	00000000000000000010000000000000	8192
BAND2 requested	00000000000000000100000000000000	16384
BAND3 requested	00000000000000001000000000000000	32768
BAND4 requested	00000000000000010000000000000000	65536
BAND5 requested	00000000000000100000000000000000	131072
BAND6 requested	00000000000001000000000000000000	262144
fp execute flag	00000000000010000000000000000000	524288
FP run flag	00000000001000000000000000000000	1048576
low resolution scan	00000000010000000000000000000000	2097152
reference scan	00000000100000000000000000000000	4194304
photometric check	00000001000000000000000000000000	8388608
defined dark measurement	00000010000000000000000000000000	16777216
SW grating run flag	00000100000000000000000000000000	33554432
LW grating run flag	00001000000000000000000000000000	67108864
SW scan direction[2]	00010000000000000000000000000000	134217728
LW scan direction[2]	00100000000000000000000000000000	268435456

Notes:

1. The value of SWSPSTAT may represent the sum of two or more bits.
2. If one of these flags is set it means the scanner is moving in the down direction.

Table A.8: *Decoding of Flag word SWSPFLAG*

Meaning	Bits set	
No glitch	00000000000	0
1 glitch	00000000001	1
2 glitches	00000000010	2
3 glitches	00000000011	3
Partly Out of limit	00000000100	4
Totally Out of limit	00000001000	8
No data	00000010000	16
Order 1	00000100000	32
Order 2	00001000000	64
Order 3	00001100000	96
Order 4	00010000000	128
Multiple orders (confused)	00011100000	224
Gain bit 1 = gain 1	01000000000	512
Gain bit 2 = gain 4	10000000000	1024
Gain bit 3 = gain 16	11000000000	1536

Notes:

1. Bits 11 to 22 of SWSPFLAG are used internally by Derive-SPD and therefore contain no information useful to the observer.
2. The value of SWSPFLAG may represent the sum of two or more bits.
3. No order flag set indicates no order could be calculated for the data.

A.3.2 SWS Glitch History Data

This product has been produced from OLP Version 5, with the files named SWGH*.FITS.

A.3.2.1 Headers

The SWGH files contain primary headers described in Table A.9, filled with example information. Most keywords are self explanatory, or have been described before.

Table A.9: *SWGH primary headers*

Header keyword	Contents	Comment
SIMPLE =	T	/
BITPIX =	8	/
NAXIS =	0	/
EXTEND =	T	/
ORIGIN =	'ESA '	/ European Space Agency
TELESCOP=	'ISO '	/ Infrared Space Observatory
INSTRUME=	'SWS '	/ Instrument used
COMMENT		SWS Glitch History Data
FILENAME=	'SWGH28600101'	/ File name
DATE =	'17/10/95'	/ Creation date 95/290
FILEVERS=	'0399 '	/ Version ID in ISO archive
OLPVERS =	'LATEST '	/ SOC OLP system version
CALGVERS=	'CALG_40 '	/ SOC OLP CAL-G files version
USERNAME=	'JSTERNBE'	/ Unofficial data product
VERS1 =	'0298/SSTA26400248'	/ Version ID of each input file
VERS2 =	'0298/GEHK26400248'	/ Version ID of each input file
VERS3 =	'0298/EOHI264'	/ Version ID of each input file
VERS4 =	'0298/SWER26400248'	/ Version ID of each input file
VERS5 =	'0976/SC03_010'	/ Version ID of each input file
VERS6 =	'0976/SC04_010'	/ Version ID of each input file
VERS7 =	'0976/SC02A_010'	/ Version ID of each input file
VERS8 =	'0976/SC02B_010'	/ Version ID of each input file
VERS9 =	'0976/SC05_010'	/ Version ID of each input file
VERS10 =	'0976/SC02_010'	/ Version ID of each input file
VERS11 =	'0976/SC01_010'	/ Version ID of each input file
VERS12 =	'0976/SC06_010'	/ Version ID of each input file
VERS13 =	'0976/SC16E_013'	/ Version ID of each input file
VERS14 =	'0976/SC12_010'	/ Version ID of each input file
VERS15 =	'0976/SC23_010'	/ Version ID of each input file
VERS16 =	'0976/SC24_010'	/ Version ID of each input file
VERS17 =	'0976/SC18_010'	/ Version ID of each input file
VERS18 =	'1261/SC16A_011'	/ Version ID of each input file
VERS19 =	'0976/SC16B_010'	/ Version ID of each input file
VERS20 =	'0976/SC16C_010'	/ Version ID of each input file
VERS21 =	'1490/IRPH28200427'	/ Version ID of each input file
VERS22 =	'1350/ORBIT'	/ Version ID of each input file
VERS23 =	'0718/SISR28200427'	/ Version ID of each input file

A.3.2.2 Records

The SWGH file contains records with the fields described in Table A.10.

Table A.10: *Records in the SWGH file*

Field name	Number	Format	Unit	Comment
GPSCTKEY	1	I*4		Instrument time key
SWGHS_S1	52	I*2		Start sample of first glitch
SWGHS_E1	52	I*2		End sample of first glitch
SWGHHGT1	52	R*4	bits[1]	Glitch height of first glitch
SWGHS_S2	52	I*2		Start sample of second glitch
SWGHS_E2	52	I*2		End sample of second glitch
SWGHHGT2	52	R*4	bits[1]	Glitch height of second glitch
SWGHN_GL	52	I*2		Number of glitches

Notes:

1. Bits can have values between 0 and 4095.

A.4 Auto-Analysis Results (AAR) files

There is one file in this section, the SWS Auto-Analysis Results file.

A.4.1 SWS Auto-Analysis Results

A.4.1.1 Headers

The AAR files, normally named SWAA* by the IDA, contain primary headers described in Table A.11. In this table example information is used to fill the header.

Most keywords are self explanatory, or have been described above. Those that are not are INSTRA, INSTDEC and INSTROLL. These are the instruments pointing direction and roll, and are described in the ISO Handbook Volume 2.

Table A.11: *AAR primary headers*

Header keyword	Contents	Comment
SIMPLE =	T	/
BITPIX =	8	/
NAXIS =	0	/
EXTEND =	T	/
ORIGIN =	'ESA '	/ European Space Agency
DATE =	'17/10/95'	/ Creation date 95/290
TELESCOP=	'ISO '	/ Infrared Space Observatory
INSTRUME=	'SWS '	/ Instrument used
COMMENT		SWS Auto Analysis Results
FILENAME=	'SWAA26400248'	/ File name in ISO archive
FILEVERS=	'0399 '	/ Version ID in ISO archive
OLPVERS =	'LATEST '	/ SOC OLP system version
USERNAME=	'JSTERNBE'	/ Unofficial data product
OBJECT =	'TEST_OBJ'	/ Target ID as given by proposer
OBSERVER=	'KLEECH'	/ Proposer ID in ISO Mission DB
EQUINOX =	2000.0	/ Equinox
TMRATE =	32	/ Telemetry rate in Kbps (Kbits/sec)
EOHAUTCS=	'96166223020'	/ Approx. UTC of start of observation
EOHAUTCE=	'96166223818'	/ Approx. UTC of end of observation
EOHAAOTN=	'S07 '	/ AOT name
EOHAPLID=	'KL_TEST'	/ Proposal ID
EOHAOSN =	'48 '	/ Observation sequence number
EOHAPSN =	'0 '	/ Pointing sequence number
EOHAPCAT=	'1 '	/ Proposal category
EOHACIND=	' '	/ Calibration indicator
EOHATTYP=	'2 '	/ Target type
ATTUTCSL=	'96166222532'	/ UTC of start time of slew to intended target
ATTUTCS =	'96166222627'	/ UTC of time of first arrival at intended target
ATTOTFTH=	10.0	/ On-target flag threshold (arc secs)
ATTRA =	102.66	/ Intended Right Ascension of instrument viewing
ATTDEC =	27.8	/ Intended DEClination (with ATTRA)
ATTTYPE =	'P '	/ Type of attitude operation (P/R/T)
ATTGUIDE=	150002	/ Guide star reference number
ATTSAANG=	115.9	/ Solar aspect angle (degrees)
ATTERROR=	2	/ CONTINGEncy flag(0=success; 1=target not acq'd)

```
TREFUTC1=              235175420  / UTC (whole seconds since 01-01-1989)
TREFUTC2=                8505250  / UTC (remaining fraction of second)
TREFUTK =             1857816480  / ISO Uniform Time Key (UTK)
TREFITK =             1857816480  / ISO INSTRUMENT Time Key (ITK)
TREFITKU=       0.04166666666667  / ITK unit length in seconds
TREFCOR1=              235175420  /UTC of 1st reference time
TREFHEL1=                -253.41  /Heliocentric correction +(s) at TREFCOR1
TREFDOP1=                -13.92  /ISO velocity towards target (km/s) at TREFCOR1
TREFCOR2 =             235175659  /UTC of 2nd reference time
TREFHEL2 =               -253.40  /Heliocentric correction +(s) at TREFCOR2
TREFDOP2 =               -13.93  /ISO velocity towards target (km/s) at TREFCOR2
TREFCOR3 =             235175898  /UTC of 3rd reference time
TREFHEL3 =               -253.39  /Heliocentric correction +(s) at TREFCOR3
TREFDOP3 =               -13.94  /ISO velocity towards target (km/s) at TREFCOR3
INSTRA =                102.66474  /Reference instrument J2000 right ascension (deg)
INSTDEC =               +27.81240  /Reference instrument J2000 declination (deg)
INSTROLL=                318.89  /Reference instrument J2000 roll angle (deg)
CALGVERS=             'CALG_40 '  / SOC OLP CAL-G files version
AOTVERS =               '03.30 '  / AOT-to-OCT logic version
TREFPHA1=               282.19191  / Orbital phase at TREFCOR1
TREFPHA2 =              282.20301  / Orbital phase at TREFCOR2
TREFPHA3 =              282.21411  / Orbital phase at TREFCOR3
CINSTRA =               309.77666  / Corrected reference instrument J2000 right ascension (deg)
CINSTDEC=               68.037530  / Corrected reference instrument J2000 declination (deg)
CINSTROL=               336.08000  / Corrected reference instrument J2000 roll angle (deg)
ISRRSEV =                       1  / RTA maximum severity level = WA
ISRQSEV =                       1  / QLA maximum severity level = WA
ISRRWARN=                 'OK '  / RA-warning flag from IS user
ISRNOOSL=                       0  / No. of out-of-soft-limit errors
ISRNOOHL=                       0  / No. of out-of-hard-limit errors
ISRNMW =                        0  / No. of monitor warnings
ISRNCVW =                       2  / No. of command verification errors
ISRNBTW =                       0  / No. of bad telemetry errors
ISRNMVW =                       0  / No. of memory verification errors
ISRNSQLA=                     122  / No. of severe QLA errors
VERS31      = 'cal21_1_011.fits'  / calfile 21_1 for dark subtraction
VERS32      = 'cal21_2_011.fits'  / calfile 21_2 for dark subtraction
VERS33      = 'cal21_4_011.fits'  / calfile 21_4 for dark subtraction
VERS34      = 'cal21_8_010.fits'  / calfile 21_8 for dark subtraction
VERS37      = 'cal25_1a_030.fits' / calfile 25 used for flux conversion
VERS38      = 'cal25_1b_030.fits' / calfile 25 used for flux conversion
VERS39      = 'cal25_1d_030.fits' / calfile 25 used for flux conversion
VERS40      = 'cal25_1e_030.fits' / calfile 25 used for flux conversion
VERS41      = 'cal25_2a_030.fits' / calfile 25 used for flux conversion
VERS42      = 'cal25_2b_030.fits' / calfile 25 used for flux conversion
VERS43      = 'cal25_2c_030.fits' / calfile 25 used for flux conversion
VERS44      = 'cal25_3a_030.fits' / calfile 25 used for flux conversion
VERS45      = 'cal25_3c_030.fits' / calfile 25 used for flux conversion
VERS46      = 'cal25_3d_030.fits' / calfile 25 used for flux conversion
VERS47      = 'cal25_3e_031.fits' / calfile 25 used for flux conversion
VERS50      = 'cal25_5b_010.fits' / calfile 25 used for flux conversion
VERS51      = 'cal25_5c_010.fits' / calfile 25 used for flux conversion
```

```
VERS52          = 'cal25_5d_010.fits'   / calfile 25 used for flux conversion
VERS53          = 'cal25_6_010.fits'    / calfile 25 used for flux conversion
VERS54          = 'cal13_116.fits'      / calfile 13 for flux conversion
```

A.4.1.2 Records

The AAR file contains records with the fields described in Table A.12. In the FITS file they are defined in the binary header.

Table A.12: *Records in the AAR file*

Field name	Number	Format	Unit	Comment
SWAAWAVE	1	R*4	μm	Wavelength of data point
SWAAFLUX	1	R*4	Jy	Flux
SWAASTDV	1	R*4	$\mu V/sec$	Standard deviation of the slope
SWAATINT[1]	1	I*4	samples	Number of samples used
SWAADETN[2]	1	I*4		detector number
SWAAITK	1	I*4		SWS instrument time key
SWAAUTK	1	I*4		ISO uniform time key
SWAARPID[3]	2	I*1		raster point id
SWAASPAR	2	I*1		Contains error information[8]
SWAALINE[4]	1	I*4		line number
SWAASDIR[5]	1	I*4		scan direction
SWAASCNT[4]	1	I*4		scan number
SWAASTAT[6]	1	I*4		status word
SWAAFLAG[7]	1	I*4		flag word

Notes:

1. SWAATINT is the total number of 1/24 second samples used to calculate the flux of this data point. See section 5.3 for a definition of this. The units for this for pre-OLP V7 files were given as seconds, rather than the correct (1/24 seconds) samples.

2. SWAADETN can be used to determine which detector observed each data point by referring to table 2.2.

3. SWAARPID, the raster point id, is copied over from the GPSCRPID in the SPD. As SWS has no raster AOTs it is always (1,1) (unless a Solar System Object is being tracked), but is included so that the format of SWS AA is compatible with LWS AA.

4. Section A.4.2 discusses SWAALINE and SWAASCNT.

5. SWAASDIR is used to identify if the datapoint is from an up-scan (1) or a down scan (-1). 0 is undefined (and don't use the data). See section 3.9.1 for a definition of up-down scans.

6. SWAASTAT is copied over from SWSPSTAT. For a description of this see Table A.7.

7. SWAAFLAG is copied over from SWSPFLAG. For a description of this see Table A.8. Note that while the bits described in Table A.8 will remain unchanged, the Derive-AAR processing stage may change bits 11 and above. These bits are of no use to the observer.

8. These two bytes contain the error information described in section 4.4.

A.4.2 SWAALINE and SWAASCNT

SWAALINE and SWAASCNT are both counts of the valid data present in an AAR. All valid data means data that are flagged as 'Data', with the 'SW', 'LW' or 'FP' runflags set but without being flagged simultaneously as 'darkcurrent', 'photometric check'. Additionally the data should have a valid order assigned.

SWAALINE is a count of the valid ranges in a dataset. For AOT 1, it is filled with the AOT band number (see table 2.2). For an AOT 2 observing X lines it will count from 1 to X, with 0 reserved for any datapoints not associated with a line. Note that the datapoints associated with SWAALINE set to, e.g. 1, may not correspond to the first entered line number in your AOT as the logic may re-arrange them to increase efficiency. For AOT 6 it effectively counts the number of scans, including reference checks etc. For an example see table A.13.

Table A.13: *Line number against detector band*

Operation	line number for detector band			
	1	2	3	4
REF	1	2	3	4
SCAN UP	5	6	7	8
REF	9	10	11	12
SCAN DOWN	13	14	15	16
REF	17	18	19	20
.	.	.	.	.

Note that this is an example of an 'old' (pre mid-1997) AOT 6 and that the scans may be different for a different AOT 6 operation.

SWAASCNT has nothing to do with the number of scans required for an AOT. It is a count of the number of lines/bands containing requested (i.e. what was requested in the AOT) data, starting with 1. Any data outside the requested ranges will have SWAASCNT set to 0. Note that even if SWAASCNT is greater than 0, the flag and status word should be checked to ensure the data is okay. For AOT 1 SWAASCNT is filled with 1.

The decision whether to increment SWAALINE or SWAASCNT depends on whether a scan starts and ends at the same grating position as the preceeding scan. Initially both are set to one. If a scan starts and ends at the same grating position as the preceeding scan the line counter is not incremented but the scan counter is. If the wavelength range is different the line counter is incremented and the scan counter is (re-)set to one. Users should note that this effectively results in a difference in the behaviour of SWAALINE for AOT 2's and 6's. For AOT 2 there is one value per each up-down pair, whereas for an AOT 6 there is one value per individual up- or down-scan.

A.5 Calibration-G files

There are fifty five files in this section, listed below. For each of these files there can be several versions, one for each phase in the mission. Which version is used to process a dataset is defined in the STIMDEP file.

Table A.14: *SWS Cal-G Files*

SC01	SWS Cal-G 1	Electrical crosstalk matrices
SC02	SWS Cal-G 2	RC correction timescales
SC02A	SWS Cal-G 2A	Midbit values
SC02B	SWS Cal-G 2B	Shape correction values
SC03	SWS Cal-G 3	Reset cutout lengths
SC04	SWS Cal-G 4	Amplifier limits
SC05	SWS Cal-G 5	Switchable gains
SC06	SWS Cal-G 6	Glitch reject levels
SC07	SWS Cal-G 7	Grating detector noise characteristics
SC08	SWS Cal-G 8	Grating calibration specifications
SC09	SWS Cal-G 9	LVDT-Angle relation
SC10	SWS Cal-G 10	Key wavelengths
SC11	SWS Cal-G 11	FP calibration spectrum
SC12	SWS Cal-G 12	Gap-position relation
SC13	SWS Cal-G 13	Relative flux
SC14	SWS Cal-G 14	Intensity of internal calibration sources
SC15	SWS Cal-G 15	Intensity of calibration sources
SC16A	SWS Cal-G 16A	Aperture offsets
SC16B	SWS Cal-G 16B	Element offsets
SC16C	SWS Cal-G 16C	Grating constants
SC16D	SWS Cal-G 16D	Telescope area
SC16E	SWS Cal-G 16E	Scanner curve coefficients
SC16ET	SWS Cal-G 16ET	Scanner curve polynoms
SC18	SWS Cal-G 18	Effective gap correction
SC19	SWS Cal-G 19	AOT 1 resolution factors
SC20	SWS Cal-G 20	Relative detector responsivity
SC21_1	SWS Cal-G 21_1	Detector dark current/noise for 1 sec reset
SC21_2	SWS Cal-G 21_2	Detector dark current/noise for 2 sec reset
SC21_4	SWS Cal-G 21_4	Detector dark current/noise for 4 sec reset
SC21_8	SWS Cal-G 21_8	Detector dark current/noise for 8 sec reset
SC22	SWS Cal-G 22	Detector response to internal diffuse source and flusher
SC23	SWS Cal-G 23	Wave limits for bands
SC24	SWS Cal-G 24	Wave limits for apertures
SC25_1A	SWS Cal-G 25_1A	Spectral responsivity for band 1A - RSRF file
SC25_1B	SWS Cal-G 25_1B	Spectral responsivity for band 1B
SC25_1D	SWS Cal-G 25_1D	Spectral responsivity for band 1D
SC25_1E	SWS Cal-G 25_1E	Spectral responsivity for band 1E
SC25_2A	SWS Cal-G 25_2A	Spectral responsivity for band 2A
SC25_2B	SWS Cal-G 25_2B	Spectral responsivity for band 2B
SC25_2C	SWS Cal-G 25_2C	Spectral responsivity for band 2C
SC25_3A	SWS Cal-G 25_3A	Spectral responsivity for band 3A
SC25_3C	SWS Cal-G 25_3C	Spectral responsivity for band 3C
SC25_3D	SWS Cal-G 25_3D	Spectral responsivity for band 3D
SC25_3E	SWS Cal-G 25_3E	Spectral responsivity for band 3E
SC25_4	SWS Cal-G 25_4	Spectral responsivity for band 4

SC25_4A	SWS Cal-G 25_4A	Spectral responsivity for band 4A
SC25_4C	SWS Cal-G 25_4C	Spectral responsivity for band 4C
SC25_4D	SWS Cal-G 25_4D	Spectral responsivity for band 4D
SC25_5A	SWS Cal-G 25_5A	Spectral responsivity for band 5A
SC25_5B	SWS Cal-G 25_5B	Spectral responsivity for band 5B
SC25_5C	SWS Cal-G 25_5C	Spectral responsivity for band 5C
SC25_5D	SWS Cal-G 25_5D	Spectral responsivity for band 5D
SC25_6	SWS Cal-G 25_6	Spectral responsivity for band 6
SC41	SWS Cal-G 41	Average shape of flux calibration sources
STIMDEP		Time dependency file

Some of these files have identical formats and so are discussed together.

In all cases the ISO Data Product Document should be referred to for the exact file layout.

A.5.1 SWS Cal-G 1 Electrical crosstalk matrices

This file is used in Derive-SPD to correct for the effects of electrical crosstalk (see section 4.2.6).

The file contains 12 records, each 52 integers in length. The first 12 numbers in each record contain the crosstalk for band 1, the next 12 for band 2 etc. Record 1 contains the crosstalk between detector 1 in each band and the other detectors in that band, record 2 contains the crosstalk between detector 2 in each band and the other detectors in that band, etc. Only records 1 and 2 contain information for bands 5 and 6 (the FP bands with only 2 detectors in each).

A.5.2 SWS Cal-G 2 RC correction timescales

This file, used in Derive-SPD, contains the time constants for the high pass filter in the amplifier chain (see section 4.2.4). It contains 52 numbers, the timescales per detectors in seconds.

A.5.3 SWS Cal-G 2A Midbit values

This file, used in Derive-SPD, contains the midbit value for each detector (see section 4.2.3). The detector readouts are between 0 and 4095 (bits) corresponding to -10 to 10 Volts. The midbit is the bit value that corresponds to 0 Volts, approximately 2048, and is different for each detector.

Currently this calfile is filled with 2047.50.

A.5.4 SWS Cal-G 2B Shape correction values

This is used in Derive-SPD. After the slope has been corrected for the reset pulse it is not straight. This files contains values to correct it, see section 4.2.5.

Currently this calfile is filled with zeros which results in the OLP chain not correcting for reset pulse shape.

A.5.5 SWS Cal-G 3 Reset cutout lengths

This file, used in Derive-SPD and Auto-Analysis, contains the number of 24Hz readouts to ignore after a reset (short circuit of the capacitor) (see section 4.2.2). It contains 52 numbers, the number of readouts minus one to ignore per detector. i.e. one more readout than these numbers is ignored.

A.5.6 SWS Cal-G 4 Amplifier limits

This file, used in Derive-SPD, contains the SWS amplifier limits, the minimum and maximum allowable voltages from the amplifiers (see section 4.2.2). There are 52 records, each of which contains the minimum and maximum voltages (in bits between 0 and 4095) for the three gains (gain 1, 4 and 16), in telemetry units.

A.5.7 SWS Cal-G 5 Switchable gains

This file, used in Derive-SPD, contains the gains used to convert between the slopes generated from the 24Hz information and the voltages on the detectors (see section 4.2.9). There are 52 records, one per detector. Each record contains three numbers, one for each gain.

A.5.8 SWS Cal-G 6 Glitch reject levels

This file, used in Derive-SPD, contains information used to recognise glitches and reject them (see section 4.2.7). It contains 52 records, one per detector. Each record contains four numbers: α; the number of readouts to ignore before and after a glitch; and the minimum width of a glitch. The last three are in units of 24 Hz samples.

A.5.9 SWS Cal-G 7 Grating detector noise characteristics

Currently not used.

A.5.10 SWS Cal-G 8 Grating calibration specifications

Currently not used.

A.5.11 SWS Cal-G 9 LVDT-Angle relation

Currently not used.

A.5.12 SWS Cal-G 10 Key wavelengths

Currently not used.

A.5.13 SWS Cal-G 11 FP calibration spectrum

Currently not used.

A.5.14 SWS Cal-G 12 Gap-position relation

This file, used in Derive-SPD, contains information on the gap, current and position relationship of the two FPs (see sections 4.2.12 and 5.7). Each record contains the FP position (a telemetered number) applicable to both FPs, and then for each FP the main current and two correction currents necessary to achieve this position, and then the corresponding gap for those currents, in μm.

A.5.15 SWS Cal-G 13 Relative flux

This file, used in Auto-Analysis, contains information used in the flux calibration. There is one row per key wavelength. Each row has the name of the AOT band, the key wavelength, two numbers defining the passband used. Then come conversion numbers for each detector in that band (by default 12, with 10 blank for FP bands) in $\mu V/sec/Jy$, then 12 internal calibration signals (in $\mu V/sec$), then 12 relative flux calibrations (in Jy), then errors on the conversion numbers (in $\mu V/sec/Jy$), errors on the internal calibrations (in $\mu V/sec$), errors on the relative flux calibrations (Jy) and finally the grating start and end position (although the grating start is unused in the pipeline due to memory effects).

A.5.16 SWS Cal-G 14 Intensity of internal calibration sources

Currently not used.

A.5.17 SWS Cal-G 15 Intensity of calibration sources

Currently not used.

A.5.18 SWS Cal-G 16A Aperture offsets

This file, used in Derive-SPD, contains the angles, in degrees, from the optical axis to the entrance or light source used, as seen from the SW and LW collimators (see section 5.7).

A.5.19 SWS Cal-G 16B Element offsets

This file, used in Derive-SPD, contains the angles, in degrees, from the optical axis to the detectors for each of the detectors (see section 5.7).

A.5.20 SWS Cal-G 16C Grating constants

This file, used in Derive-SPD, contains two grating constants, in μm, for the SW and LW gratings (see section 5.7).

A.5.21 SWS Cal-G 16D Telescope area

Currently not used.

A.5.22 SWS Cal-G 16E Scanner curve coefficients

This file, used in Derive-SPD, contains the scanner curve coefficients (see section 5.7).

A.5.23 SWS Cal-G 16ET Scanner curve polynoms

This contains the scanner curve polynoms (see section 5.7).

A.5.24 SWS Cal-G 18 Effective gap correction

This file, used in Derive-SPD, contains information of the effective gap correction. For each possible FP wavelength there is a gap correction for each of the two FPs. All units are μm.

A.5.25 SWS Cal-G 19 AOT 1 resolution factors

Cal-G 19 is used in the processing of all speed AOT 1's. It contains the factors needed to smooth the RSRF's of each AOT band down to the spectral resolution of the AOT 1 being processed and hence match the resolutions.

This was added in OLP V5.0.

A.5.26 SWS Cal-G 20 Relative detector responsivity

Currently not used.

A.5.27 SWS Cal-G 21_x Detector dark current/noise for x sec reset

These 4 files, Cal-G 21_1, Cal-G 21_2, Cal-G 21_4 and Cal-G 21_8 contain information on the dark current. There is one file per reset interval. Each file contains 52 records, each containing the detector number, the average measured dark current (from ground and PV phase tests). the noise in the dark current and finally the minimum and maximum valid dark currents. Dark currents are measured in $\mu V/sec$. The values are used to check the dark currents in the data against, with a flag raised if they are exceeded.

A.5.28 SWS Cal-G 22 Detector response to internal diffuse source

Currently not used.

A.5.29 SWS Cal-G 23 Wave limits for bands

This file, used in Derive-SPD, contains information on the wavelength limits for the six detector bands. There is one row for each band, and each row contains the lower and upper wavelength limits in μm.

A.5.30 SWS Cal-G 24 Wave limits for apertures

This file, used in Derive-SPD, contains information on the wavelength limits for the three apertures. There are five rows, one row for each aperture plus two for calibrators, and each row contains the lower and upper limit wavelength limit for the two subsystems, in μm.

A.5.31 SWS Cal-G 25_x Spectral responsivity for band x

These files, Cal-G 25_1A, Cal-G 25_1B, Cal-G 25_1D, Cal-G 25_1E, Cal-G 25_2A, Cal-G 25_2B, Cal-G 25_2C, Cal-G 25_3A, Cal-G 25_3C, Cal-G 25_3D, Cal-G 25_3E, Cal-G 25_4, Cal-G 25_5A, Cal-G 25_5B, Cal-G 25_5C, Cal-G 25_5D and Cal-G 25_6, contain the spectral responsivity information (RSRF) for each band.

Each is composed of the number of detectors in that band (twelve for grating, two for the FP files Cal-G 25_x and 25_6) times three numbers. These are the wavelength at which the responsivity is measured (in μm), the responsivity and the error on it, both in $\mu V/sec/Jy$.

Files 25_4A, 25_4B and 25_4C are used for off-band data.

A.5.32 SWS Cal-G 41 Slope of calibration source

This file is compared with the observed calibration source.

A.5.33 STIMDEP Time dependency file

Defines which version of the Cal-G files is used to process an observation.

Appendix B

List of Acronyms and Symbols

This appendix lists acronyms and symbols specific to SWS. For a more general list refer to the Handbook Volume 2.

AA	Auto Analysis – software used to process data, see section 4.3
AAR	Auto Analysis Result file - output of AA, defined in section A.4.1
AOT	Astronomical Observation Template – see chapter 3
CAM	ISO Camera – one of the four instruments onboard the satellite
d	Fabry-Pérot gap width
Derive-AAR/DAAR	The OLP stage that processes SPD data to the AAR level. See section 4.3
Derive-SPD/DSPD	The OLP stage that processes ERD data to the SPD level. See section 4.2
Dwell time	The time during which the grating is stationary and hence the detectors are illuminated by light of one wavelength.
ERD	Edited Raw Data – raw data from the satellite, defined in section A.2.1
FITS	Flexible Image Transport System
FM	Flight Model (of SWS)
FS	Flight Spare model (of SWS)
FWHM	Full Width at Half Maximum
F-P	Fabry-Pérot Spectrometer
IA	Interactive Analysis
ILT	Instrument Level Test (SWS laboratory test)
ITK	Instrument Time Key - see the ISO Handbook Volume II for a description of this key
JFET	Junction Field Effect Transistor
LW	Long Wavelength section of SWS
LWS	ISO Long Wavelength Spectrometer – one of the four instruments onboard the satellite
LVDT	A measure of the angle of the scan mirror for the gratings. It is given the term 'LVDT' as this angle is measured by a Linear Voltage Differential Transducer
L_{AOT}	Number of scan steps per AOT band
L_F	Number of scan steps per FWHM of spectral resolution
L_s	Step size in scanner steps
λ	Wavelength
n	Fabry-Pérot order
n_i	Number of integrations
n_{int}	Number of samples taken from a single spectral resolution element
n_{scan}	Number of scans

n_{step}	Number of steps
N_D	Dark current noise
N_R	Read noise
N_S	Shot noise
OLP	Off-Line Processing – the pipeline, also known as SPG
PHT	ISO Photopolarimeter – one of the four instruments onboard the satellite
QLA	Quick Look Analysis - a quick assessment carried out on the data
RTA	Real Time Assessment - a quick assessment carried out on the data
R	Spectral Resolution
SNR	Signal-to-Noise Ratio
SOC	Science Operations Center (Villafranca)
SPD	Standard Processed Data file - output of DSPD, defined in section A.3.1
SPG	Standard Product Generation – the pipeline, also known as OLP
SW	Short Wavelength section of SWS
SWGH	SWS Glitch History Data file - output of DSPD, defined in section A.3.2
SWS	ISO Short Wavelength Spectrometer – one of the four instruments onboard the satellite
S	Signal Strength (μV/s)
S_ν	Flux density (Jy)
TDATA	Transparent Data
TDF	Telemetry Distribution Format
TDT	Target Dedicated Time
t_r	Detector reset time (sec)
UTK	Uniform Time Key - see the ISO Handbook Volume II for a description of this key

Bibliography

[1] van den Ancker, M.E., Voors, R. & Leech, K.J., Grating instrumental profile and resolution, issued 1 July 1997 and accessible at URL http://www.iso.vilspa.esa.es/users/expl_lib/SWS/doc/sws_ip/

[2] Beintema, D.A. & Kunze, D., SWS AOT Design Description, 24 June 1996 and available at URL http://www.iso.vilspa.esa.es/users/expl_lib/SWS/aot_design_doc.ps.gz

[3] FITS, NASA Science Data Systems Standards Office (NSDSSO), see URL http://www.cv.nrao.edu/fits/

[4] Feuchtgruber, H., Status of SWS Fabry-Pérot wavelength calibration and instrumental profile, issued 5 May 1998, and available at URL http://www.iso.vilspa.esa.es/users/expl_lib/SWS/fp_wavecal.html

[5] Feuchtgruber, H., Status of study on Gam-Dra fluxes and related pointing errors, issued 10 June 1998 and available on the web at URL http://www.iso.vilspa.esa.es/users/expl_lib/SWS/gamdrareport.html

[6] Feuchtgruber, H., Status of study of AOT02 line profiles and fluxes on NGC6543, issued 2 June 1998.

[7] de Graauw, T., *et al*, 1996, A&A 315, L49, Observing with the ISO Short Wavelength Spectrometer, published in the A&A special issue (November 1996 Vol 315) devoted to ISO and available at URL http://www.iso.vilspa.esa.es/ISO/AandA/I0102.html

[8] Heras, A.M., Single Detector Signal Jumps, issued 9 June 1997 and accessible at URL http://www.iso.vilspa.esa.es/users/expl_lib/SWS/doc/jumps_rep_web/jumps_rep_web.html

[9] Heras, A.M., CROSS AOT COMPARISON, PART 1, issue 1.1, issued on 6 February 1997, and available at URL http://sws.ster.kuleuven.ac.be/documents/X_AOT_COMPARISON/x_aot_comp1.txt

[10] Heras, A.M., Cross AOT comparison-part 2, issued 21 April 1997 and published in part in the 'First ISO Workshop on Analytical Spectroscopy', Eds A.M. Heras, K. Leech, N.R. Trams & M. Perry, ESA SP-419, p77.

[11] Heras, A.M., The effects of the pointing jitter on SWS observations, issued 6 August 1998 and available on the web at URL http://www.iso.vilspa.esa.es/users/expl_lib/SWS/point_jitter.ps.gz

[12] Kester, D., Beintema, D. & Valentijn, E., End-of-Mission Report: Wavelength Calibration Status, issued 2 July 1998 and available at URL http://www.iso.vilspa.esa.es/users/expl_lib/SWS/wavecal.ps.gz

[13] Leech, K.J., ISO Satellite & Data Manual (ISDM), SAI/98-094/Dc

[14] Leech, K.J., *et al*, SWS Observers Manual. Version 3.0 was the post-launch version issued with the supplemental call, while Version 2.0 (van der Hucht, K.A. *et al*) was the pre-launch version. Available at URL http://www.iso.vilspa.esa.es/manuals/SWS_man/obsman.html

[15] Leech, K.J., SWS Instrument Data Users Manual (IDUM), SAI/95-221/Dc

[16] Leech, K.J. & Heras, A.M., Effects seen in data induced by incorrect target coordinates or crowded fields, issued 12 June 1997 and accessible at URL http://www.iso.vilspa.esa.es/users /expl_lib/SWS/doc/pointing/

[17] Leech, K.J. & Morris, P., Possible Detector Memory Effects in SWS Grating range spectra (AOT S06) due to SWS Reference Scans, issued 27 May 1997 and available at URL http: //www.iso.vilspa.esa.es/users/expl_lib/SWS/ref_scan/

[18] Salama, A., SWS Beam Profiles and ISO Pointing, issued 9 September 1998 and available at URL http://www.iso.vilspa.esa.es/users/expl_lib/SWS/beam_doc.ps.gz

[19] Saxton, R., ISO Data Products Document (IDPD), ISO-SSD-9111A

[20] Schaeidt, S.G., *et al*, 1996, A&A 315, L55, The Photometric Calibration of the ISO Short Wavelength Spectrometer, published in the A&A special issue (November 1996 Vol 315) devoted to ISO and available at URL http://www.iso.vilspa.esa.es/ISO/AandA/I0103.html

[21] Shipman, R.F., 2000, 'Testing of SWS Flatfield', and available at http://sws.ster.kuleuven.ac.be/ documents/flatfield/fftest.html

[22] Valentijn, E., *et al*, 1996, A&A 315, L60, The Wavelength Calibration and Resolution of the Short Wavelength Spectrometer, published in the A&A special issue (November 1996 Vol 315) devoted to ISO and available at URL http://www.iso.vilspa.esa.es/ISO/AandA/e_valentijn.html

[23] Vandenbussche, B., 1999, The ISO-SWS Relative Spectral Response Calibration available at URL http://www.iso.vilspa.esa.es/users/expl_lib/SWS/rsrf_v1.1.ps.gz

[24] Wieprecht, E., Wiezorreck, E. & Hauser, L. 2000, ExA 10/2-3, 1999, SWS-detector glitch effect correction.

[25] Wieprecht, E. & Feuchtgruber, H., "The Error Propagation of the SWS Pipeline", 31 August 1999 and available at URL http://www.iso.vilspa.esa.es/users/expl_lib/SWS/errorprop_2_1.ps.gz

Index